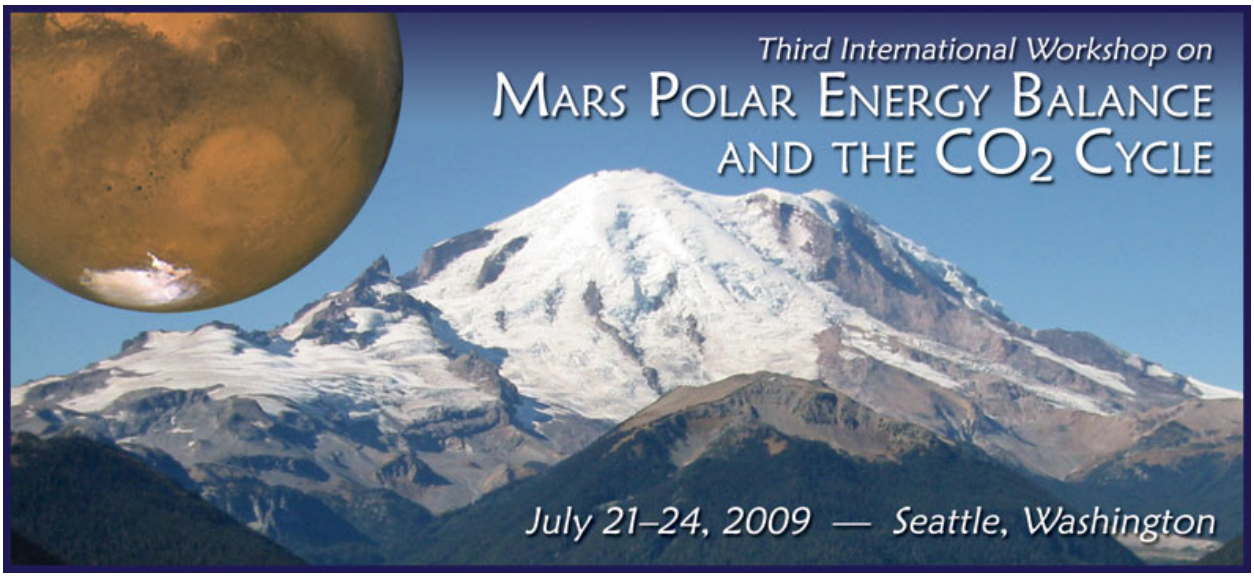

Program and Abstract Volume

LUNAR AND PLANETARY INSTITUTE

LPI Contribution No. 1494

THIRD INTERNATIONAL WORKSHOP ON
MARS POLAR ENERGY BALANCE AND THE CO_2 CYCLE

July 21–24, 2009

Seattle, Washington

Sponsors

Lunar and Planetary Institute

U.S. Geological Survey

Convener

Timothy Titus
U.S. Geological Survey

Scientific Organizing Committee

Timothy Titus
U.S. Geological Survey

Joshua Bandfield
University of Washington

Anthony Colaprete
NASA Ames Research Center

Thomas Prettyman
Planetary Science Institute

Lunar and Planetary Institute 3600 Bay Area Boulevard Houston TX 77058-1113

LPI Contribution No. 1494

Compiled in 2009 by
LUNAR AND PLANETARY INSTITUTE

The Lunar and Planetary Institute is operated by the Universities Space Research Association under a cooperative agreement with the Science Mission Directorate of the National Aeronautics and Space Administration.

Abstracts in this volume may be cited as

Author A. B. (2009) Title of abstract. In *Third International Workshop on Mars Polar Energy Balance and the CO_2 Cycle*, p. XX. LPI Contribution No. 1494, Lunar and Planetary Institute, Houston.

This volume is distributed by

ORDER DEPARTMENT
Lunar and Planetary Institute
3600 Bay Area Boulevard
Houston TX 77058-1113, USA
Phone: 281-486-2172
Fax: 281-486-2186
E-mail: order@lpi.usra.edu

A limited number of copies are available for the cost of shipping and handling.
Visit the LPI Online Store at https://www.lpi.usra.edu/store/products.cfm.

ISSN No. 0161-5297

Preface

This volume contains abstracts that have been accepted for presentation at the Third International Workshop on Mars Polar Energy Balance and the CO_2 Cycle, July 21–24, 2009, Seattle, Washington.

Administration and publications support for this meeting were provided by the staff of the Publications and Program Services Department at the Lunar and Planetary Institute.

Contents

Program

Tuesday, July 21, 2009
INTRODUCTION
8:30 a.m. Blakely/Camano Room

8:30 a.m. Workshop Goals and Objectives

EATING SWISS CHEESE AT THE SOUTH POLE
9:00 a.m. Blakely/Camano Room

Convener: **Sylvain Piqueux**

9:00 a.m. Session Introduction

9:15 a.m. Thomas P. C. * James P. B. Calvin W. M. Haberle R. M.
Residual South Polar Cap: How old, How is it Changing? **[#7017]**

9:45 a.m. Haberle R. M. * Kahre M. A. Malin M. Thomas P. C.
The Disappearing South Residual Cap on Mars: Where is the CO_2 Going? **[#7002]**

10:15 a.m. Break

10:30 a.m. Wood S. E. * Griffiths S. D.
Epochal Seasonal Thermal Modeling of Mars' Polar Surface Energy Balance: Perennial CO_2 Ice and Atmospheric Collapse **[#7032]**

11:00 a.m. James P. B. * Thomas P. C. Calvin W. M. Haberle R.
CTX Observations of Seasonal Albedo Variations in the "Tooth Region" of the RSPC **[#7019]**

11:30 a.m. Soto A. * Guo X. Richardson M. I.
On the Mystery of the Perennial Carbon Dioxide Cap at the South Pole of Mars **[#7012]**

12:00 p.m. SPRC Poster Synopses and General Discussion

12:30 p.m. Lunch in Orcas/Lopez Room

Tuesday, July 21, 2009
DUSTY SEASONINGS AND FROZEN MUD PIES
1:30 p.m. Blakely/Camano Room

Convener: **Joshua Bandfield**

1:30 p.m. Session Introduction

1:45 p.m. Kahre M. A. * Haberle R. M.
Mars' CO_2 Cycle: Effects of Airborne Dust and CO_2 Ice Emissivity on the Growth of Seasonal CO_2 Caps **[#7010]**

2:15 p.m. Millour E. * Forget F. Diez B. Montabone L.
Simulating the Martian CO_2 Cycle with the LMD Global Climate Model **[#7011]**

2:45 p.m. Bandfield J. L. *
Thermophysical Properties of Martian High Latitude Surfaces Derived from Seasonal Temperature Measurements **[#7006]**

3:15 p.m. Break

3:30 p.m. Vincendon M. * Mustard J. Forget F. Kreslavsky M. Spiga A. Murchie S. Bibring J.-P.
Mid Latitude CO_2 Ice Deposits Analyzed with CRISM and OMEGA **[#7021]**

4:00 p.m. Doute S. * Schmidt F. Schmitt B. Vincendon M. Langevin Y. Gondet B.
Physical State of the "Bright" South Seasonal Polar Cap from OMEGA Observations **[#7033]**

4:30 p.m. Calvin W. M. * James P. B. Haberle R. M. Malin M. C. Thomas P. C. Brown A. J.
MARCI Views of the Martian Polar Ices and Their Evolution **[#7020]**

5:00 p.m. CO_2 Ice Properties Poster Synopses and General Discussion

5:30 p.m. Adjourn

Thursday, July 23, 2009
SPICING YOUR MEAL WITH CAP SEASONINGS
8:30 a.m. Blakely/Camano Room

Convener: **Thomas Prettyman**

8:30 a.m. Session Introduction

8:45 a.m. Prettyman T. H. * Titus T. N. Colaprete A.
Constraints on Mars' Polar Energy Balance from Nuclear Spectroscopy **[#7026]**

9:15 a.m. Titus T. N. *
Mars Polar Cap Edges Tracked Over Four Full Mars Years Using MGS TES **[#7018]**

9:45 a.m. Litvak M. L. * Boynton W. V. Kozyrev A. S. Mitrofanov I. G. Sanin A. B. Tretyakov V. I. Varenikov A. B. Golovin D.
Seven Years of Observations of Martian Seasonal Caps Onboard Mars Odyssey by HEND Instrument **[#7003]**

10:15 a.m. Break

10:30 a.m. Langevin Y. * Bibring J.-P. Douté S. Vincendon M. Poulet F. Gondet B.
Investigations of Mars Polar Processes by OMEGA/Mex Over Three Martian Years **[#7025]**

11:00 a.m. Schmitt B. * Appéré T. Douté S. Beck P. Forget F. Langevin Y. Bibring J.-P.
Microphysical Cycle of Evolution of the Northern Martian Seasonal Condensates **[#7027]**

11:30 a.m. Appéré T. * Schmitt B. Douté S. Forget F. Langevin Y. Bibring J.-P. Gondet B.
Spring Evolution of the Northern Seasonal Condensates on Mars from OMEGA on Mars Express **[#7004]**

12:00 p.m. Seasonal Cap Poster Synopses and General Discussion

12:30 p.m. Lunch in Orcas/Lopez Room

Thursday, July 23, 2009
DUSTY AND FROSTY JETS
1:30 p.m. Blakely/Camano Room

Convener: **Timothy Titus**

1:30 p.m. Session Introduction

1:45 p.m. Hansen C. J. *
HiRISE Images of Southern Seasonal Polar Cap Sublimation for a Second Spring on Mars **[#7029]**

2:15 p.m. Langevin Y. * Hansen C. Thomas N. Vincendon M. Titus T. Piqueux S. Bibring J.-P. Gondet B. Seelos K.
Investigations of the Cryptic Region of the South Seasonal Cap of Mars in 2009 **[#7008]**

2:45 p.m. Gardin E. * Quantin C. Allemand P. Thollot P.
Dark Spot and Dark Flow Development During the Seasonal Frost Retreat on the Russell Crater Megadune, Mars **[#7013]**

3:15 p.m. Break

3:30 p.m. Pilorget C. * Forget F. Millour E. Madeleine J.-B.
A Physical Model of Surface CO_2 Ice: New Clues to Dark Spots Formation **[#7007]**

4:00 p.m. Piqueux S. * Christensen P. R.
Basal Sublimation and Venting of the North Translucent ("Cryptic") Seasonal Cap **[#7001]**

4:30 p.m. Lorenz R. D. *
Pushing Frost Uphill: The Martian Polar CO_2 Cycle as a Heat Engine **[#7005]**

5:00 p.m. Jets and Atmospheres Poster Synopses and General Discussion

5:30 p.m. Adjourn

Thursday, July 23, 2009
POSTER SESSION
5:30 p.m. Orcas/Lopez Room

Cornwall C. Titus T. N.
Martian Cold Spot Activity in the Northern and Southern Hemispheres and the Effects of the Global Dust Storm of 2001 **[#7015]**

Eluszkiewicz J. AER Team
Current Status of Atmospheric and Surface Retrievals in the Mars Polar Regions **[#7034]**

Michaels T. I.
Modeling Microscale Mars Polar Phenomena Related to CO_2 Ice **[#7014]**

Vincendon M. Langevin Y. Douté S. Bibring J.-P.
3 Mars Years of Dust Optical Depth Mapping by OMEGA Above the South Pole **[#7022]**

Withers P. Tellmann S.
Simplifying the Martian Carbon Dioxide Cycle: An Empirical Method for Predicting Surface Pressure **[#7009]**

Friday, July 24, 2009
POLAR SCIENCE MIT GAS
8:30 a.m. Blakely/Camano Room

Convener: **Tim Michaels**

8:30 a.m. Session Introduction

8:45 a.m. Tellmann S. * Withers P. Pätzold M. Häusler B. Tyler G. L. Hinson D. P.
The Polar Atmosphere as seen by the Radio Science Experiment MaRS on Mars Express **[#7024]**

9:15 a.m. Määttänen A. Montmessin F. Gondet B. * Hoffmann H. Scholten F. Hauber E. Gonzalez-Galindo F. Forget F. Bibring J.-P. Bertaux J.-L. Neukum G.
High-Altitude CO_2 Clouds on Mars: OMEGA and HRSC Observations **[#7023]**

9:45 a.m. Hayne P. * Paige D. A.
Carbon Dioxide Snow Cloud Activity and Polar Winter Emissivity: Mars Climate Sounder Observations and Model Results **[#7030]**

10:15 a.m. Break

10:30 a.m. Barnes J. R. * Sprague A. L. Hinson D. P. Tyler D. Boynton W. V.
Further Examination of the Role of Atmospheric Eddies in Wintertime Polar Argon Enhancement and CO_2 Supersaturation **[#7016]**

11:00 a.m. Forget F. * Millour E. Montabone L. Lefevre F.
Non Condensable Gas Enrichment and Depletion in the Martian Polar Regions **[#7031]**

11:30 a.m. Discussion
White Papers and Top Priorities

1:00 p.m. Adjourn

SPRING EVOLUTION OF THE NORTHERN SEASONAL CONDENSATES ON MARS FROM OMEGA ON MARS EXPRESS

T. Appéré, B. Schmitt, S. Douté, *Laboratoire de Planétologie de Grenoble, CNRS/UJF, France (Thomas.Appere@obs.ujf-grenoble.fr)*, **F. Forget,** *[3]Laboratoire de Modélisation Dynamique, Université Paris 6, Paris, France*, **Y. Langevin, J.-P. Bibring, B. Gondet,** *Institut d'Astrophysique Spatiale, CNRS - Université Paris-Sud, Orsay,France.*

Introduction: Seasonal condensates are one of the most important martian meteorological processes. The determination of the physical state and coexistence modes of the ices and dust composing the seasonal condensates, as well as their extent, abundance and temporal evolution, are of prime importance for the understanding of the deposition and sublimation processes of volatiles on Mars. The spatial and temporal distributions of the condensates are strongly linked with the seasonal cycle of CO_2 and H_2O exchanges between the surface and the atmosphere. The knowledge of these distributions should help to constrain these cycles. They may also provide clues to understand the current and past climatic cycles through inter-annual evolutions. Before the Mars Express mission (ESA) the evolution of the seasonal condensates have been essentially monitored by the albedo and temperature changes of the surface [1, 2, 3].

OMEGA observations: The OMEGA imaging spectrometer aboard Mars Express allows to directly monitor the abundance, physical state and distribution of the CO_2, water and dust components of the condensates through their visible and near-infrared spectral signatures. We report on the 2006 evolution of the northern seasonal condensates, from winter solstice to their complete sublimation around summer solstice.

Evolution of the seasonal condensates extent: The seasonal condensates were monitored using three parameters : reflectance at 1.08µm as a proxy of the albedo, CO_2 ice band depth at 1.43µm and H_2O ice band depth at 1.5µm. Maps of these parameters were created for 23 Ls intervals.

The seasonal condensates evolution in term of albedo is mostly the same as the ones observed by [1, 2, 3] in 2000 and 2002. The recession is first axisymmetric then much less symmetric after Ls 50°. Condensates albedo increases during the recession. Further analysis should help to constrain the origin(s) of this effect: a combined ice grain size and aerosols optical depth effect, or a process removing the dust from the ice, or a photometric effect of the ice?

CO_2 ice and H_2O ice distributions are also axisymmetric from Ls 350° to 50°. H_2O ice extends southern of CO_2 ice, thus a CO_2-free water ice annulus surrounds the CO_2 ice rich deposits [4]. This annulus was first detected on the basis of temperature measurements [1]. Low H_2O ice band depth is detected southern of this water ice annulus, likely mostly due to absorption by water ice in clouds forming the polar hood. After Ls 50°, CO_2 ice distribution becomes patchy until complete disappearance at Ls 80°. However, between Ls 50° and 70°, the CO_2 ice signature reappears at locations where it had disappeared. H_2O ice distribution is no more axisymmetric after Ls 50°, assuming the kind of polygonal form observed for the albedo distribution. It recesses until reaching the permanent cap at Ls ~100°.

Boundaries of the seasonal condensates in term of albedo, CO_2 ice and H_2O ice were retrieved from the dataset (see Figure 1).

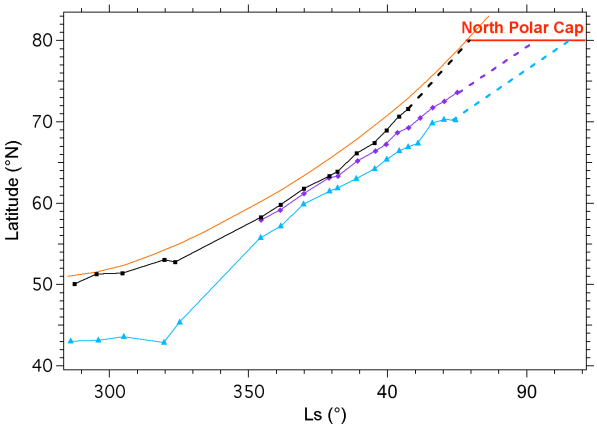

Figure 1: Comparison between seasonal condensates boundaries. All boundaries are zonally averaged. Black: CO_2 ice boundary (OMEGA). Purple: albedo boundary (OMEGA). Blue: H_2O ice boundary (OMEGA). Orange: IR boundary (TES).

First we notice that the water ice annulus is very extended before the beginning of the recession at Ls 320°. Its ~8° extension likely corresponds to daily water frost observed by the Viking Lander 2 [5]. After Ls 350°, the water ice annulus is only 2° extended and widens to more than 3° after Ls 35°. The albedo boundary of the condensates does not correspond to their outer limit, i.e. the water ice limit. Water ice detected

southern of the albedo limit probably corresponds to dusty water ice segregated with defrosted soil. CO_2 ice is systematically detected southern the TES crocus line which is the thermal stability limit of CO_2 ice [6]. CO_2 ice southern the TES crocus line is likely segregated with water ice whose temperature is above CO_2 ice temperature.

Evolution on specific regions: Values of the albedo, CO_2 ice band depth at 1.43µm and H_2O ice band depth at 1.5µm were monitored at specific regions, one which exhibits typical seasonal condensates behavior and the other exhibiting an atypical behavior.

Typical behavior: Figure 2 shows the evolution of the three parameters in a region located at 65°E, 71°N. CO_2 ice band depth decreases as soon as Ls 0° and the absorption band disappears at Ls ~45°. Albedo and H_2O ice band depth first gradually increase then sharply decrease from Ls 40° to ~66°. The water ice annulus reaches this region at Ls ~45°, when CO_2 ice disappears.

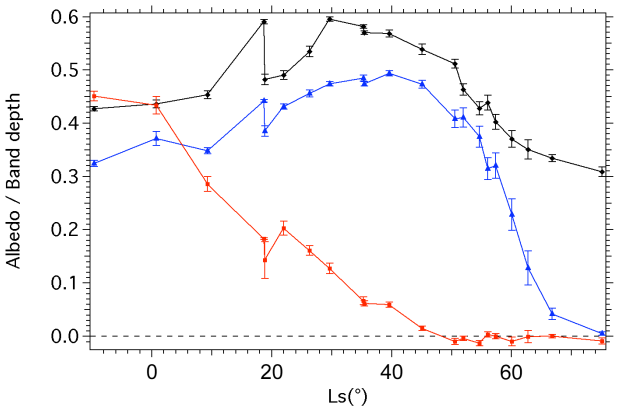

Figure 2: typical seasonal behavior of albedo and ices band depth. Black: albedo. Blue: H_2O ice band depth at 1.5µm. Red: CO_2 ice band depth at 1.43µm.

Atypical behavior: Figure 3 shows an atypical behavior observed at 347°E, 76°N. A sharp decrease of the CO_2 ice band depth is observed between Ls 35° and 50° correlated with a sharp increase of the H_2O ice band depth. The albedo stays constant during this period. Then at Ls 59° CO_2 ice band depth suddenly increases to 25% and H_2O ice band depth decreases. Both ices are no more detected after Ls 80°.

This atypical behavior is observed on the circumpolar dark dunes field, on the walls of Chasma Boreale and inside North permanent cap chasmata.

The process responsible for this behavior may be linked with the water ice annulus. Water ice sublimating in this annulus could recondense on the northern CO_2 ice rich deposits which would act as a cold trap [7]. A H_2O ice veneer would form, hiding the CO_2 ice

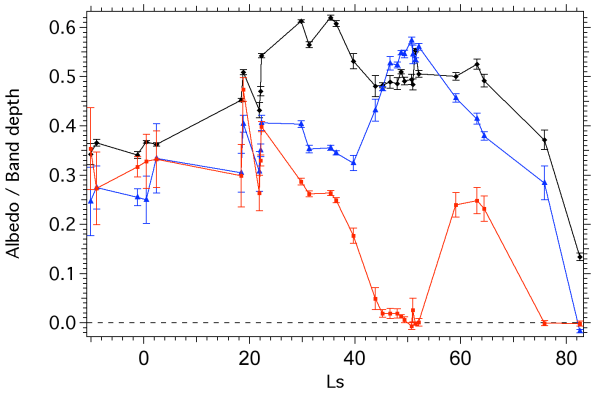

Figure 3: atypical behavior of albedo and ices band depth. Black: albedo. Blue: H_2O ice band depth at 1.5µm. Red: CO_2 ice band depth at 1.43µm.

signature. Radiative transfer modelling in layered media [8] using optical constants of CO_2 and H_2O [9,10] has shown that a 0.1 mm thick layer of H_2O ice is enough to hide the CO_2 ice signature. Then the sublimation of CO_2 ice would break up the H_2O ice veneer, revealing the CO_2 ice signature.

Conclusion: Northern seasonal condensates differ from the southern ones by the amount of H_2O ice involved. Stability temperature of water ice is higher than CO_2 ice one. Therefore a water ice annulus surrounds the CO_2 ice rich deposits. An atypical behavior is observed for CO_2 ice signatures, involving a complex interplay between H_2O frost, CO_2 ice, probably dust and the underlying terrains. The understanding of the various processes occurring during the condensates recession will provide clues to constrain the seasonal cycle of CO_2 and H_2O exchanges between the surface and the atmosphere.

References: [1] Kieffer H.H. and Titus T.N. (2001) *Icarus* 154, 131-144; [2] James P.B. and Cantor B.A (2001) *Icarus* 154, 162-180; [3] Benson J.L. and James P.B. (2005) *Icarus* 174, 513-523; [4] Schmitt B. et al. (2005) *36th LPSC*, 36, 2326+; (2006) *LPI Contribution* 1323, 8050; [5] Jones K.L. et al. (1979) *Science* 204, 799-806; [6] Titus T. N. (2005) *36th LPSC*, 36, 1993+; [7] Appéré et al. (2008) *LPI Contribution* 1443, 9008 ; [8] Douté S. and Schmitt B. (1998) *JGR E,* 103, 31367-31390; [9] Quirico E. and Schmitt B. (1997) *Icarus,* 127, 354-378. [10] Grundy W. and Schmitt B. (1998) *JGR E,* 103, 25809-25822.

THERMOPHYSICAL PROPERTIES OF MARTIAN HIGH LATITUDE SURFACES DERIVED FROM SEASONAL TEMPERATURE MEASUREMENTS. J. L. Bandfield, Department of Earth and Space Sciences, University of Washington, Seattle (joshband at u.washington.edu).

Introduction: Martian high latitude surfaces have thermal properties consistent with an extensive high thermal inertia layer within a few centimeters of the surface. This subsurface permafrost will have a thermal inertia similar to solid bedrock that is much higher than the more porous dry particulate regolith cover [e.g. 1-6]. The layered nature of the regolith makes it impossible to describe its thermophysical properties using a single thermal inertia value. This layered nature of the regolith makes it necessary to revisit the derivation of high latitude thermophysical properties.

Data and Methods: The analyses of the surface temperatures assume that any buried high thermal inertia layer is a solid mixture of regolith and ice with a thermal inertia of 2290 J m^{-2} K^{-1} $s^{-0.5}$, (MKS units are used throughout this abstract). The model assumes a relatively simple two layered geometry of relatively dry soil cover on top of a semi-infinite high inertia layer that is assumed constant throughout the measurement field of view. More complicated systems are likely to be common on Mars, but the data set does not have the leverage to converge on a unique solution based on more complex geometries.

This study utilizes the estimated surface kinetic temperature derived from Thermal Emission Spectrometer data. Spectral, rather than bolometer, measurements were used because they are less susceptible to atmospheric effects. Observations were restricted to emission angles less than 30°, 50–80° latitude (north and south), and 0100–0300 local time. The data were averaged in bins of 2° latitude, 4° longitude and 4.5° L_s.

The KRC thermal model (H.H. Kieffer, manuscript in preparation) was used to predict surface temperatures. This model allows for customization of a wide variety of parameters such as changes in subsurface thermophysical properties and atmospheric aerosol properties.

Thermal inertias derived from measurements with low angles of solar incidence are not as accurate as those derived from nighttime temperature measurements because of the dominant influence of slope, albedo, and atmospheric aerosol characteristics and their associated uncertainties. For this reason, descending orbit observations at local times of 1300–1500 were avoided. The model was set to run for two Martian years before outputting surface temperatures for the third year.

Each latitude/longitude bin of seasonal surface temperature data was fit individually using a nonlinear least squares fitting routine. All modeling parameters were fixed except surface cover thermal inertia and depth of the permafrost layer. The seasons used for fitting were restricted to summer and early fall seasons. In addition, all surface temperatures below 160K were not used for fitting because of the proximity to CO_2 condensation temperatures. These restrictions as well as the use of only 0100–0300 local time data isolated the model and data from conditions of significant modeling uncertainty.

Top layer inertias were allowed to vary from 60–800, corresponding to diurnal skin depths of ~0.3 to 11 cm. The model permafrost layer has fixed thermophysical properties (including a thermal inertia of 2290), but was allowed to vary from 1.15 to 20.3 diurnal skin depths. As a result, the model and fitting routine is sensitive to permafrost at 0.3–6 and 12–220 cm depths for surface cover thermal inertias of 60 and 800 respectively.

Uncertainties are dominated by systematic errors in derivation and modeling of surface temperatures at mid-latitudes. The seasonal energy cycle is relatively weak at lower latitudes and the model does not account for lateral heat transport from lower latitudes. Uncertainties are discussed in detail in *6*.

Results: Surface cover thermal inertia, active layer thickness, and error maps are displayed in Fig. 1. There are clear correlations between the different data sets and derived parameters. For example, between ~50-65°N, relatively low albedo surfaces are associated with relatively high surface cover thermal inertias, neutron derived water ice depths, and surface temperature derived active layer thicknesses. Similar spatial correlations are also apparent in the southern hemisphere maps, although the nature of the surface cover thermal inertia and the permafrost/water-ice distributions are significantly different from the northern hemisphere maps.

Average RMS errors are 1.93 K and 2.30 K in the north and south respectively. This excludes regions of permanent water or CO_2 ice, which will not be well fit by the model.

Discussion: Obtaining accurate thermophysical properties at high latitudes is essential for prediction of seasonal CO_2 and H_2O frost cover as well as for predicting theoretical water ice stabilities. This is a difficult determination because of a rather weak diurnal energy cycle and the influence of subsurface ice itself on the apparent thermal inertia at these latitudes.

Several studies have derived apparent thermal inertia for high latitude surfaces. Despite some quantitative differences due to the models and type of data used, these studies show that thermal inertia in the northern hemisphere is generally higher than in the southern high latitudes.

This work finds a similar pattern of surface cover thermal inertia. The southern hemisphere has average surface cover thermal inertias of 159, 208, and 251 at 70–80°, 60–70°, and 50–60°S respectively. This is in-between the relatively high values derived by *7* and low values of *8*. Putzig et al. [9] have lower thermal inertia values between ~70– 80°S and higher thermal inertia values at ~50–60°S. It is interesting to note that the southern rim of Hellas basin has high values of thermal inertia up to ~500 by *9*, but is a region of low surface cover thermal inertia (~200) and relatively shallow permafrost here. This will have a significant effect on predicted seasonal frost cover, surface temperatures, and water ice stability depths predicted by vapor diffusion models.

Where surface cover thermal inertia generally decreases poleward in the south, the pattern is more complex in the north. Elevated thermal inertias values of ~300–400 are typical of low albedo regions such as Acidalia near 50–65°N. This is about 50–150 units lower than those of *10* and *9*.

One of the reasons that the term ‘‘apparent thermal inertia’’ is used for polar studies of surface thermophysical properties is that it is impossible to characterize a layered surface with a single value. Thermal inertia derived assuming a vertically homogeneous surface will not be constant based on season [e.g., *11*]. The work presented here is an improvement on previous studies because it explicitly accounts for vertical heterogeneity (albeit in a simplistic manner) and the surface cover thermal inertia values are likely more representative of the top layer of regolith. This can lead to a significant improvement in the prediction and modeling of surface temperatures and seasonal frost cover.

References: [1] Paige, D.A. (1992) *Nature*, *356*, 43-45. [2] Mellon, M.T. et al. (2004) *Icarus*, *169*, 324-340. [3] Schorghofer, N. and Aharonson, O. (2005) *JGR*, *110*, 10.1029/2004JE002350. [4] Titus, T.N. et al. (2003) *Science*, *299*, 1048-1051. [5] Bandfield, J.L. (2007) *Nature*, *447*, 64-67. [6] Bandfield, J.L. and Feldman, W.C. (2008) *JGR*, *113*, 10.1029/2004JE002350. [7] Paige, D.A. and Keegan, K.D. (1994) *JGR*, *99*, 25993-26013. [8] Vasavada, A.R. et al. (2000) *JGR*, *105*, 6961-6970. [9] Putzig, N.E. et al. (2005) *Icarus*, *173*, 325-341. [10] Paige, D.A. et al. (1994) *JGR*, *99*, 25959-25991. [11] Putzig, N.E. and Mellon, M.T. (2008) *Icarus*, *191*, 68-94.

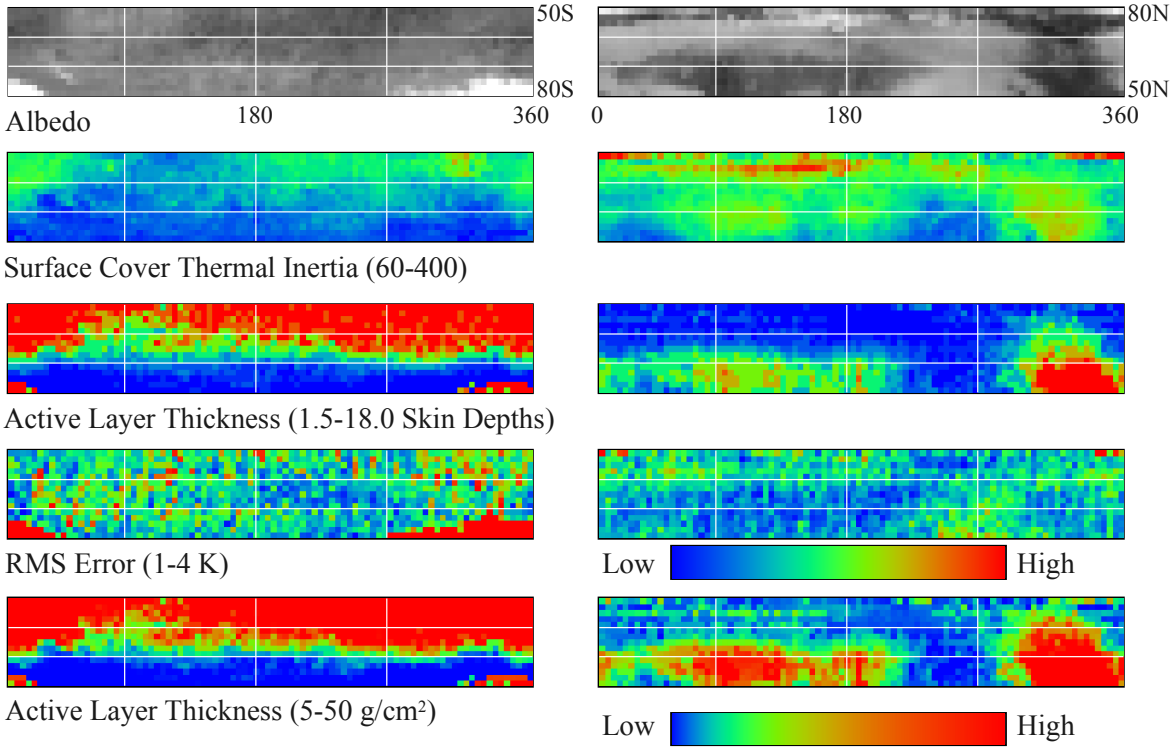

Figure 1. Albedo, surface cover thermal inertia, active layer thickness, and RMS error maps are shown for 50–80N/S at all longitudes. The bottom set of maps are in burial depth assuming a 1.5 g/cm3 surface cover bulk density and use the bottom logarithmic color scale.

Further Examination of the Role of Atmospheric Eddies in Wintertime Polar Argon Enhancement and CO_2 Supersaturation. J. R. Barnes[1], A. L. Sprague[2], D. P. Hinson[3,4], D. Tyler[1], and W.V. Boynton[2], [1]College of Oceanic and Atmospheric Sciences, 104 COAS Admin. Bldg., Oregon State University, Corvallis, OR, 97331 (barnes@oce.orst.edu), [2]Lunar and Planetary Laboratory, University of Arizona, Tucson, AZ, 85721 (sprague@lpl.arizona.edu), [3]Department of Electrical Engineering, Stanford University, 350 Serra Mall, Stanford, CA, 94305 (dhinson@stanford.edu), [4]Carl Sagan Center, SETI Institute, Mountain View, CA, 94043.

Introduction: Previous studies have shown that large-scale atmospheric eddies are of considerable importance for two basic processes which are known to take place in the winter polar regions of Mars. These are the enhancement of Argon and other noncondensing gases as a result of the condensation of CO_2 on the surface and within the atmosphere [1,2,3,4], and the presence of atmospheric regions which are significantly supersaturated with respect to CO_2 [5,6,7]. The latter may be associated with the occurrence of CO_2 convection in the winter polar regions [7]. We have been pursuing further studies of the role of atmospheric eddies in controlling the enhancement of Argon in the winter polar regions by analyzing additional TES temperature data, as well as MGS RS data. We are also carrying out studies of CO_2 supersaturation in the winter polar atmosphere, especially that in northern winter, using TES temperature data as well as MGS RS temperature data.

Winter Polar Argon Enhancement: Measurements made by the Gamma Ray Spectrometer (GRS) on the Mars Odyssey spacecraft have been analyzed to show that the absolute and relative column abundances of Argon and other noncondensing gases maximize in the winter polar regions [1,3]. These gases are left behind as CO_2 condenses on the ground and in the atmosphere. The relative enhancement of Argon is considerably larger in southern winter than in northern winter: peak enhancements are by a factor of ~ 6 in the south polar region in winter, but are only a factor of ~ 1.5-3 above the ambient mixing ratios in northern winter. Given the elevation differences between the south and the north, as well as the seasonal CO_2 cycle, the actual maximum winter column abundances of Argon in the north are quite similar to the corresponding amounts in the south. Based upon a simple model without any atmospheric mixing (condensation only), the peak Argon enhancement factors in the south polar region would be ~ 9, whereas those in the north would be only ~ 3.5 [3,4]. In both cases the actual maximum enhancements are observed to occur close to winter solstice, whereas the no-mixing model predicts maximum enhancements at spring equinox. Atmospheric mixing of Argon (and the other noncondensing gases) from the polar regions into lower latitudes is required to explain this seasonal variation and the reduced enhancements. Viewed in this way, the atmospheric mixing of Argon out of the polar region in northern winter is actually fairly comparable to that in the south during southern winter. In a GCM study of the Argon enhancements, the model mixing was found to be overly strong in both the north and the south, resulting in smaller than observed winter polar enhancements [4]. A basic aspect of the northern winter GRS measurements is that the Argon abundances exhibit substantially greater "high frequency" variability (on time scales of ~ 25 sols and longer) than in the south. No such variability is present in the GCM results, and it is of interest to try to determine if there are plausible dynamical mechanisms associated with the eddies which might be able to produce such variations.

Further studies: Additional Odyssey GRS data have now been analyzed to yield the polar Argon abundances, such that the Argon enhancements during three winters (MY26, 27, and 28) in both the north and the south have been determined. To first order, the basic behavior in the three different winter seasons is quite similar in both the north and the south. The MY26 winter seasons are the only ones for which there are also MGS TES data, which can be analyzed to characterize the basic behavior of the atmospheric eddies responsible for the Argon mixing. There is also an excellent set of MGS RS temperature profiles for northern autumn in MY26 [8], as well as data for the MY27 northern autumn and winter seasons. The RS data have been analyzed so as to characterize aspects of the low-level transient and stationary eddy activity [8]. Some analyses of the MY26 northern winter TES data have previously been carried out to characterize the transient eddy activity in relation to flushing dust storms [9]. We are pursuing much more extensive analyses of these data, as well as data from the MY26 southern winter season, for comparisons with the Argon results. Analysis of the eddy activity during MY24 and 25 is also being completed, to permit an assessment of the MY26 eddies in comparison to the eddy activity in these other years. One aspect that we are particularly focusing on is whether or not there is any "high frequency" variability in the eddy activity that could possibly be correlated with that observed in the Argon enhancements during northern fall and winter.

Winter Polar CO_2 Supersaturation: Previously, the TES temperature data for the MY24 northern winter season were examined in order to assess the extent and magnitude of polar CO_2 supersaturation; TES data for southern winter in MY25 were also analyzed [7]. MGS RS data for MY24, 25, and 26 were analyzed to look at polar supersaturation in both northern and southern winter [7]. It was found that supersaturation was relatively common in both polar regions during winter. The magnitude and vertical extent of supersaturation can be expressed in terms of a convective available potential energy or CAPE, and a potential convective energy flux [7]. The latter was found to reach a maximum value around the time of solstice in both winter polar regions, with the northern maximum value being roughly twice as large as the southern maximum. The region in which significant supersaturation was present was found to be larger – extending further equatorward – in northern winter. GCM simulations were performed and these yielded fairly good agreement with the bulk winter polar supersaturation cycle determined from the TES data, when effects of CO_2 convection (represented by a parameterization) were incorporated in the model [7]. Simulations of the distributions of noncondensing gases were also done, and these yielded generally smaller winter polar enhancements than those present in the GRS Argon data, though the intraseasonal variation in the enhancements was not examined [7].

Further studies: TES temperature data for the northern fall and winter seasons of MY25 and 26, the latter being the first year for which GRS Argon data are available, can be analyzed to assess the magnitude and extent of polar supersaturation. TES data for southern winter in MY24 and 26 can be similarly analyzed. MGS RS data for all three years can be examined in this context, to provide a comparison with the TES data. Analyses of the TES and RS temperature data yield the basic characteristics of the atmospheric eddies, and the contribution of these to the observed supersaturations can be assessed. Preliminary examinations of the TES data for MY24 northern winter showed that strong transient eddies were of considerable importance in producing the supersaturated regions, with stationary eddies and thermal tides also playing an important role. In southern winter, the stationary eddies appeared to be of greater importance for this [2]. The interannual variability of polar supersaturation is a very interesting issue, which can be studied most fully using the TES temperature data.

Results: We will present and discuss some of the key results from the various data analyses described above, in the context of both the winter polar Argon enhancements observed by the Odyssey GRS, and the winter polar CO_2 supersaturations. In relation to the Argon enhancements during southern winter, a basic picture for the mixing involving the transient eddies has previously been proposed [6]. This is based upon the substantial intensification in these eddies which takes place at L_s ~ 130-140, according to analyses of the TES temperature data [2]. We will discuss to what extent this picture holds up in the context of our more complete analyses of the TES data for southern winter. The Argon behavior in northern winter will be addressed in relation to the eddy activity as revealed by the TES and RS data analyses, especially those for MY26 and 27. One focus of this will be the high-frequency variations in the Argon enhancements. One speculative hypothesis that can be proposed is that at least some of this variation could be associated with changes in the basic eddy characteristics during northern fall and winter [2,9,10]. We will also present and discuss the most complete assessment to date of the extent and magnitude of atmospheric polar supersaturations, based upon our analyses of the TES and RS temperature data. These are related to dust abundances, eddy activity, and possible CO_2 convection. The latter is potentially very important in connection with the Argon enhancements, in producing strong vertical mixing [7]. The polar supersaturations (and CO_2 convection) are generally very important in the basic context of the winter polar thermal structure, something that circulation models have tended to have difficulty with.

References:

[1] Sprague A. L. et al. (2004) *Science, 306*, 1364-1367. [2] Barnes J. R. (2006) *The Second Mars Atmosphere Modeling and Observations Workshop,* http://www.mars.lmd.jussieu.fr/granada2006. [3] Sprague A. L. et al. (2007) *J. Geophys. Res., 112,* E03S02, doi:10.1029/2005JE002597. [4] Nelli S. et al. (2007) *J. Geophys. Res., 112*, E08S91, doi:1029/2006JE002849. [5] Colaprete A. et al. (2003) *J. Geophys. Res., 108*(E7), 5081, doi:10.1029/2003JE002053. [6] Barnes J. R. (2005) *LPS XXXVI*, Abstract #1267. [7] Colaprete A. et al. (2008) *Plan. And Space Sci., 56*, 150-180. [8] Hinson D.P. (2006) *J. Geophys. Res., 111*, E05002, doi:10.1029/2005JE002612. [9] Wang H. (2007) *Icarus, 189,* 325-343. [10] Hinson D. P. and Wang H. (2009) *submitted to Icarus*.

MARCI Views of the Martian Polar Ices and their Evolution. W. M. Calvin[1], , P. B. James[2], R. M. Haberle[3], M. C. Malin[4], P. C. Thomas[5], A. J. Brown[6],[1]Geological Sci. & Eng., University of Nevada, Reno, NV 89557, wcalvin@unr.edu, [2]Space Science Institute, Boulder, CO, [3]NASA Ames, Moffett Field, CA, [4]Malin Space Science Systems, San Diego, CA, [5]Center for Radiophysics and Space Research, Cornell University, Ithaca, NY, [6]SETI Institute, Mountain View, CA.

Introduction: The Mars Color Imager (MARCI) on MRO consists of two optical systems (visible and ultraviolet) projecting images onto a single CCD detector [1]. The camera operates in a "pushbroom" mode such that filters are adjacent to each other on the focal plane. MARCI has two ultraviolet and five visible channels. The visible channels have a nadir scale of about 900 m and the UV channels are summed to 7-8 km nadir scale. A primary goal of the MARCI VIS images is to map climate and seasonally variable phenomena as a function of Martian season (Ls).

MRO began transition phase observations at the end of September, 2006. This corresponded to an Ls ~ 113, or after the north residual cap had retreated to its nominal summer state of coarse exposed water ice [2,3]. In mapping orbit MARCI acquires roughly 10 images a day, the vast majority covering the polar regions allowing for high time fidelity synoptic coverage of the varying albedo deposits. We now have a full martian year of observations and are able to trace the onset and retreat of seasonal frosts for both the north and south poles as well as summer season changes in residual ice deposits.

North Pole Seasonal and Residual Ices: Benson and James [4] summarized the recession of the both north and south seasonal caps as observed by MOC. They noted slight asymmetry and variations in recession of the north mostly related to topography.

Calvin and Titus [3] identified large-scale variations in the north residual ice cap using binned TES albedo data. The cap undergoes a period of defrosting up to Ls ~100 to 105, followed by frost migration and transport. These results are consistent with observations reported by Langevin et al. [2], who attributed a decrease in albedo and the change in shape of absorption bands of the central cap in early summer to sublimation of fine-grained water ice frosts. While large scale patterns remain the same, interannual variability in both the persistence and location of the highest albedo deposits has been noted. In particular, sustained bright anomalies were found in several locations.

MARCI time series from MY28 (the first MRO northern summer) shows numerous persistent small bright patches throughout the north residual cap and a sustained high albedo deposits along the ridgeline west of the Chasma Boreale. In addition to the Chasma ridgeline numerous small spots are observed and tend to be located near the lower latitude margins of permanent ice. The bright spots along the ridge were observed by CTX and CRISM and found to disappear after a dust event, uncovering water ice-rich, but lower albedo material [5].

Observations in MY29 (the second MRO northern summer) shows significant variability in the early season (prior to Ls 100). We see retreat of normally water ice covered materials poleward from Tenius Rupes and Abalos Mensa. Significant retreat of water ice in the Gemini Scopuli, off ~60E longitude, is seen followed by refrosting beginning near Ls 95, when the sustained bright patches along the cap margins are also again seen. High albedo materials cover the area mapped as gypsum until well into the northern spring and a new high albedo deposit is seen on top of the dark deposits off the reentrant in Olympia Planum, that later disappears.

Figure 1: North Pole MARCI view on July 30, 2008, Ls 105. Defrosted regions noted in the text are evident as well as new lighter toned deposits in Olympia Undae.

South Pole Seasonal and Residual Ices: The south seasonal cap has a strong asymmetry in seasonal retreat with bright outliers in the Mountains of Mitchell as well as the development of a low-albedo and cold "cryptic" region [6,7,8]. Benson and James [4] note that the south cap recession, though asymmetric, is very similar from year to year between 1999 and 2003.

South seasonal cap recession in MY28 (the southern summer in calendar 2007 with the occurrence of a global dust storm) is similar to past recessional curves, but may have earlier loss of seasonal frost in some areas due to the large dust storm. Outlier ice deposits that have been mapped as water ice by Piqueux et al. [9] stay frosted well into the southern summer, beginning to sublime after Ls 315. These deposits also brighten in early fall suggesting cold trapping of frosts as lower temperatures return.

We have noted the presence of CO_2 frosts in the area of residual carbon dioxide ice until approximately Ls 320 [10,11]. Analysis of CRISM data shows that water ice is highly spatially variable and that many of the low albedo units still contain the spectral features of coarse CO_2 ice [10]. Early season, CO_2 frost is ubiquitous and albedo decreases over the summer, showing remnant "seasonal" ice continues to disappear until Ls 320 or later. The diagnostic CO_2 ice features at 2.28 and 2.34 μm in dark terrain are seen both early and late in the season and are associated with large pathlengths suggesting carbon dioxide ice is intermixed with soils in the dark lanes. This is similar to the situation in the north, where low albedo material darkens, but does not obscure, the ice signatue. However, the southern cap has at least some regions where the ice is solid CO_2, rather than water. There is an apparent transition zone that has more water ice that occurs between high albedo residual cap units to underlying dark polar layered deposits. Late in the summer season, water ice is more apparent in dark material in some locations, especially those areas that have been previously mapped as water based on temperature. Water ice appears to be both intrinsic to the PLD and as a "patina" or surface veneer deposited by winds or cold-trapped on shaded surfaces. Based on previous mixture modeling no place surveyed appears to have more than a few % water ice, though the analysis is not yet comprehensive.

References: [1] Malin, M.C. et al. (2001) JGR, 106, p. 17651. [2] Langevin, Y., et al. (2005), Science, 307, p. 1581. [3] Calvin, W.M. and T.N Titus, (2008) Planet. Space Sci., vol., pg. [4] Benson, J.L. and P. B. James (2005) Icarus, 174, p. 513. [5] Calvin W. M. et al. (2008) 39th LPSC, #1939 [6] James P. B. et al. (1992) in *Mars*, U AZ Press, p. 934 [7] Kieffer H. H. et al. (2000) JGR, 105, p. 9653. [8 James P. B. et al. (2001) JGR 106, p. 23635. [9] Piqueux, S. et al. (2008) JGR, 113, E08014, doi:10.1029/2007JE003055. [10] Calvin W. M. et al. (2009) 40th LPSC, #1984. [11] Thomas P. C. et al. (2009) Icarus, in press.

Figure 2: South Pole MARCI view on August 30, 2007, Ls 305. High albedo region offset above the residual cap is the region mapped as water ice based on temperature.

MARTIAN COLD SPOT ACTIVTY IN THE NORTHERN AND SOUTHERN HEMISPHERES AND THE EFFECTS OF THE GLOBAL DUST STORM OF 2001. C. Cornwall[1,2] and T. N. Titus[2],
[1]Department of Geology, Northern Arizona University, Flagstaff, Arizona 86001 (cc269@nau.edu),
[2]United States Geological Survey, Flagstaff, Arizona.

Introduction: Mariner and Viking were the first to observe cold spot activity in the polar regions of Mars in the 1970s [1]. Cold spots are identified as areas with 20μm brightness temperatures that are as low as 130 K, which is significantly below the CO_2 ice sublimation temperatures [1]. Studies of data from Mars Global Surveyor (MGS) Thermal Emission Spectrometer (TES) [2, 3], Mars Orbital Laser Altimeter (MOLA) [4] and Viking Infrared Thermal Mapper (IRTM) [5] indicate that cold spots are a combination of surface deposits of CO_2 atmospheric condensates and active CO_2 snow storms [2].

This study focuses on differences found between cold spots in the southern hemisphere and the northern hemisphere. We also examined the effects that the 2001 global dust storm had on cold spot formation and activity in both hemispheres. The global dust storm had a significant effect on cold spots in the northern hemisphere [6] and may have also influenced southern hemispheric cold spots.

Data: Three Mars years of data from MGS TES were used in this study. Observations were divided into polar ring data (latitudes 86° to 87.2°) and "cold spot only" data, where bolometer brightness temperatures less than 135 K were used. Due to the high-frequency of repeat coverage, polar ring data were used to obtain accurate size and half-life estimations of cold spots. "Cold spot only" data were used to evaluate seasonal and spatial distributions of cold spots outside the polar ring.

Analysis techniques: We used data from the TES database and a brightness temperature difference between 18μm and 25μm (T_{18}-T_{25}) to analyze the spatial and temporal characteristics of cold spots [2]. Values are obtained by fitting TES data to a two dimensional spatial Gaussian convolved with a temporal exponential decay. These fits provide estimates for both radius and amplitude (intensity) of a cold spot.

Results:

Polar ring cold spot activity in the northern and southern hemispheres. In the South Polar Ring, cold spot activity is restricted to the perennial cap. Since the perennial cap is not centered at the geographic pole, the south polar ring exhibits less cold spot activity than the north by an average of 25 cold spots per year. Cold spots that formed in relation to topography (topographic cold spots), possibly by orographic lifting [7] or gravity waves [8, 9] were not as common on the southern perennial cap as cold spots independent from topographic features (non-topographic cold spots). In the north, topographic cold spot activity was more abundant than non-topographic activity [6]. Cold spot amplitudes varied considerably from year to year in the South Polar Ring, whereas in the North Polar Ring, cold spots averaged 23° C (Fig. 1). In general, South Polar Ring topographic cold spot half-lives were comparable to those in the north [6]. Non-topographic cold spot half-lives were shorter by an average of 1.5 Julian days in the South Polar Ring. North Polar Ring cold spots were usually larger than South Polar Ring cold spots [6].

"Cold spot only" cold spot activity in the northern and southern hemispheres . Cold spots outside the polar night in the south were more common than in the north. The majority of cold spots in both hemispheres formed within the polar night [6]. Cold spots frequently recurred in the same place every year for both the northern and southern hemispheres. Recurring cold spots were often linked to prominent topographic features, such as craters, the "Mountains of Mitchel", and areas of deeply dissected terrain.

Effects of the 2001 global dust storm. The global dust storm of MY 25 occurred between L_s 180° and 270°, and significantly affected North Polar Ring cold spots (Fig. 1). During the storm in the North Polar Ring, topographic cold spot activity decreased, while non-topographic cold spot activity increased [6]. Radii for both topographic and non-topographic cold spots increased. Non-topographic amplitudes decreased and half-lives increased. Topographic cold spot amplitudes increased and their half-lives changed very little. Outside the North Polar Ring, cold spot activity decreased southward of 65°N latitude, but increased in frequency at higher latitudes, which is similar to the observations made by Forget et al. [5].

In the southern hemisphere, the global dust storm occurred during the spring, which resulted in a more subtle effect on cold spot formation. Prior to the storm (MY 25), topographic activity increased and topographic cold spots increased in

size and amplitude. Non-topographic cold spots decreased in size, but increased in amplitude. In addition, topographic and non-topographic cold spot half-lives were shorter in MY 25. Following the storm (MY 26), the majority of cold spots increased in size. Average amplitudes for all cold spots continued to rise and half-lives doubled for both topographic and non-topographic cold spots. Cold spots outside the polar ring the year prior to and the autumn following the dust storm decreased in number and did not form north of 62°S latitude.

Significance: The most prominent difference between North and South Polar Ring cold spots is their half-life and size. These differences might be due to a difference in elevation between the two hemispheres. Outside the Polar Ring, southern cold spots were more frequent than those in the north. In the north, cold spots outside the polar ring were closely tied to topography [6]. The ancient cratered terrain in the southern hemisphere could explain the increased southern cold spot activity.

The variations in cold spot behavior for the northern and southern hemispheres during MY 25 and MY 26 can be attributed to the effects of the global dust storm of 2001. These changes could be due to a blockage of sunlight caused by suspended dust particles in the atmosphere.

References: [1] Kieffer H. H., T. Z. Martin, S. C. Chase, E. D. Miner, F. D. Palluconi, G. Muench, and G. Neugebauer (1976), Infrared thermal mapping of the Martian surface and atmosphere: First results, *Science*, 193, 780-786. [2] Titus, T. N., H. H. Kieffer, K. F. Mullins, and P. R. Christensen (2001), TES premapping data: Slab ice and snow flurries in the Martian north polar night, *J. Geophys. Res.*, 106, 23,181-23,196. [3] Hansen, G. B. (1997), The infrared absorption of carbon dioxide ice from 1.8 to 333 μm, *J. Geophys. Res.*, 102, 21,569-21,587. [4] Ivanov, A. B., and D. O. Muhleman (2001), Cloud reflection observations: Results from the Mars Orbiter Laser Altimeter, *Icarus*, 154, 190-206. [5] Forget, F., G. B. Hansen, and J. B. Pollack (1995), Low brightness temperatures of Martian polar caps: CO_2 clouds or low surface emissivity?, J. Geophys. Res., 100, 21,219-21,234. [6] C. Cornwall and T. N. Titus (2009), Spatial and temporal distributions of Martian north polar cold spots before, during, and after the global dust storm of 2001, *J. Geophys. Res.*, 114, E02003, doi:10.1029/2008JE003243. [7] Forget, F., F. Hourdin, and O. Talagrand (1998), CO_2 snowfall on Mars: Simulation with a general circulation model, *Icarus*, 131, 302-316. [8] Colaprete, A., O. Toon (2002), Carbon dioxide snowstorms during the polar night on Mars, *J. Geophys. Res.*, 107, 5051-5066. [9] Tobie, G., F. Forget, and F. Lott (2003), Numerical simulation of the winter polar wave clouds observed by Mars Global Surveyor Mars Orbiter Laser Altimeter, Icarus, 164, 33-49.

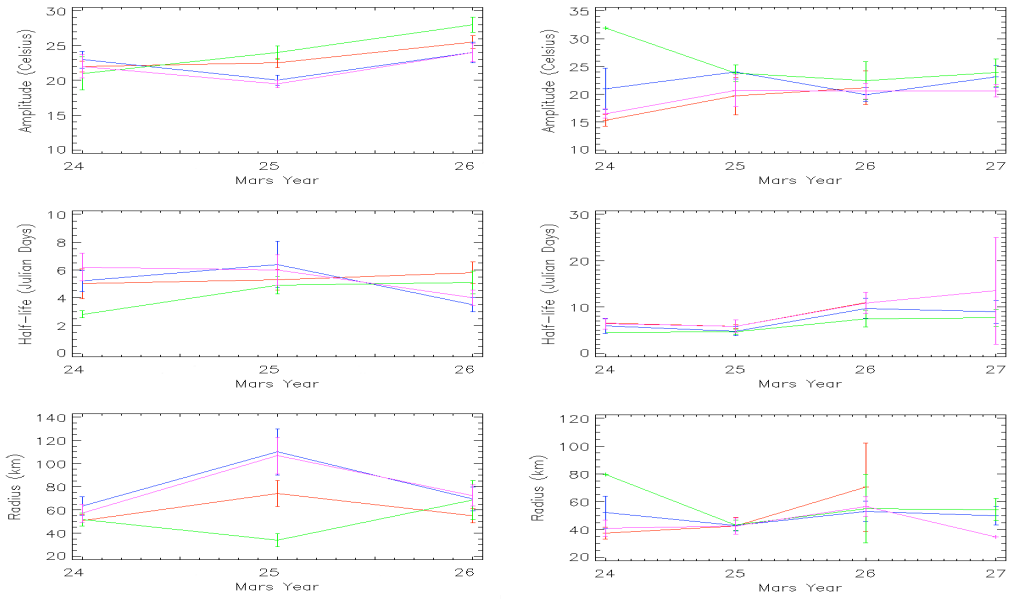

Figure 1. Plot averages for amplitude, half-life, and radius for Mars Years 24-27 with standard deviation. Left column depicts the values for the North Polar Ring cold spots and the right column displays values for the South Polar Ring cold spots. Topographic cold spots are graphed as red lines; non-topographic, blue; isolated activity (where there was no neighboring cold spot activity), green; and local activity (where cold spots occurred in small clusters), violet.

PHYSICAL STATE OF THE "BRIGHT" SOUTH SEASONAL POLAR CAP FROM OMEGA OBSERVATIONS. S. Doute[1], F. Schmidt[2,1], B. Schmitt[1], M. Vincendon[3,4], Y. Langevin[4], B. Gondet[4], [1]*Laboratoire de Planetologie de Grenoble Bat D de Physique B.P. 53 Grenoble Cedex 09 France sylvain.doute@obs.ujf-grenoble.fr*, [2]*European Space Astronomy Centre (ESAC), P.O. Box - Apdo. de correos 78, 28691 Villanueva de la Canada, Madrid, Spain*, [3]*Department of Geological Sciences, Brown University, Providence, Rhode Island, 02912, U. S. A.* , [4]*Institut d'Astrophysique Spatiale, CNRS / Universite Paris XI, Orsay Campus, 91405, France*.

Introduction The composition, physical state and texture of the South Seasonal Polar Cap (SSPC) have important consequences on energy balance. The imaging spectrometer OMEGA on board Mars Express has acquired the most comprehensive set of observations to date in the near-infrared (0.93-5.1 microns) on the SSPC from mid-winter solstice (Ls=110° , December 2004) to the end of the recession at Ls=320° (November 2005) [1]. The time resolution is 3 days to one month and the spatial resolution ranges from 700m to 10 km/pixel. The spectral range covered by OMEGA is particularly relevant for our studies since it samples numerous absorption bands distinctive of CO2 and H2O in their solid state. [1] showed that, during southern spring and summer, there is a very complex evolution in terms of effective grain size of CO2 ice and contamination by dust or H2O ice. H2O ice does not play a significant role except close to the end of the recession. [2] systematically segmented the South Seasonal Polar Cap into different spectral units and tested diverse surface representations by the modeling of spectral end-members and average unit spectra. Here we focus on the "bright" part of the SSPC corresponding to spectral unit SSPC1 (I.b of [1]). Regions belonging to this unit have a very bright albedo ($\approx$ 0.6-0.8) associated with strong CO2 ice absorption features. According to [1] such characteristics are compatible with granular CO2 deposits with grain size in the range of 5 cm implying an extremely low contamination by dust and water ice. Furthermore, from their study of a representative region at 34° E, 76° S, the albedo increases from Ls=223° up to a maximum at Ls=240° and then decreases until total disappearance of the ice. The albedo increase would require a decrease of grain size if the granular model is really relevant. However the mean free path within CO2 ice as well as its thermodynamic behavior would rather favor a porous CO2 slab model [3]. Then strong photometric effects could be expected that could explain the brightening. In this paper we propose to further study the physical state of the "bright" part of the SSPC and its evolution by monitoring two reference regions from Ls 223° to 260° of martian year 27.

Observations Regions 1 ($\approx 6000\mathrm{km}^2$) and 2 ($\approx 9900\mathrm{km}^2$) are centered at 77°40′S 53°15′W and 79°25′S 136°22′W respectively. They were observed by OMEGA 28 and 32 times respectively during the selected time period. From the original spectral cubes, we extract the spectra falling in each region as well as the corresponding auxiliary data: incidence, emergence and phase angles as well as the solar longitude Ls. Accurate characterization of surface icy materials requires the modeling and the correction of the atmospheric (gas and aerosols) spectral effects. Thus we use efficient radiative transfer algorithms and methods tailor-made for operational use in order to retrieve Mars surface reflectance [4]. A line-by-line radiative transfer model which is fed by the vertical compositional and thermal profiles predicted by the European Mars Climate Database (EMCD) calculates the gaseous spectral transmission. The system that removes the aerosol effects uses radiative properties and maps of total column optical depth evaluated by [5] for the aerosols over large portions of the SSPC.

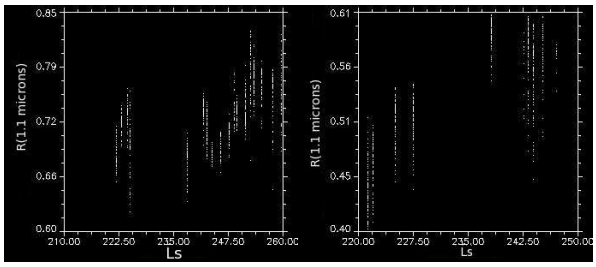

FIG. 1 – *Scatter plots of reflectance at 1.1 μm versus solar longitude. Left: region1, right: region 2.*

Photometric and spectral trends We conducted our analysis according to three dimensions that are sampled by the observations: spectral, angular and temporal.

Note that time and acquisition geometry are correlated since solar incidence increases with time as we progress into spring. Excursion of the emergence angle is quite limited, often close to a few degrees, never higher than $\approx$ 20 °. As a consequence, incidence and phase angles are in comparable range, [55°,80°] and [57°,75°] for region 1 and 2 respectively. Previous calculations with a dedicated spectral reflectance model [2] showed that, with a rough CO2 slab, an increase of surface reflectance with a decreasing solar incidence is to be expected if the mean slope is sufficient ($\gtrsim 8°$). The relative enhancement factor is much higher deep into the saturated 2.64 μm CO2 absorption band than in continuum at 1.1 μm. Unfortunately the former channel is dominated by the aerosol scattering and deconvolution of the slab and aerosol effects is extremely difficult. Whereas region 2 exhibits in the continuum at 1.1 μm a broad trend compatible with the slab model, no such behavior is observed for region 1. Similarly no clear correlation emerges with the emergence nor the azimuth angle. At contrary (Fig. 1) we note a clear evolution of the surface reflectance at 1.1 μm with time for both regions. From Ls=223° the reflectance rises steadily to reach a maximum at Ls=252° for region 1 and Ls=240° for region 2 with a 13% and 30% relative increase respectively. Then we see the beginning of a decline.

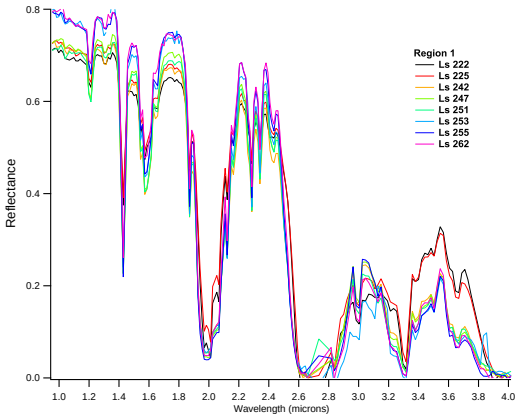

FIG. 2 – *Spectral evolution of region 1*

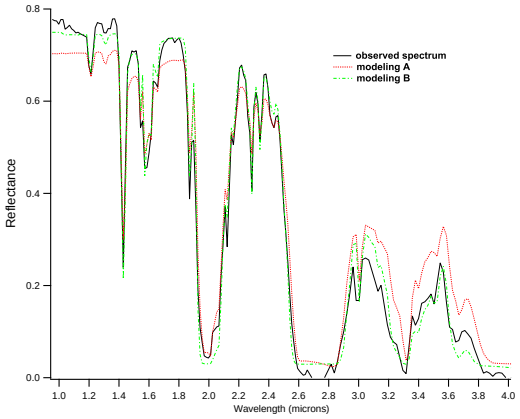

FIG. 3 – *Comparing two modelings of a representative spectrum of region 1*

The temporal evolution of the continuum level is accompanied by a joint transformation of the spectral morphology as illustrated by Fig. 2. The 2 μm CO2 absorption band progressively saturates whereas the band depth of the 2.28 and 2.34 μm features increases strongly. These changes suggest that the mean free path of photons within the ice also lengthens very significantly.

Modeling and discussion In order to understand the physical meaning of the trend affecting the spectral reflectance and, possibly, to discriminate between a granular and compact superficial texture of the icy deposits we test two models:(A) an optically thick layer of granular CO2 ice contaminated by dust and water [6] (B) a substratum composed of a similar granular

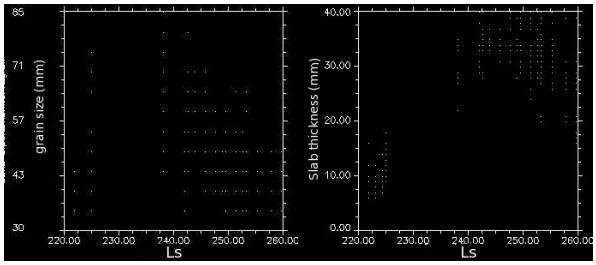

FIG. 4 – *Temporal evolution of the main physical parameter of models A and B*

mixture but overlaid by an extremely compact ($\approx$ 0.02 % of porosity) and rough CO2 slab [2]. Databases of OMEGA synthetic spectra are generated accordingly by a radiative transfer model simulating the reflection of solar light. Then we use the GRSIR method [7] based on these databases and statistics to evaluate quantitatively the physical parameters associated to both models from the observed spectra. Model (A) describes CO2 ice as contaminated by dust at the level of $\approx$ 0.01 wt% with $\approx$ 4 cm (region1) and $\approx$ 12 cm (region2) grains in diameter. Model (B) requires the presence of a compact slab in the upper 1 to 4 centimeters of the deposits, the rest being grains $\approx$ 8 mm in diameter. Fig. 3 exemplifies that it is more difficult with model (A) than with model (B) to reconcile the increase of albedo conjointly with an enhancement of the CO2 band depths at 1.43, 1.59, 2.28 and 2.34 μm. Model (A) gives a 2 μm band saturation that is often more realistic but this is the only spectral feature for which it is in better position. Furthermore scatter plots of retrieved slab thickness LCO2 and grain size DCO2 against Ls for hundred of observed spectra show a more regular and less dispersed evolutionary path for model B than for model A (Fig. 4). Finally LCO2 increases with time whereas DCO2 decreases so that model (B) alone supports the observed lengthening of photon path within CO2 ice.

Conclusion A spectral study of two representative regions of the "bright" south seasonal polar cap in the range Ls 220 to 260° suggests that the upper 1 to 4 centimeters of the CO2 deposits form a slab of very compact ice. The slab thickness increases with time until CO2 ice demise. Increase of albedo due to a decreasing dust contamination first comes with this evolution, before the appearance of ice-free patches within the pixels that reverses the trend. Existence of the slab implies strong photometric and radiative effects. We have not be able to detect unambiguously the former, likely because the range of phase angles covered by our selected observations is too limited.

References

[1] Langevin, Y., et al., 2007, *J. Geophys. Res.*, **112**, .

[2] Douté, S., et al., 2008, in *Lunar and Planetary Institute Science Conference Abstracts*, vol. 39 of *Lunar and Planetary Institute Science Conference Abstracts*, 1736–+.

[3] Eluszkiewicz, et al., 2005, *Icarus*, **174**, 524.

[4] Douté, S., et al., 2007, in *Lunar and Planetary Institute Conference Abstracts*, vol. 38 of *Lunar and Planetary Institute Conference Abstracts*, 1836–+.

[5] Vincendon, M., et al., 2008, *Icarus*, **196**, 488.

[6] Doute, S., et al., 2007, *Planetary and Space Science*, **55**(1-2), 113.

[7] Bernard-Michel, et al., 2009, *J. of Geophys. Res.*, **in press**.

CURRENT STATUS OF ATMOSPHERIC AND SURFACE RETRIEVALS IN THE MARS POLAR REGIONS. J. Eluszkiewicz and the AER Team[1], [1]Atmospheric and Environmental Research, Inc., 131 Hartwell Ave., Lexington, MA 02421, jel@aer.com.

Introduction: The Mars polar regions and the global atmospheric circulation are intimately coupled through the CO_2 condensation/sublimation cycle driven by the polar energy balance [1-4]. The caps and the atmosphere also interact on the regional scale [5]. Signatures of these interactions may be expected in the surface and atmospheric properties retrieved from remote sensing observations, but polar retrievals to-date have been somewhat limited in scope. For example, the opacity product in the Planetary Data System (PDS) retrieved from Thermal Emission Spectrometer (TES) radiances is essentially non-existent when the surface temperature drops below about 220 K. This is principally due to the generally small thermal contrast between the atmosphere and the surface, particularly in situations when the surface has near-black-body emissivities [6]. This limitation has been addressed through a modification of the TES opacity retrievals [7], but this modification does not attempt a simultaneous retrieval of atmospheric temperatures, relying instead on the PDS profiles [8]. The latter have been obtained without specifically accounting for either dust or the polar surface emissivities (which are often very different from the non-polar emissivities) and they exhibit little vertical structure (see below). Surface emissivities are also not reported in the retrievals performed from the Planetary Fourier Spectrometer (PFS) data [9]. Polar atmospheric retrievals from the Mars Climate Sounder (MCS) limb radiances are emerging [10], but with a scarcity of concurrent surface observations and without a scattering parameterization.

Simultaneous Atmospheric/Surface Retrievals: In a pilot study [11], we performed simultaneous atmospheric and surface retrievals on a limited number of TES spectra in the northern polar ring data around 87°N during fall and winter. The retrieved quantities were atmospheric temperatures, spectral surface emissivities, and optical depths of atmospheric water ice and dust. For the atmospheric particulates, we ignored scattering, instead using their spectral absorption coefficients available from the PDS [6] and retrieving their optical depth. The impact of neglecting scattering is, in general, not large. For the small dust and ice optical depths we retrieve, the differences between non-scattering radiances and radiances computed using the scattering version of our radiative transfer code [12] are, on average, within the instrument noise level.

Figure 1 shows the atmospheric temperature profiles retrieved for locations characterized by near-unity emissivities ("low-BD_{25}" [13], panel *a*) and the so-called "cold spots" ("high-BD_{25}") where emissivities are significantly lower than unity (panel *b*). Since cold spots are usually attributed to the occurrence of snowfall [5, 13-18], it is encouraging to see that the associated temperature profiles do fall below the CO_2 condensation line (plotted in green in Figure 1) more often than in the "low-BD_{25}" locations (where the CO_2 frost is likely to form directly on the ground). The supersaturated region in Figure 1 is confined to the lowest 20 km, consistent with the altitude range of previous detections of CO_2 clouds [19, 20].

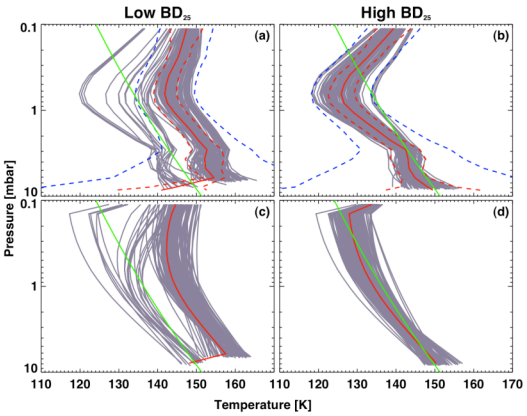

Figure 1: (*a*) and (*b*): Atmospheric temperature profiles retrieved using AER's algorithm for the low and high BD_{25} spectra. (*c*) and (*d*) Their PDS counterparts. The solid red lines represent the mean retrieved profile in each case, while the green lines represent the profile of the CO_2 condensation temperature. For our profiles, the dashed blue and red lines represent *a priori* and *a posteriori* errors, respectively, around the mean profile.

The shape of our retrieved profiles in Figure 1 exhibits a warming between 1 and 0.1 mbar. While the reality of this shape is somewhat questionable, given the limited number of degrees of freedom and a very coarse vertical resolution [11], the small *a posteriori* errors in this altitude region indicate that the warming is real. The qualitative aspects of the shape in our temperature profiles around 1 mbar are consistent with the newest GCM runs that take into account interplays between cloud microphysics, convection, and large-scale dynamics [21]. Furthermore, the polar warming has also been detected in the PFS and MCS retrievals [9, 10], albeit without evidence of supersaturation and at somewhat greater heights (0.1 vs. 1 mbar).

For comparison, in panels (*c*) and (*d*) of Figure 1 we show the corresponding TES temperature profiles available from the PDS. As in our retrievals, the PDS profiles are generally colder for high-BD_{25} locations,

but are significantly more linear above 1 mbar, particularly over the cold spots.

Of particular interest to the polar energy balance studies are the retrieved surface emissivities, shown in Figure 2. As expected, for the cold spots the emissivities do deviate significantly from unity in the 25-micron (400 cm^{-1}) "transparency band" of solid CO_2 [22] and their spectral shape is qualitatively consistent with simulated snow emissivities [16]. In contrast, for the low-BD_{25} spectra, the retrieved emissivities are flat, but significantly less than unity (0.8-0.9), which is not supported by modeling. The cause of these spectrally uniform deviations from blackbody behavior remains to be investigated, but they might be caused by systematic errors not accounted for in our retrieval (with a zero-radiance-level correction applied to the TES spectra [13], the retrieved emissivities are somewhat closer to unity [11]). In any case, a comparison between the magnitudes of the *a priori* and *a posteriori* errors in Figure 2 reveals that there is enough information in the TES radiances to reduce the *a priori* errors on surface emissivity significantly. Furthermore, the estimated number of degrees of freedom is unity at each emissivity spectral point within the range shown in Figure 2, underscoring the ability of the retrieval to "move away" from the *a priori*. The retrieved dust opacities are generally low [11], consistent with the "flushing" of the wintertime polar atmosphere by precipitating snow, with a hint of lower opacities in the high-BD_{25} case (suggesting more active flushing in the putative snowfall locations).

Future Plans: We plan to extend the study described in [11] to a comprehensive sample of TES polar measurements and establish the reasons for the AER/PDS differences via a detailed intercomparison of the respective retrieval algorithms (the PDS algorithm has been kindly provided by Michael Smith). We will attempt to remove the remaining artificial deviations from blackbody behavior by retrieving empirical correction factors necessary to yield blackbody emissivities while constraining T_{skin} to be close to T_{frost} and fitting these factors using the correction software developed by Joshua Bandfield. The retrieved cap emissivities will be compared with frost emissivity models [13, 16, 23] and their (and the associated atmospheric temperatures') spatial distribution and evolution used to provide insights on the frost formation mechanisms. The development of a limb-scattering code for Mars is also underway [24] and this will enable a quantitative assessment of scattering effects on the limb retrievals. Eventually, the new retrievals (both polar and non-polar) will be utilized in the Mars Data Assimilation System being developed at the University of Maryland.

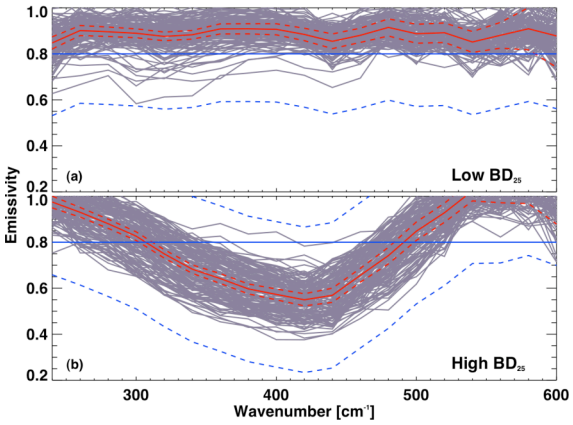

Figure 2: Seasonal cap emissivities retrieved from TES spectra. The red solid and dashed lines represent the mean retrieved emissivity and its *a posteriori* errors and the blue solid and dashed lines represent the *a priori* emissivity and its errors.

Acknowledgements: The extensive contributions of my AER colleagues are gratefully acknowledged. The adaptation of our retrievals to Mars has been supported by the NASA Mars Fundamental Research and Mars Data Analysis Programs.

References: [1] Leighton R. R. and B. C. Murray (1966) *Science, 153,* 136. [2] Paige D. A. and A. P. Ingersoll (1985) *Science, 228,* 1160. [3] Pollack J. B. et al. (1990) *J. Geophys. Res., 95,* 1447. [4] Forget F. et al. (1998) *Icarus, 131,* 302. [5] Colaprete A. et al. (2005) *Nature, 435,* 184. [6] Smith M. D. (2004) *Icarus*, *167,* 148. [7] Horne D. and M. D. Smith (2009) *Icarus, 200,* 118. [8] Conrath B. J. et al. (2000) *J. Geophys. Res., 105,* 9,509. [9] Giuranna M. et al. (2008) *Icarus, 197,* 386. [10] McCleese D. J. et al. (2008) *Nature Geoscience, 1,* 745. [11] Eluszkiewicz J. et al. (2008) *J. Geophys. Res., 113,* E10010, doi:10.1029/2008JE003120. [12] Moncet J.-L. et al. (2008) *J. Atmos. Sci., 65,* 3917. [13] Kieffer H. H. et al. (2000) *J. Geophys. Res., 105,* 9653. [14] Eluszkiewicz J. (1993) *Icarus, 103,* 43. [15] Titus T. N. et al. (2001) *J. Geophys. Res., 106,* 23,181. [16] Eluszkiewicz J. et al. (2005) *Icarus, 174,* 524. [17] Langevin Y. et al. (2006) *Nature, 442,* 790. [18] Cornwall C. and T. N. Titus (2009) *J. Geophys. Res., 114,* E02003, doi:10.1029/2008JE003243. [19] Pettengil G. H. and P. G. Ford (2000) *Geophys. Res. Lett., 27,* 609. [20] Ivanov A. B. and D. O. Muhleman (2001) *Icarus, 154,* 190. [21] Colaprete A. et al. (2008) *Planet. Space Sci., 56,* 150. [22] Hansen G. B. (1997) *J. Geophys. Res., 102,* 21,569. [23] Hansen G. B. (1999) *J. Geophys. Res., 104,* 16,471. [24] Eluszkiewicz et al. (2008) The Mars Atmosphere: Modeling and Observations, Williamsburg, VA, abstract # 9031.

NON CONDENSABLE GAS ENRICHMENT AND DEPLETION IN THE MARTIAN POLAR REGIONS.

François Forget[1], Ehouarn Millour[1], Luca Montabone[1] and Franck Lefevre[2]. [1]Laboratoire de Météorologie Dynamique, Université Paris 6, BP 99, 75005 Paris, FRANCE (forget@lmd.jussieu.fr), [2]LATMOS, Paris, FRANCE

Introduction

The condensation of 30% of the Martian atmosphere every year induces large surface pressure variations all over the planet. However, while carbon dioxide condenses onto the surface to form CO_2 ice, the 5% of non-condensible gases that form the martian atmosphere (mostly N_2, Ar, O_2, or CO) is left in the atmosphere. This process is well observed by the Gamma Ray Spectrometer (GRS) [1,2] aboard Mars Oddyssey, but has also been detected by monitoring CO using the imaging spectrometer OMEGA on Mars Express [3] or CRISM on Mars Reconnaissance Orbiter [4].

. Sprague et al. [1, 2] showed that the mean Argon mixing ratio in the south polar region is enhanced by as much as a factor of 6 during winter. That means that the air composition strongly vary with location and season and that non-condensible gases makes up to 30% of the bulk southern polar atmosphere around winter solstice (and probably much more locally) compare to about 5% on average.

Parametrisation in the LMD Mars General Circulation Model

We have developped a detailed parametrisation of this effect in our Mars General Circulation Model. The LMD GCM [5] includes a dedicated parametrisation of the CO2 cycle and its condensation in the polar caps and clouds [6,7]. Modelling the non-condensible gases enrichment in a 3D atmospheric models using terrain-following vertical coordinates (i.e. "sigma" or "hybrid" coordinate) requires a specific algorithm that is detailed in [8]. It is completed with a modified convection sheme able to simulate the convection forced by the enrichment of lighter gas near the surface.

Some results

Our simulations (figures 1 and 2) predict a polar night atmosphere where non-condensable gas such as argon are highly enriched near the surface. This occurs in spite of the various mixing mechanism that are taken into account.

Comparison with Ar observations (figure 1)

In the **north polar region**, the simulation seems to be realistic, with a very limited enrichment around Ls=270^o The seasonal evolution is in acceptable agreement with the Argon observation [1,2]

In the **south polar region**, our preliminary results seems to match the GRS observations from Sprague et al. (2004, 2007) poleward of 75^{o}S. Interestingly The double peaked seasonal evolution (two maxima around Ls=80^o and Ls=170^o) predicted by the model is not seen in the observations. However, it is not observed in all our simulations. More interestingly, a detailed analysis reveals that our simulations disagree with Sprague et al.'s quantitative measurements. In order to calibrate their Argon retrieval, these authors used Viking Lander 2 GCMS measurements. On this basis, they showed that Argon is severely enriched in the polar nigh by a factor of 6, but only slightly depleted in the summer. In our simulation, we also find a factor of 6 difference between southern summer and winter, but it is enriched by a factor of 3 to 4 in the polar nigh and depleted by a factor of 3 in summer. This is in good agreement with the available CO observations as well as with the Mars Exploration Rover APXS Ar observations (see below). To reconcile these datasets and our modeling results, we suggest to alter 30-40% the absolute « calibration » of Argons.

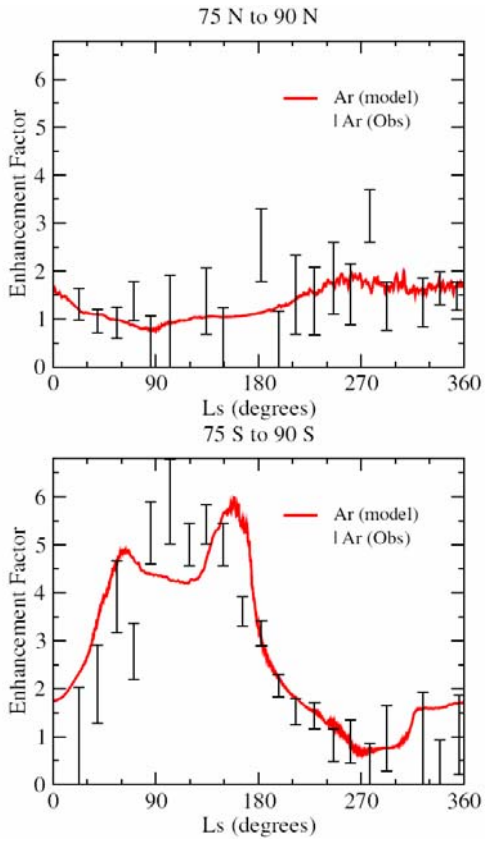

Figure 1: Seasonal evolution of the mean argon column estimation of the atmospheric temperature in the southabundance in both polar regions (from 75 latitude to the ern polar night (compared to radio occultation or therpole) compared to the Argon abundance measured by the Gamma Ray Spectrometer (GRS) aboard Mars Oddyssey from June 2002 to March 2004 (Sprague et al. 2004,). The abundance are normalized and shown as an enhancement factor over

what is expected from an homogeneously mixed atmosphere (see Sprague et al. 2007).

Comparison with CO observations. Figure 2 shows a comparison between CRISM CO observations [4] and the prediction with the GCM. Unfortunately, no data are available in the polar night. Nevertheless, enhancement related to the polar night condensations and CO depletion due to the CO2 sublimation are well observed and modeled.

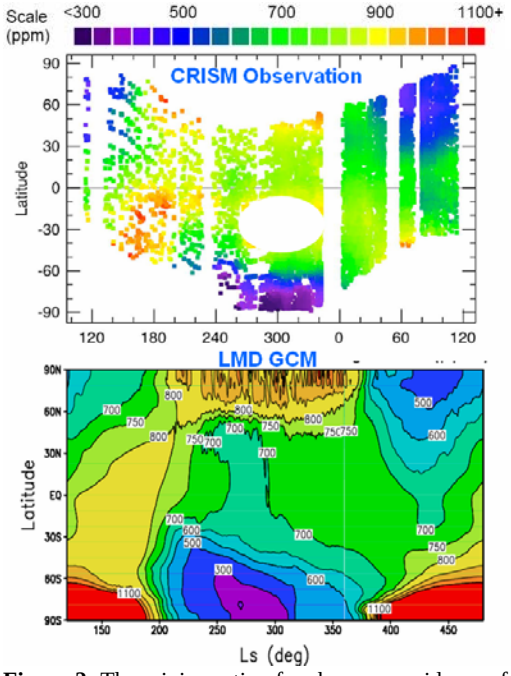

Figure 2: The mixing ratio of carbon monoxide as a function of season (Ls) and latitude as observed by CRISM during Mars Years 28 and 29 [4] compared to the GCM prediction. The local maximum observed near Ls=300 is hidden to facilitate the comparison since it is an artifact due to a planet-encircling dust storm [4]

Comparison with the APXS observations. Using the APXS on board the Opportunity rover on MER mission, Econmou et al. [9] have been able to measure the argon density variation in the martian atmosphere as a function of seasons. It is characterized by a detectable oscillation which is very well predicted by the GCM. If Argon was enriched by a factor of 6 in the polar night, that means that at least during the first part of the winter all the Argon going in the southern polar regions would be trapped there [2]. Consequently the Argon mixing ratio at the MER latitude should not vary, whereas variations are then detected...

Impact of the non-condensible gas enrichment on the polar cap energy balance.

The local depletion of CO_2 in the polar night strongly reduces the partial pressure of CO_2, decreasing the CO_2 frost point temperature by several kelvins, and the surface thermal infrared cooling decreased by a few %. This can be simulated in the model (Figure 3)

In addition, the winter winter martian atmosphere is characterized by a significant latitudinal gradient of molecular weight through a deep layer at the edge of the polar vortex. Meteorologists have never needed to consider such gradients, and a closer analog would be a gradient of salinity in oceanography. In practice, the enrichment observed around winter solstice would have an effect on the circulation as large as a 13 K temperature horizontal gradient (as used in the traditional thermal wind equation, for instance). The gradient should tend to reduce the intensity of the polar vortex, and favor the transport of non-condensible gas outside the polar region, acting as a negative feedback. This effect, however, will be quite difficult to simulate in a GCM.

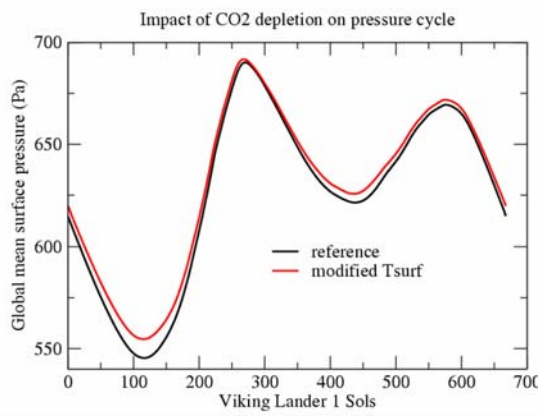

Figure 3. The impact of the CO2 depletion and enrichment on the global CO2 cycle resulting from its impact on the CO2 cap energy balance due to the modification of the CO2 frost point temperature

Reference

[1] Sprague et al. Science, Volume 306, Issue 5700, pp. 1364-1367 (2004)

[2] Sprague et al. J. Geophys. Res., 112, E03S02, doi:10.1029/2005JE002597 (2007)

[3] Encrenaz et al., A&A 459, 265-270 (2006)

[4] Smith et al., JGR, in press (2009)

[5] Forget et al. JGR. 104 , 24,155-24,176 (1999)

[6] Forget et al. Icarus, Volume 131, Issue 2, pp. 302-316. (1998)

[7] Millour et al., this issue.

[8] Forget et al. abstract at the 3rd workshop on "Mars Atmosphere: Modeling And Observations" , Williamsburg, 2008. Available on : http://www.lpi.usra.edu/meetings/modeling2008/pdf/9106.pdf

[9] Economou et al. abstract at the 3rd workshop on "Mars Atmosphere: Modeling And Observations" , Williamsburg, 2008

DARK SPOT AND DARK FLOW DEVELOPMENT DURING THE SEASONAL FROST RETREAT ON THE RUSSELL CRATER MEGADUNE, MARS E. Gardin[1], C. Quantin[1], P. Allemand[1] and P. Thollot[1], Laboratoire des Sciences de la Terre, Université de Lyon, Ecole Normale Supérieure de Lyon, Université Claude Bernard Lyon 1, CNRS, France, Bat Géode, 43 bd du 11 Novembre, 69622 Villeurbanne cedex, France (emilie.gardin@univ-lyon1.fr)

Introduction: Defrosting features have been observed on the megadune of Russell Crater (54.6°S; 12.4°E). Throughout spring, the south polar CO_2 cap retreats and leads to dalmatian spots named dark spots [1], spiders [2], fans [3] and polygonal crack patterns [4]. [5] proposed a semi-quantitative model to explain all of these processes. The dark spots, fans and spiders are probably formed by the venting of sub-ice CO_2 gas under pressure. This model implies a pure CO_2 ice slab and solar rays responsible for heating and defrosting the lower part of the ice slab by translucency [5].

The high resolution images of Russell Crater, first by MOC, and then by HiRiSE, display features never observed further north in the southern hemisphere. Some south-facing scarps in middle latitudes are partly frosted during the local winter and are able to record the defrosting sequence during the spring retreat. This is the case in Russell Crater, a large crater of the southern hemisphere with a large dune field in its center. The aim of this work is to describe the active features produced by the defrosting on the megadune of Russell Crater and to discuss the possible mechanisms that are responsible for these features.

Data set: MRO (Mars Reconnaissance Orbiter) targeted HiRiSE images acquired at different times throughout the two acquisition years over Russell Crater megadune. We studied the HiRiSE images and described our observations throughout the defrosting period (Table 1).

Season	HiRiSE	Ls	res.(cm/px)	Low d.s	Up d.s	D.f	Polygons	D.D
Winter	PSP_1440_1255	136.3°	50					
	PSP_1981_1255	157.7°	50					
	PSP_2337_1255	172.6°	25					
	PSP_2482_1255	178.9°	25					
Spring	PSP_2548_1255	181.8°	25					
	PSP_2904_1255	197.9°	25					
	PSP_3326_1255	217.7°	25					
	PSP_3748_1255	238.4°	25					
	PSP_4038_1255	252.7°	25					
	PSP_4249_1255	263.1°	25					
Summer	PSP_5238_1255	310.3°	25					
	PSP_5383_1255	316.8°	25					
Autumn	PSP_6873_1255	17.2°	50					
	PSP_7018_1255	22.5°	25					
	PSP_7229_1255	30.1°	50					
Winter	PSP_9879_1255	122.2°	100					
	PSP_10090_1255	130.1°	100					
	PSP_10301_1255	138.1°	100					
	PSP_10446_1255	143.7°	50					
	PSP_10868_1255	160.6°	50					
Spring	PSP_11580_1255	191.5°	50					

Table 1: List of processed HiRiSE images on the Russell Crater megadune (54.6°S and 12.4°E) with their local season time, solar longitude (Ls) and spatial resolution of acquisition in cm/px. The vertical bars symbolize evidence of the observing features. "Low d.s": dark spots, which appear in the lower part of the megadune's slope. "Up d.s": dark spots located in the upper part of the megadune and on the plateau. "D.f": dark flows located in the upper part of the megadune. "Polygons": evidence near the brink of the megadune. "D.D": occurrence of dust devil tracks on the megadune.

Regional context: Russell is a 134 km diameter crater located to the west of Hellas Basin (fig. 2). This crater hosts a 1,704 km^2 dune field with an unusual megadune on its north-eastern boundary. This megadune, visible on MOLA data is around 500 m high and is highly studied because its south-facing scarp displays gullies [6-7-8]. The south-facing slope of the asymmetric megadune is steep with an average slope of 30°. Many ripples (1-3 m in height) are present all over the slope.

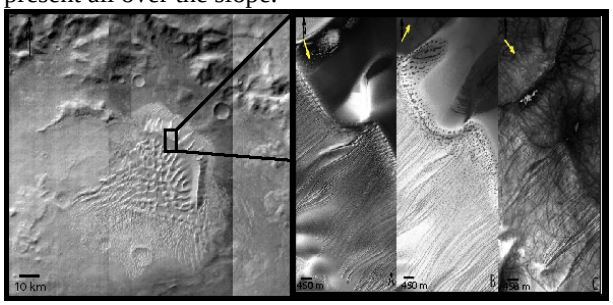

Figure 2: On the left: Mosaic of THEMIS IR images of the Russell Crater dune field. On the right: HiRiSE images of the south-facing megadune's slope during the defrosting season. A: Ls 158°, B: Ls 182° and C: Ls 215°. Yellow arrows are the solar incidence angles.

Distribution of defrosting features: At the beginning of the defrosting sequence, several features appear over the Russell Crater megadune and are visible on many HiRiSE images. During the early winter, we observe polygonal structures in the upper part of the alcoves forming the submittal part of the south-facing slope of the megadune. These polygonal structures are only visible between Ls 122.2° and Ls 130.1°.

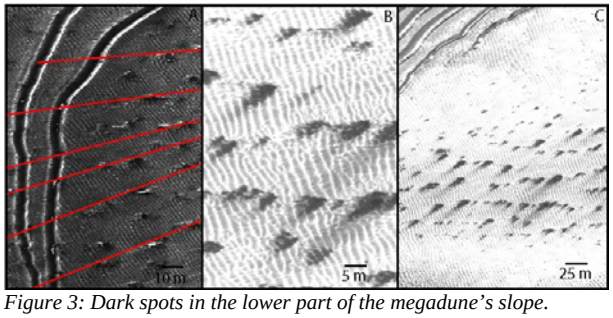

Figure 3: Dark spots in the lower part of the megadune's slope.
A: Dark spots are aligned and independent of the gullies' location.
B: Dark spots and their dust tracks.
C: Alignment of dark spots and dust that has been blown by the wind.

From Ls 130°, dark spots appear in the lower part of the megadune with diameters between 5 and 10 m. At full spatial resolution they seem to be aligned and independent of the gullies' presence (fig. 3A). They

appear as diffuse patches (fig.3 B-C), where the dust has been blown by the wind. Throughout the season, the dark spots grow reaching diameters up to 25 m. From Ls 143.7°, the dark spots also develop in the submittal part of the megadune (Table 1). The distribution of these dark spots follows lines parallel to the iso-elevations in the slope whereas on the plateau, the dark spots distribute perpendicular to the brink (fig. 4). On the upper part of the megadune's slope the dark spots appear on up-facing scarps and on the plateau, they appear on meter scale araneiform cones.

Figure 4: HiRiSE image at Ls 136.3°: dark spots in the upper part of the Russell Crater megadune and on the plateau. Dark spots are aligned and perpendicular to the brink on the plateau.

From Ls 172.6°, on the upper part of the megadune, in addition to the growing of the dark spot, dark streaks develop down the slope. These dark streaks are channelized. Comparing HiRiSE images very few days apart, the dark streaks are growing, spreading more and more down the slope and more channels. On the latest HiRiSE images, we observe that the large dark streaks are composed by darker and fresher individual steaks overlapping oldest and relatively lighter toned dark streaks. These albedo variations attest of refrosting processes (Table 1 and fig. 5). The observation also argues for short and repeated events more than a viscous and continuous spreading. The hypothesis is also supported by the observations at Ls 181° of single dark streak channels that are overlapping few meter high ripples. A minimum velocity is required to explain such a run-up. These dark spreading streaks that we will call "dark flows" in the rest of the paper, are the last features observed during the defrosting sequence. At Ls 217.7°, dust devil tracks (Table 1 and [10]) re-appear attesting of the complete frost retreat at this time in the area.

Spectral analysis: A CRISM observation data set is also available on the studied location of Russell Crater megadune at this period. The multiple spectra taken in winter and during the early spring present the characteristic signatures of the CO_2 frost, mixed with a small amount of water ice consistent with the atmospheric composition. From Ls 242°, no more CO_2 or water frost is present in the spectra.

Discussion: We interpret the dark spots as dust depositions consecutive to small eruptions of dust trough a frost slab as proposed by [5]. We propose that the dark spots are growing with successive eruptions and depositions as the season advances. The distribution of the dark spots is correlated to araneiform cones on the plateau and up-facing scarps on the slope. Even if these small scale topographies are observed in summer, we do not know if the defrosting features created these topographies or if the dark spots are located on the warmer north-facing scarps of these little topographies. At the end of the defrosting process and only at the steep submittal part of the megadune, dark flows develop. We interpret these features as avalanches of dust mixed with CO_2 and water vapour released under pressure. The same process creates dark spots of flat terrain but would trigger avalanches in case of steep slopes. This hypothesis is supported by the asymmetry of the dark flows. The flows develop only down the slope. The CO_2 and water vapour released with the dust at time of eruption is unstable as regard to the surface conditions and may play a role in the avalanche development and channelization.

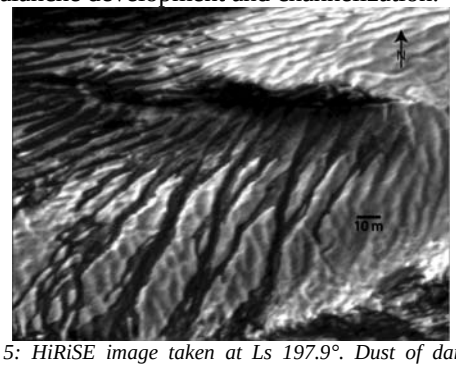

Figure 5: HiRiSE image taken at Ls 197.9°. Dust of dark flows spreading down the CO_2 frost on the Russell Crater megadune.

Conclusion: Dark spots and dark flows on steepest slopes mark the transitional period between the seasonal frost and its complete retreat. The channelized dark flows observed for the first time on the Russell Crater megadune, may be new flow mechanisms implying unstable vapour. We do not know yet the relationship between this newly highlighted flow mechanism and the underlying gullies.

Acknowledgements: We thank the 'Région Rhône-Alpes' of France for supporting this 'project CIBLE 2006'. We thank the HiRiSE team for the availability of data. We also thank Jessica Flahaut, Kylie Sedon, the LPG team of Grenoble, France.

References: [1]: Bridges et al. (2001), *LPS XXXII*. [2]: Piqueux et al (2003), *JGR*. [3]: Piqueux and Christensen (2008), *JGR*. [4]: Kossacki et al. (2004), *Icarus*. [5]: Kieffer (2007), *JGR*. [6]: Mangold et al. (2003), *JGR*. [7]: Costard et al. (2002), *Science*. [8]: Reiss and Jaumann (2003), *GRL*. [10] : Verba et al. (2009), *LPS XXXX*.

THE DISAPPEARING SOUTH RESIDUAL CAP ON MARS: WHERE IS THE CO_2 GOING? R. M. Haberle[1], M. A. Kahre[2], M. Malin[3] , and P.C. Thomas[4]. [1]Space Science Division, NASA/Ames Research Center, Moffett Field CA, 94035, Robert.M.Haberle@nasa.gov, [2]Bay Area Environmental Research Institute / NASA Ames Research Center, Moffett Field, CA, 94035, [3]Malin Space Science Systems, P.O. Box 910148, San Diego, CA. 92191, [4]Center for Radiophysics and Space Research, Cornell University, Ithaca, NY 14853.

Introduction: The familiar seasonal advance and retreat of the polar caps on Mars is due to the condensation and sublimation of CO_2, the main constituent of the Martian atmosphere. At both poles, the CO_2 that condenses during fall and winter completely sublimes by early summer, yet residual ice remains. In the north, the residual ice is water and when exposed it warms and sublimates into the atmosphere where winds transport it to other regions of the planet. In the south, however, the residual ice is mainly CO_2, though some water is mixed in around the edges, and possibly underneath the cap itself [1,2].

The existence of the South Residual Cap (SRC) is a mystery. For one thing, it is not located precisely at the pole and is instead offset by several degrees of latitude. This may be related to unique weather patterns spawned by the nearby Hellas basin [3]. For another thing, it is exposed when Mars is closest the sun and solar insolation is high. It must therefore have a very high albedo to survive. Furthermore, since the existence, location, and basic shape of the SRC have not grossly changed since at least as far back as the early 1700's [4], its albedo must be precisely tuned to avoid net erosion or accumulation [5].

Yet the cap now appears to be eroding. Images from the Mars Observer Camera (MOC) on Mars Global Surveyor reveal circular depressions in the ice that are growing with time. The volume of material lost between 1999 and 2001 is estimated to be 2-10x10^9 m^3 [6]. For plausible values of CO_2 ice density, this corresponds to a loss rate of as much as 1% of the present atmospheric mass per Mars decade. More recent detailed mapping using the Context Camera (CTX) images on the Mars Reconnaissance Orbiter (MRO) suggest an even faster loss rate equivalent to about 2.5% of the atmospheric mass per Mars decade [7].

A natural question then is: Where is the CO_2 going? There are three possibilities: the atmosphere; the seasonal caps, and/or the regolith. Of these, the regolith is the least likely to take up much CO_2 given the presence of so much water ice near the surface at middle and high latitudes [8] and the long time periods required to diffuse CO_2 to depths deep enough for this to be a significant reservoir [9].

GCM Simulations: A general circulation model (GCM) with a validated CO_2 cycle can address this question. Here we use a version of the Ames GCM recently used to study the role of the CO_2 ice emissivity in stabilizing the CO_2 cycle against interannual variations in atmospheric dust content [10,11]. The model gives a good fit to the Viking pressure data and for this purpose runs with unit CO_2 ice emissivities and subsurface water ice as suggested in [12].

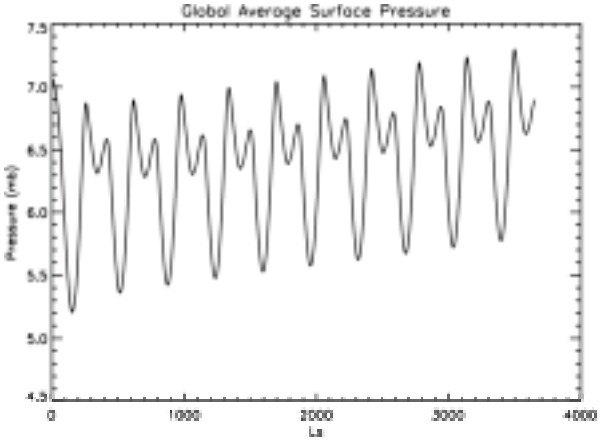

Fig. 1. Global average surface pressure (mb) vs Ls.

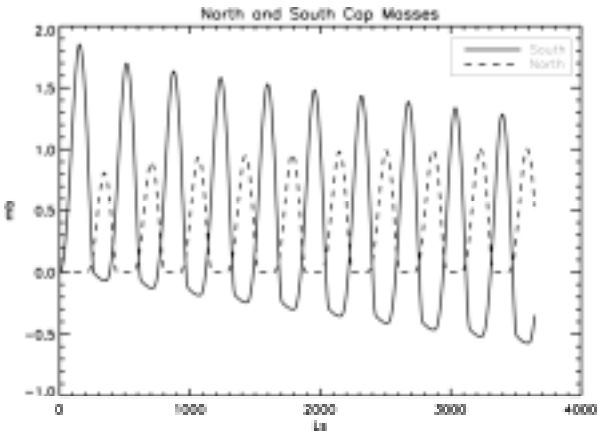

Fig. 2 South (solid) and North (dashed) cap masses (mb) vs Ls.

To simulate the disappearing cap, we place a large reservoir of CO_2 ice at those grid points in the model that give approximately the same area and location as the SRC. We then tune its albedo to loose CO_2 at a rate of about 0.6 mb (global equivalent) per Mars decade. This is about an order of magnitude greater than reproted above, but allows us to accelerate the process to

get a glimpse at how the system might respond. The results are shown in Figs 1 and 2.

About 70% of the net loss from the SRC appears in the atmosphere. Thus global mean annual surface pressure in this accelerated run increases by about 0.04 mb per Mars decade. Scaling this back to real time changes suggests an increase of about 0.004 mb per Mars decade assuming the system is linear. The is approximately the interval of time beween the Viking and Pathfinder missions which both measured surface pressure, a parameter directly related to atmospheric mass. Unfortunately, the accuracy and stability of the Viking and Pathfinder pressure sensors is not good enough to detect such small changes.

The remaining 30% lost by the SRC is taken up by the seasaonl caps, and virtually all of this is going into the north cap. Elevation differences account for the asymmetric behavior. Lower elevations in the north lead to higher surfrace pressures and therefore higher cap frost point temperatures. Since the condensation rate is proportional to the cap temperature through σT^4, the north cap gains at the expense of the south cap.

However, it is not clear from this simulation that the 70/30 partioning between atmosphere and caps is real. In Fig. 2, the gains for the north cap appear to be asymptoting rather than showing a steady gain year after year as is the case for the atmosphere (Fig. 1). This may indicate that the model subsurface temperatures where ground ice is present have not yet equilibrated and that a longer run would show a higher fraction of the net annual loss going into the atmosphere afterall.

What we can conclude at this stage of our study is that most of the CO_2 lost by the SRC is likely to end up in the atmosphere, and that best way to detect this would be from long-term direct measurements of surface pressure with sensors that have high accuracy and minimal zero drift.

References: [1] Titus T. et al. (2003) Science, 299, 1048-1051. [2] Bibring J.P. et al. (2004) Nature, 428, 627-630. [3] Colaprete T. et al. (2005) Nature, 453, 184-188. [4] Thomas P. et al. (2005) Icarus, 174, 535-559. [5] Bonev B.P. et al. (2007) Planet. Space Sci., 56, 181-193. [6] Malin M.C. et al. (2001) Science, 294, 2146-2148. [7] Thomas P.C. et al. (2009) Icarus, submitted. [8] Boynton W.V. et al. (2002) Science 297, 81-85. [9] Toon O.B. et al. (1980) Icarus, 44, 552-607. [10] Kahre M.A. et al. (2008) DPS abstract, BAAS, 40, p. 390. [11] Kahre, M.A. and Haberle R.M. (2009) 3rd International Workshop on Mars Polar Energy Balance and the CO2 Cycle, Seattle, WA. [12] Haberle R.M. et al. (2008) Planet. Space Sci. 56, 251-255.

HIRISE IMAGES OF SOUTHERN SEASONAL POLAR CAP SUBLIMATION FOR A SECOND SPRING ON MARS. C. J. Hansen[1] and the HiRISE team, [1]Jet Propulsion Laboratory / California Institute of Technology, 4800 Oak Grove Dr., Pasadena, CA 91109, Candice.j.hansen@jpl.nasa.gov

Introduction: Enigmatic surface morphologies at high southern latitudes are erosional features formed by sublimation of the seasonal carbon dioxide ice cap. The Mars Reconnaissance Orbiter (MRO) High Resolution Imaging Science Experiment (HiRISE) has imaged this terrain in unprecedented detail throughout two southern spring seasons. It has been postulated [1, 2, 3] that translucent ice traps gas sublimating from the bottom of the ice layer. Where the pressure is released the escaping gas jet entrains loose surface material and carries it to the top of the ice where it is carried downwind and deposited in a fan shape. Radially-organized channels (dubbed "spiders") eroded into the surface were hypothesized to channel sublimating gas [4]. Originally it was thought that this process was confined to the cryptic region at high southern latitudes [4] however we have found these erosional features, preferably refered to as "araneiform terrain" [5] in areas not previously identified as cryptic. Araneiform terrain is covered with radially-organized channels, 1 to 2 m deep. Similar terrain with interconnecting channels, not radially-organized, is refered to as lace [5].

Investigation: Several areas in the south polar region were selected for observation of the seasonal sublimation process. These areas were imaged numerous times throughout southern spring in Mars years 28 and 29. Some sites were the same as the first year in order to investigate interrannual variability. Other new areas were also selected in the second year in order to broaden the types of terrain imaged systematically.

Second Spring First Impressions: There are significant differences between the two Mars springs in the level of activity. Figure 1a and Figure 1b compare Mars year 28 and year 29. The difference in L_s between the two images is just 0.25^0. The high density of fans in Figure 1a corresponds to the araneiform terrain and the number of fans is ~similar between the two years. The area with few fans at the top of Figure 1a, lace terrain, can be contrasted with the same region in Figure 1b. There are many more fans in the lace terrain at approximately the same time in the second year.

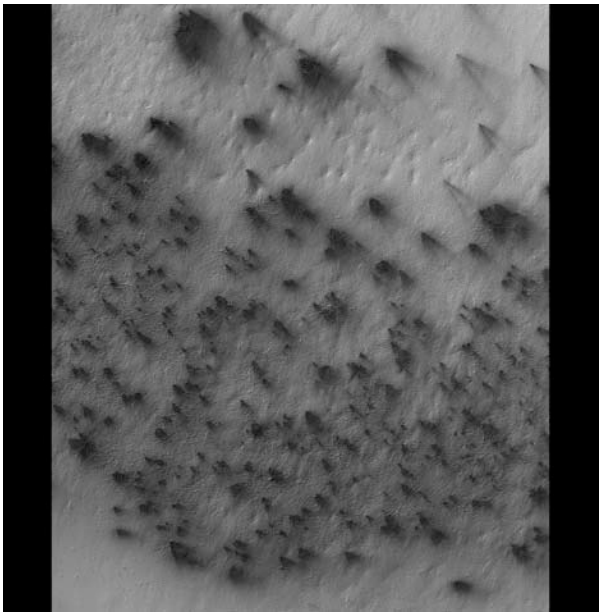

Figure 1a. PSP_002850_0935 was acquired on L_s = 195.40. The higher density of fans covers araneiform terrain. Note the lack of fans at the top of the image. The latitude / longitude is -86.387 (planetocentric) / 99.002 E. The width of the image is ~5 km.

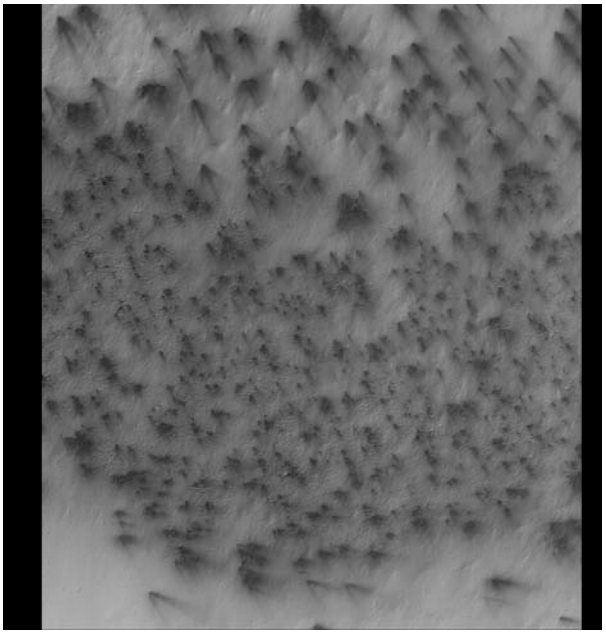

Figure 1b. ESP_011671_0935 was acquired on L_s = 195.65. The top of the image has a significantly greater number of fans.

What could cause this difference in activity? Possibilities could be a difference in ice thickness or a difference in ice albedo, that would allow ruptures and gas release to occur earlier in the season. Year-to-year differences in seasonal cap properties are not unusual both on small and large scales.

The seasonal process of sublimation was tracked for the "spiders" shown in Figure 2a [5], a sub-image of PSP_002850_0935. In the second Mars year imaged by HiRISE we zoom in on the same two spiders, in the sub-images shown in Figure 2b, a sub-image of ESP_01671_0935. Even in this region of araneiform terrain we see more small fans in the second year than were observed in the first year. The fans were larger in the first year however, so it will be important to quantify the amound of material moved – the overall gas flow may be equivalent.

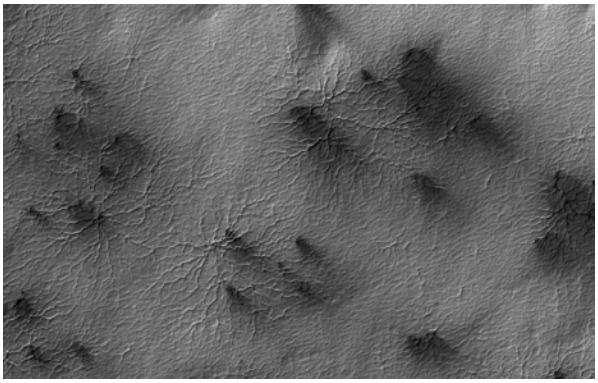

Figure 2a. This sub-image of PSP_002850_0935 zooms in on two spiders studied in detail in the first year of HiRISE operation [5].

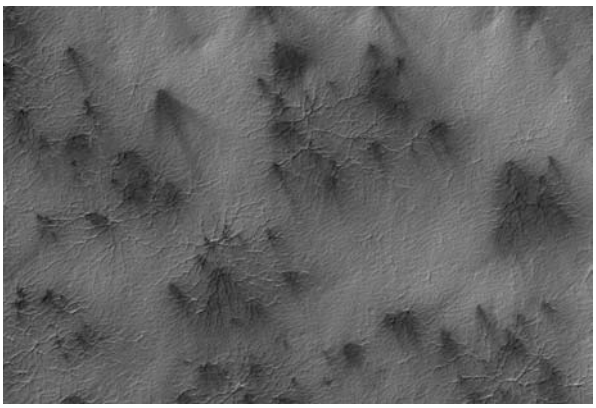

Figure 2b. This sub-image of ESP_011671_0935 zooms in on the same area. More small fans are visible at the same L_s.

Other New Findings: Images taken in areas previously not identified as cryptic terrain show similar erosional morphologies and fans. This suggests that if this mechanism of trapped gas release is correct then the seasonal ice may at least at times be translucent, or that subsurface thermal conduction alone is an adequate source of energy [6].

New images obtained show fans associated with polygonal cracks as described in [7]. Gas flow from polygonal cracks preceeds flow from the spiders, forming fans earlier in the season, shown in Figure 3.

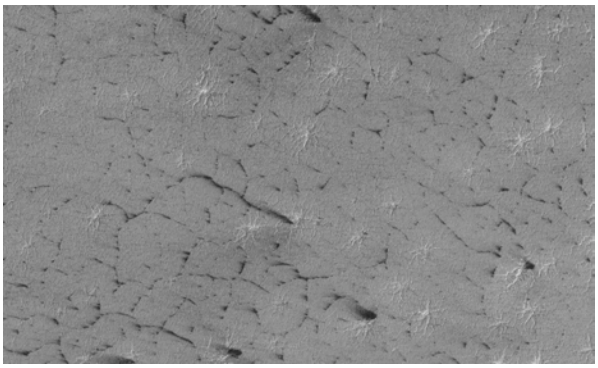

Figure 3. Sub-image of ESP_012821_0865 shows fans emerging from polygonal cracks before spiders.

References: [1] Kieffer, H. (2000) LPI Contribution #1057. [2] Kieffer, H. (2006) Nature 442:793. [3] Kieffer, H. (2007) JGR 112:E08005. [4] Piqueux, S., S. Byrne, and M. Richardson (2003) JGR 108(E8):3-1. [5] Hansen, C. J. et al., submitted to Icarus (2008). [6] Aharonson, O., et al. (2004) JGR 109:E05004. [7] Piqueux, S. and P. R. Christensen (2008) JGR 113:E06005.

Acknowledgement: This work was partially supported by the Jet Propulsion Laboratory, California Institute of Technology, under a contract with the National Aeronautics and Space Administration.

CARBON DIOXIDE SNOW CLOUD ACTIVITY AND POLAR WINTER EMISSIVITY: MARS CLIMATE SOUNDER OBSERVATIONS AND MODEL RESULTS. P. Hayne[1], D. A. Paige[1]. [1]University of California, Los Angeles (595 Charles Young Blvd E, Los Angeles, CA 90095; phayne@ucla.edu)

Introduction: Carbon dioxide snow clouds near the winter pole of Mars have long been predicted on theoretical grounds [1, 2], and have been detected indirectly through their effects on the emitted [3, 4] and reflected [5] infrared radiation field. We previously reported direct observations of clouds in the polar atmosphere during southern winter using data from the Mars Climate Sounder (MCS), and presented preliminary model results supporting the hypothesis that they are precipitating CO_2 snow clouds centered at ~ 20 – 30 km altitude [6, 7].

Here, we present maps of cloud activity and effective emissivity recorded by MCS. In the southern winter, sporadic activity occurs at all latitudes poleward of ~ 60°, and persistent activity occurs poleward of ~ 80°. Lowest effective emissivities are found in a ~ 500 km diameter region strongly correlated with the location of the south perennial cap. Orographic clouds due to local topography occur predominantly late in the winter, consistent with earlier studies using TES data [8]. Mapping of cloud activity in the north polar region is in progress. Radiative transfer modeling indicates that most "low emissivity regions" (LERs, a.k.a. "cold spots") are due to clouds, though small (< 50 km diameter) and low-lying clouds are difficult to detect in MCS limb observations [9].

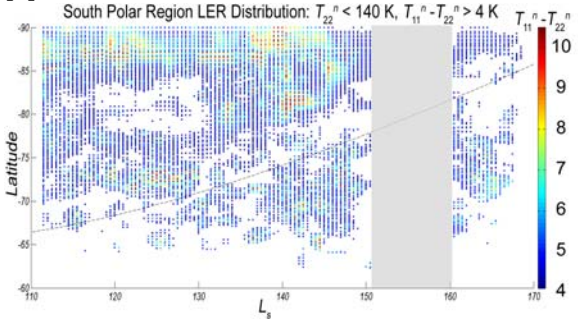

Figure 1: South Polar LER distribution as a function of latitude and L_s, during late southern winter (L_s = 111°–148°). Dashed line indicates extent of polar night. Bin-average $T_{11}^n - T_{22}^n$ ranges from 4 K up to 10 K, indicating smaller grain sizes for higher values.

Observations: The Mars Climate Sounder [10] onboard the Mars Reconnaissance Orbiter records nadir and limb radiance measurements in nine spectral channels, from ~1–40 μm wavelength. The longest continuous period of coverage spanned a range of solar longitude, L_s = 111° to 148°, corresponding to southern winter. We convert radiances to equivalent brightness temperatures using the radiometric response of each filter and the Planck function. Observations are binned by latitude and longitude (1–5° bins) and L_s, and we generate maps of nadir brightness temperatures, T_b^n, and limb profiles, $T_b^l(z)$ (where b is the center wavelength of the filter, and z is the center of the altitude bin). Figure 1 shows southern winter LER activity.

Model: To simulate multiple scattering in the cloudy polar atmosphere, we employ an algorithm based on the δ-Eddington approximation for the equation of transfer [11], modified for the infrared [12] and with full spherical geometry for limb viewing [9]. Scattering parameters (g, Q_{ext}, and ϖ_0) are calculated from Mie theory with optical constants for dust, water ice, and carbon dioxide ice for the model atmospheric composition and size distribution. Surface temperature is taken at the mean CO_2 frost point (e.g., ~ 145 K for the south polar region), and the atmospheric temperature is approximated by the mean "clear" polar profile retrieved from MCS radiances [10]. Monochromatic radiances are calculated at high spectral resolution for the full range of viewing geometries, then convolved to each MCS filter's response and the instantaneous field of view.

Results: Maximum and minimum effective emissivities (ε_{min} and ε_{max}) for the south polar region during the period L_s = 111° to 148° are shown in Figure 2, for the MCS 22 μm channel. The effects of topography on the partial pressure of CO_2, p_{CO_2}, have been accounted for using MOLA topography and a pressure scale height of 7.5 km. Bins ~ 50 km in size and 1° L_s are used to average point observations (> 2 per bin, generally ~ 10 per bin). ε_{max} is relatively symmetric around the south pole, with values < 1 for nearly the entire region > 60° S, and values < 0.75 at the south polar residual cap (SPRC) location. Measured T_{22}^n is affected by CO_2 ice grain size and dust contamination [13], with smaller grains resulting in lower T_{22}^n (hence lower effective emissivity). Our results for ε_{max} and for $T_{11}^n - T_{22}^n$ (indicating the depth of the CO_2 transparency band) suggest grains remain small (< 1 mm) and/or are replenished throughout the study period, in the south polar region.

Minimum effective emissivities are quite low, especially in regions where high cloud activity is observed. ε_{min} < 0.8 roughly indicates these active re-

gions, and ε_{min} over the SPRC is < 0.5 during this period, indicating a high level of persistent cloud activity. Many of the smaller features are associated with pixel-scale (~ 50 km) topography, indicating local orographic effects, which increase in frequency late in the winter.

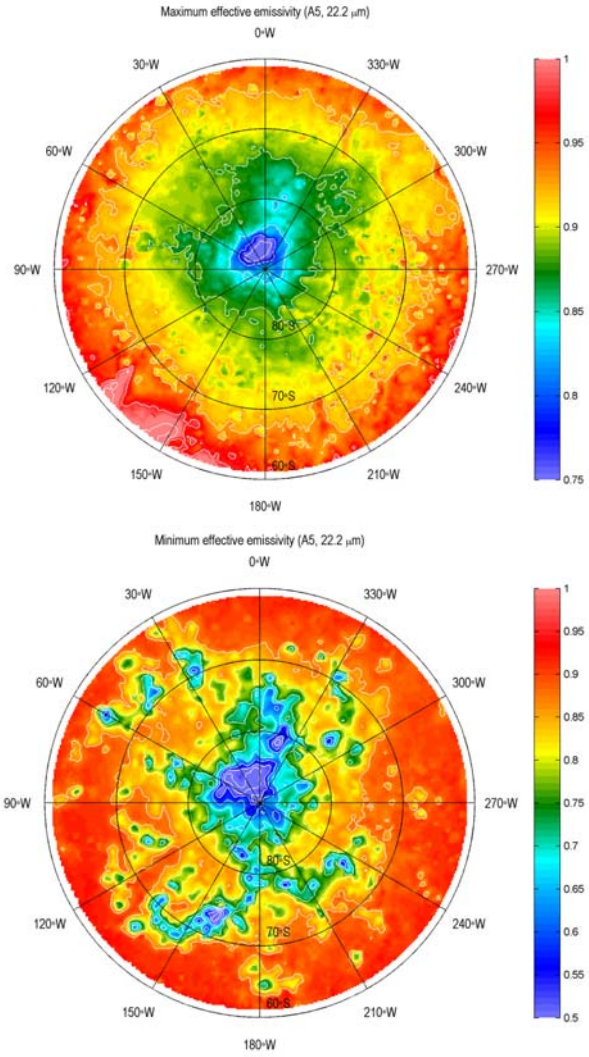

Figure 2: Maximum (top) and minimum (bottom) effective emissivities (22 μm) for the south polar region during the period L_s = 111° to 148°. The two scales are ε = 0.75 to 1.0, and 0.5 to 1.0, respectively. Reduction of p_{CO_2} due to elevation has been taken into account (see text).

Cloud activity recorded in MCS limb observations over the polar region is well correlated with nadir LERs. Figure 3 shows a "snapshot" of $T_{22}{}^{l}$(25 km) for the 1° L_s bin centered at L_s = 116°. The low-$T_{22}{}^{l}$ ring 70-80°S is likely due to the relatively clear atmosphere inside the polar vortex; the large high- $T_{22}{}^{l}$ region over the pole is due to clouds. Although little correlation between $T_{22}{}^{l}$(25 km) and $T_{22}{}^{n}$ is observed lower than ~ 75°S latitude, modeling indicates this is most likely due to the difficulty in spatially resolving smaller clouds. Also, modeling and comparison with limb data is necessary in order to determine whether low-lying CO_2 clouds are also present in these regions.

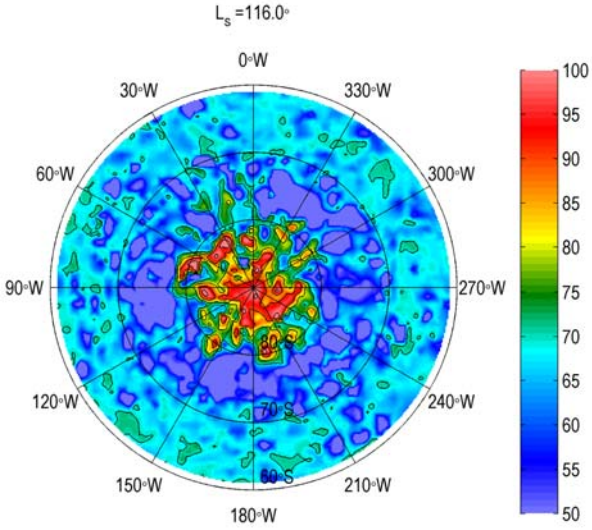

Figure 3: Limb brightness temperature (K) at 22 μm, for a 5-km vertical bin centered at 25 km altitude, at L_s = 116°.

Discussion: Our results indicate that cloud activity in the south polar region is dominated by two distinct types, likely related to two modes of deposition: 1) A large (~ 500 km diameter) optically thick cloud persists poleward of ~ 80°S throughout the winter, and 2) smaller scale, shortler lived clouds form sporadically at all latitudes higher than ~ 60°S. The latter form preferentially late in the season and are often associated with topography, implying an orographic effect. Effective emissivities are highly variable, but remain lower than unity for most of the polar region. The lowest effective emissivities (< 0.5) are recorded over the SPRC and its vicinity. A similar study of the north polar region is currently in progress.

References: [1] Paige, D. A. and Ingersoll, A. P. (1985) *Science* 228, 1160. [2] Pollack, J. B. et al. (1990) *JGR* 95, 1447. [3] Forget, F. et al. (1995) *JGR* 100, 21219. [4] Titus, T. N. et al. (2001) *JGR* 106, 23181. [5] Colaprete, A. et al. (2003) *JGR* 108, 5081. [6] Hayne, P. and Paige, D. A. (2008) *LPS* XXXIX, p. 2516. [7] Hayne, P. and Paige, D. A. (2009) *LPS* XL, p. 1849. [8] Cornwall, C. and Titus, T. N. (2009) *JGR* 114, E02003 [9] Hayne et al. (2009) *in prep.* [10] McCleese et al (2008) *Nature Geosci.* 1, 745. [11] Joseph, J. H. et al. (1976) *J. Atmos. Sci.*, 33, 2452. [12] Paige, D. A. (1985) Ph.D. Thesis, Caltech, Pasadena. [13] Hansen, G. B. (1999) *JGR* 104, 16471.

CTX observations of seasonal albedo variations in the "Tooth Region" of the RSPC. P. B. James[1], P. C. Thomas[2], W. M. Calvin[3], R. Haberle[4] [1]Space Science Institute Boulder CO 80301 [2]Center for Radiophysics and Space Research, Cornell University, Ithaca NY [3] Department of Geological Sciences, University of Nevada, Reno NV [4]Space Science Division, NASA Ames Research Center, Moffet Field CA.

Introduction: The tandem of Context Imager (CTX) and Mars Color Imager (MARCI) on Mars Reconnaisance Orbiter (MRO) is ideal for sorting out the behaviors of frost units at two complementary scales: 5 meters/ pixel and 1 km/pixel, respectively. Both cameras have been well calibrated, and the Lambert albedos determined from simultaneous observations of identical regions by the two cameras are consistent with each other. We have used CTX and MARCI to study the evolution of albedos in the Residual South Polar Cap (RSPC).

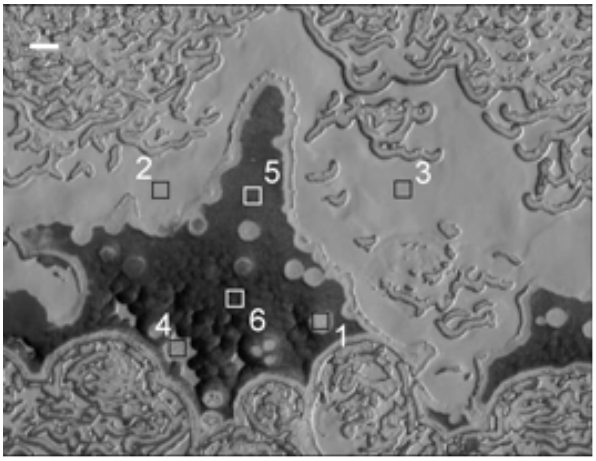

Figure 1: The Tooth Region at Ls=353. Boxes indicate regions corresponding to albedo measurements in Fig. 3. CTX image P13_006229_0951_XN_84S014W

The area, which we call the "tooth," (Fig.1) has survived as a recognizable feature since at least Mariner 9 but has undergone changes in the intervening time that seem to include both erosion and deposition (Fig. 2). We studied the brightness variations of several features in this region that include examples of units B and A as well as a down wasted region [1]. Comparison of the behaviors of units within a small region has the advantage that atmospheric aerosols and photometric angles are essentially equal throughout the scene, thus avoiding problems with interpretation of Lambert albedos at different locations.

Albedoes of Units in the Tooth Region: The seasonal albedo behaviors of the various units are shown in Figure 3. The earliest view at L_s=286.5° indicates that all of the units start with the same albedo, ~0.78, characteristic of the seasonal CO_2 deposits in the region. The albedos of all of the units other than the down wasted sample 5 remain equal in the second image at L_s=303.7°; the slight increase is possibly produced by a decrease in dust opacity over the cap after the large 2007 dust event. During the next two time steps, L_s=309.8° and L_s=328.6°, the albedos of all of the units decrease, but those of the 5 and 6 samples decrease more rapidly. The downwasted units continue to become darker into late summer L_s=352.5°, though at a reduced rate, while the albedos of the bright units increase to values more characteristic of early summer.

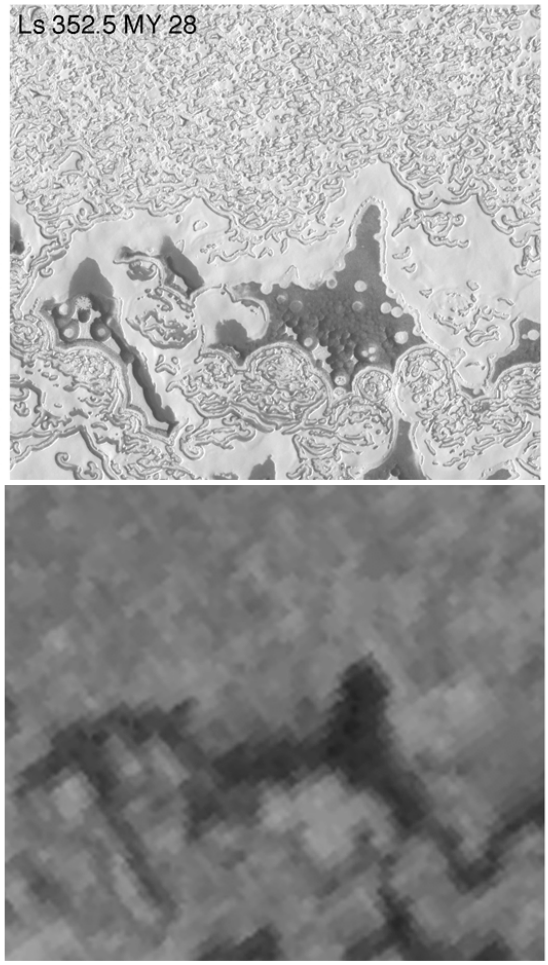

Figure 2: Comparison of MY 28 (CTX image P13_006229_0951_XN_84S014W, L_s=352º.; Mariner 9 image 231b01, L_s =356º)

Our favored interpretation of these observations is that the albedo decreases are a result of the sublimation of bright, small grain CO_2 deposits over the entire area. The physical

mechanism could be either that, as the deposits get thinner, more of the subsurface shows through the frost or that the nature of the frost (e.g. the grain size) changes with depth. In essence either scenario requires that the depth of the bright, seasonal frost in the darker samples 5 and 6 is less than in the bright regions. The albedo decreases more rapidly as the areas get darker and absorb more energy. We attribute the upturn in the albedo to the onset of recondensation of CO_2 in the brighter areas in the vicinity of L_s=330°. Note that, even at the end of summer, the albedos of the relatively dark units are greater than would be expected for bare ground; evidently these areas reveal either dirty water ice deposits or CO_2 with large grains size.

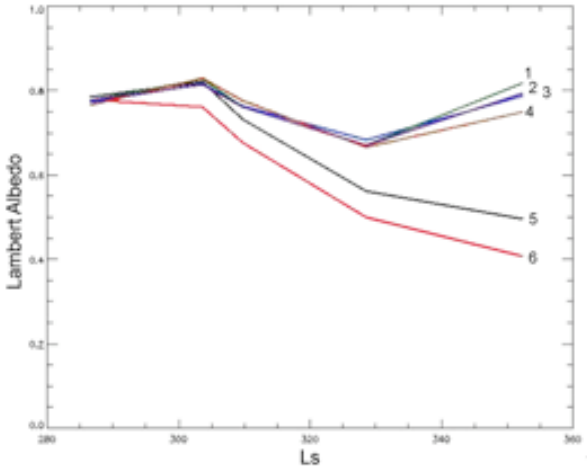

Figure 3: Time evolution of the Lambert albedos of the six regions identified in Figure 1.

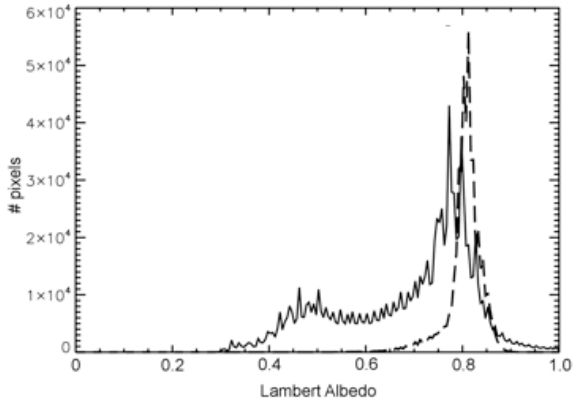

Figure 4: Distributions of albedos of pixels in the Tooth Region at Ls= 303.7° and at Ls=352.5°.

Relation to large-scale behavior: There is a general downward trend in the large scale (~kms/pixel) Lambert albedo in the RSPC during mid to late summer [2]. There are several possible explanations for this: a change in the intrinsic properties of the CO_2 frost; a change in the distribution of light and dark areas at higher resolution; a failure of the Lambert approximation at large incidence angles. The change in the distribution of pixels within the Tooth Region from early summer to late summer (Fig. 4) strongly favors the second interpretation.

References:

[1] Thomas, P. C. et al. (2009), Icarus, submitted. [2] James, P.B. et al. (2007), Icarus 192, 318-326.

MARS' CO_2 CYCLE: EFFECTS OF AIRBORNE DUST AND CO_2 ICE EMISSIVITY ON THE GROWTH OF SEASONAL CO_2 CAPS. M.A. Kahre[1] and R.M. Haberle[2], [1] Bay Area Environmental Research Institute / NASA Ames Research Center, Moffett Field, CA, 94035 (melinda.a.kahre@nasa.gov), [2]NASA Ames Research Center, Moffett Field, CA, 94035.

Introduction: The dust and CO_2 cycles have long been known to greatly affect the current climate and weather of Mars. Tens of percent of the main constituent of Mars' atmosphere, CO_2, cycles between the surface and the atmosphere annually. The formation and subsequent regression of the north and south CO_2 caps control the mass of the atmosphere as a function of time. Airborne and surface dust can affect the formation and regression of the annual CO_2 polar caps by influencing the polar heat balance through the alteration of the radiation balance and dynamics of the atmosphere and by altering the thermal properties of the surface [1,2].

Multiple years of surface pressure measurements by the Viking landers strongly suggest that the CO_2 cycle is highly repeatable on annual timescales[3]. This result is significant and somewhat unexpected given the highly variable nature of the dust cycle during the multiple years of Viking observations[4]. A comprehensive physical explanation for the repeatable nature of the CO_2 in the presence of a variable dust cycle has not yet been put forth in the literature. Here we present one possible explanation.

This current work began because we were trying to reproduce the results of [1] that indicated that increasing atmospheric dust inhibits CO_2 condensation. Our current GCM predicted the opposite--that increasing atmospheric dust enhances CO_2 condensation during cap growth. We traced this result to the low CO_2 cap emissivities that are necessary to fit the Viking lander pressure data in simulations in the absence subsurface ice. This led us to appreciate the critical importance of one parameter-- CO_2 ice emissivity--in determining the the manner in which increasing atmospheric dust affects the CO_2 cycle. We show here that a low ice emissivity leads to enhanced CO_2 condensation rates when the atmospheric dust is increased and a high ice emissivity leads to suppressed CO_2 condensation rates when the atmospheric dust is increased. This leaves open the possibility that the explanation for the highly repeatable nature of the CO_2 cycle is that the surface ice emissivities are equal to an intermediate value such that increasing the atmospheric dust has no effect on CO_2 condensation rates.

The NASA Ames General Circulation Model and Simulations: The NASA Ames GCM is a three-dimensional gridpoint model of the Martian atmosphere. The model version (1.7.3) used here runs on an Arakawa C-grid with a horizontal resolution of 5° in latitude by 6° in longitude. The radiative effects of airborne dust and CO_2 gas are accounted for at visible and infrared wavelengths (see [1] for details). A temporally and spatially fixed dust loading is assumed. Surface and atmospheric CO_2 condensation and surface CO_2 sublimation occurs when necessary to balance the polar heat budget. When condensation occurs in the atmosphere, the latent heat of condensation is deposited locally but the mass of the condensed gas is instantaneously deposited on the surface. No CO_2 ice cloud microphysics is included. Simulations are executed for three Martian years to fully equilibrate the CO_2 cycle; analyzes are performed on the second and third years of simulation.

To investigate the affects of dust on the CO_2 cycle we first tune the model to reproduce the Viking pressure data using a low dust opacity (τ = 0.3) and two different CO_2 emissivity/subsurface ice scenarios. For the first scenario, we find a good match to the Viking observations with low CO_2 ice emissivities (0.5 and 0.7 for the north and south, respectively), assuming no subsurface water ice. For the second scenario, we utilize the spatial pattern of inferred subsurface water ice from observations from Mars Odyssey's Gamma Ray Spectrometer. We find a good fit to the Viking observations assuming unity for the north and south CO_2 ice emissivities with depths to the ice table of 5 and 12 centimeters for the north and south, respectively.

Results: To investigate the affect of atmospheric dust on the CO_2 cycle, the two simulations described above were repeated but with a large dust loading (τ = 5.0).

Total Cap Mass. The seasonal evolution of the mass and spatial extent of the seasonal CO_2 ice cap depends on the net effects of condensation and sublimation. The total mass of CO_2 condensed in the north polar region differs in each of the four cases (Fig. 1). The two low dust (τ = 0.3) cases predict similar north cap masses because both of the simulations are tuned to fit the Viking pressure curves. The magnitudes of the peak north cap mass range from approximately 1.3 $\times$ 10^{15} kg to 3.8 $\times$ 10^{15} kg for the high dust (τ = 5.0) cases. When the surface ice emissivity is low (ε = 0.5), increasing the atmospheric dust opacity leads to a more massive CO_2 ice cap. Conversely, when the surface ice emissivity is high (ε= 1.0), increasing the at-

mospheric dust opacity leads to a less massive CO_2 ice cap.

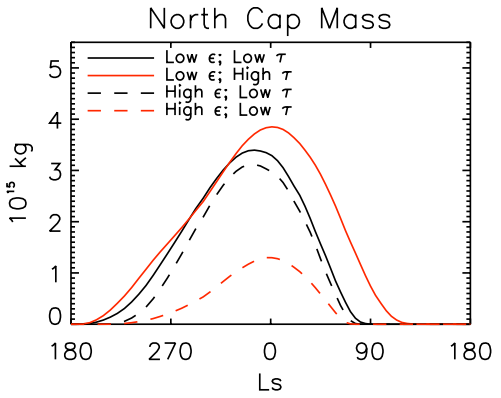

Figure 1: Total ice mass contained in the north seasonal CO_2 cap as function of season for each of four GCM simulations. This figure demonstrates that the surface ice emissivity dictates the manner in which airborne dust affects the CO_2 cycle: When the emissivity is high, increasing the dust opacity suppresses CO_2 condensation but when the emissivity is low, increasing the dust opacity enhances CO_2 condensation.

CO_2 Cap Formation. CO_2 condensation and sublimation combine to regulate the growth and recession of the seasonal CO_2 cap. The magnitude of the peak mass of the cap depends on the seasonally averaged CO_2 condensation rate during cap growth. For this reason, we focus on the growth phase of the northern seasonal CO_2 cap in order to understand the manner in which atmospheric dust and surface emissivity affects the how massive the cap becomes.

The CO_2 condensation rate is dictated by the polar heat balance. To first order, the latent heat released when CO_2 condenses balances the net radiation loss at the top of the atmosphere and heat transported into or out of the region by the atmosphere. An analysis of the components of the heat balance is necessary to understand the simulated behavior that increasing the atmospheric dust opacity enhances CO_2 condensation with a low surface ice emissivity but suppressed CO_2 condensation with a high surface ice emissivity.

During cap formation, the heat transported by the atmosphere at high latitudes (i.e., poleward of 70 N) becomes much less efficient than at lower latitudes, which dictates that the latent heat of CO_2 condensation must balance the net radiative loss at the top of the atmosphere. Therefore, the net radiative loss of the atmosphere dictates the CO_2 condensation rate. When the CO_2 ice emissivity is high, atmospheric dust decreases the net radiative loss by a small amount (i.e.,less than 5 W m^{-2}) and therefore reduces the CO_2 condensation rate. This is because the dusty, high emissivity atmosphere is radiating at cooler temperatures than the surface, causing the radiative loss to be suppressed a small amount. When the CO_2 ice emissivity is low, atmospheric dust increases the radiative loss by a more significant amount (i.e., approximately 10 W m^{-2}), and therefore increases the CO_2 condensation rate. This occurs because the contribution to the radiation balance from the surface is greatly reduced; thus, a dustier atmosphere (even though it is colder than the surface) increases the radiative loss from the atmospheric column and enhances the CO_2 condensation rate.

Discussion and Conclusions: This work highlights the criticality of the surface ice emissivity on determining the sign of the effect of airborne dust on CO_2 condensation. A high surface emissivity results in the suppression of CO_2 condensation with increasing dust, while a low surface emissivity results in the enhancement of CO_2 condensation with increasing dust (Fig. 2). This raises the intriguing possibility that the CO_2 cycle is highly repeatable because the CO_2 ice emissivity is equal to the critical value such that increasing the atmospheric dust load does not result in more or less CO_2 condensation. For this explanation to be substantiated, further questions need to answered, including: 1. What is the "perfect" ice emissivity and is this value consistent with the observations? 2. Is this emissivity reached by chance or are there feedbacks driving the emissivity to this value? 3. How do other possible interactions between the dust and CO_2 cycle complicate this scenario?

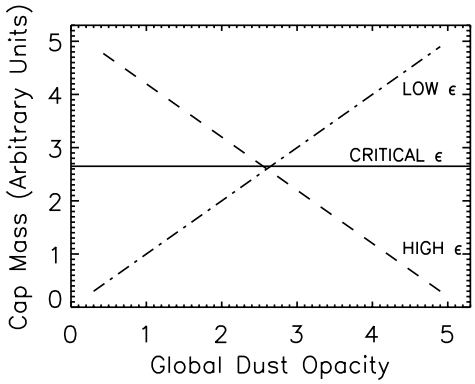

Figure 2: Theoretical depiction of the 'perfect' CO_2 ice emissivity, which is the emissivity that leads to no net increase or decrease in CO_2 condensation when the atmospheric dust opacity increases.

References: [1] Pollack et al., (1990) *JGR 95*, 1447-1473; [2] Paige, D.A. and Ingersoll, A.P. (1985) *Science, 228*, 1160-1168; [3] Hess et al. (1980), *GRL*, *7*, 197-200; [4] Tillman, J.E. (1986) *MECA Workshop on Dust on Mars II*, p. 72

INVESTIGATIONS OF MARS POLAR PROCESSES BY OMEGA/MEX OVER 3 MARTIAN YEARS.

Y. Langevin[1], J-P. Bibring[1], Sylvain Douté[2], M. Vincendon[3], F. Poulet[1], B. Gondet[1], [1]IAS CNRS / Univ. Paris Sud 11, Bat. 121, 91405 Orsay Campus, Orsay, France, yves.langevin@ias.u-psud.fr, [2]LPG CNRS / Univ. Joseph Fourier, [3]Brown University

Introduction: The seasonal and perennial polar caps of Mars play a major role in the polar energy balance as well as the CO_2 and H_2O cycles. Until 2004, the main results on the extent and evolution of the caps were obtained in the visible (bright regions being associated with ices) by orbiting cameras (from the very first Mariner missions to Viking, then MGS/MOC) then in the thermal IR (MGS/TES and Odyssey Themis). Ices could then be detected from their characteristic equilibrium temperatures. Since January 2004, the OMEGA Vis-NIR imaging spectrometer on board Mars Express has provided a powerful new tool for investigating ices on Mars. Both CO_2 and H_2O ices present strong characteristic absorption bands in the near-IR (Fig. 1). The relative strength of these bands provides information on grain size while the albedo is controlled by dust contamination within the ice or at the surface.

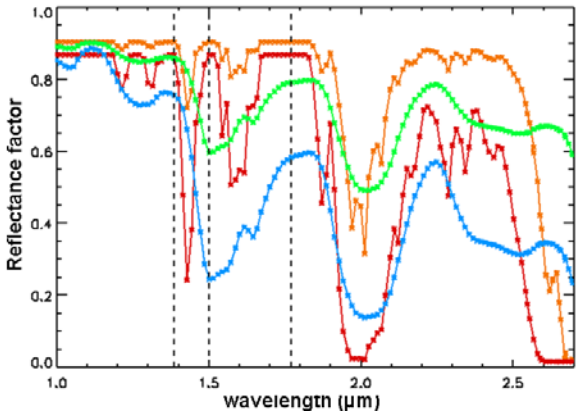

Fig. 1: spectral signatures of CO2 ice (orange: 1 mm size; red: 5 cm size) and H2O ice (green: 10 µm size; blue: 100 µm size)

Observations started in January 2004 at Ls 331°. They now cover nearly 3 full martian years (20/07/2009: Ls 306°). The precession of the pericenter of the elliptical orbit of Mars Expess (300 km x 10400 km, 6.7 h) and the combination of the precession of the orbit plane with the orbital motion of the planet generate a wide range of observation conditions of high latitude regions in terms of altitude and local time. As an example, for observations at Ls 90° in 2004 (Fig. 2a), the orbit was close to the terminator with an altitude over the north pole of 4000 km while it was at a local time of 2 AM – 2 PM with an altitude of 500 km over the north pole in 2006 (Fig. 2h).

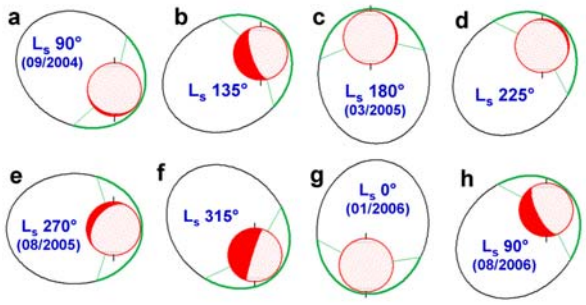

Fig. 2: Evolution of the orbit of Mars Express during one martian year (Ls 90° to Ls 90°)

Main results: Observations of southern polar regions after one month in orbit yielded a first important result, with the detection of the spectral signature of H_2O ice in well defined areas (dark blue in Fig. 3) at the edge of the southern perennial cap [1]. Spectral modeling provided constraints on H_2O ice grain size both in these regions and as contamination of CO_2 ice over the perennial cap [2].These regions have an albedo similar to dust covered terrains, hence they could not be identified in imaging data.

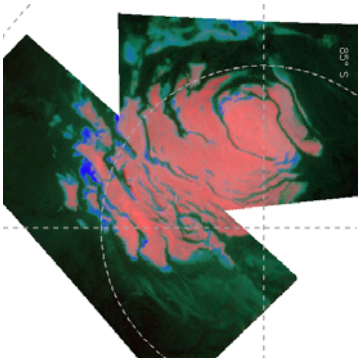

Fig. 3: Signatures of CO_2 ice (pink) and H_2O ice (blue) near the South pole observed by OMEGA at L_s 335° in early 2004.

In the early phases of the mission, observations near apoapsis were not authorized, hence the first comprehensive observations of the North high latitude regions were obtained shortly after the northern summer solstice. The observations of the North perennial cap demonstrated that it is constituted of large grained H2O ice covered by small-grained H_2O frost until shortly after the summer solstice [3]. Part of the observed evolution of the albedo of ice covered surfaces results from a decrease of the aerosol optical thickness after summer solstice [4]

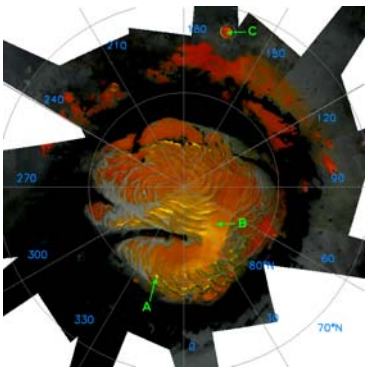

Fig. 4: large grained perennial H_2O ice (red) and residual seasonal frost (yellow) over the North cap at Ls 115° (from [3])

Low albedo areas with weak H2O ice signatures have been observed in NPLD. As these signatures correspond to large grained H2O ice (~ 1 mm), these areas correspond to ice-dust mixtures (permafrost).

A comprehensive set of observations on the retreat of the seasonal cap was obtained in 2005 [5], the swath width decreasing in step with the retreat of the cap as the altitude over the South pole decreased (Fig. 2c to 2f). These observations revealed a very complex role of CO2 ice, H2O ice and dust both on the ground and as aerosols for H2O ice and dust. The "cryptic region" (a dark, cold area within the cap which is prominent in mid-spring [6]) was of particular interest as its low albedo had been attributed to the underlying surface observed through clear CO_2 ice. OMEGA observations exhibited much weaker CO_2 ice signatures in this region, which demonstrated that its low albedo could be attributed to surface dust contamination [7].

In the South, H_2O frost is observed as aerosols close to the spring equinox. It sediments in well defined areas within the cap, which sublimate in late spring (Fig. 5). Contrary to the situation in the North, there is no evidence for a ring of H_2O frost lagging behind the retreat of CO_2 frost [5,8].

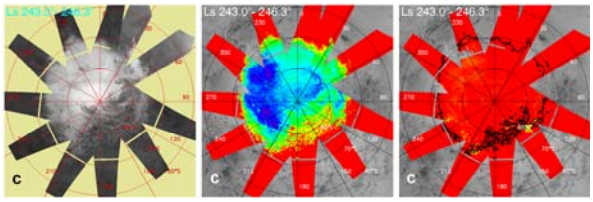

Fig. 5: albedo (left), CO_2 ice signatures (center) and H_2O ice signature (right) over the south seasonal cap in late spring; at this stage, only a few small patches of H_2O frost are observed along the sublimation front (from [5]).

Observations in the North in 2006 and 2008 revealed a completely different pattern: after mid-spring, H_2O ice signatures spectrally dominates over the seasonal cap, except from a few patches where CO_2 ice signatures are still observed, even when it is clear that the bulk of the cap is still constituted by CO_2 ice.

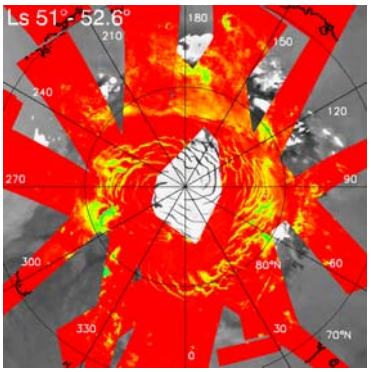

Fig. 4: signatures of CO2 ice (green) observed as patches within the limits (black) of the north seasonal cap in mid spring

The saturated bands of CO_2 ice provide a very powerful diagnostic tool for evaluating the optical thickness of aerosols over icy regions, as only photons scattered by airborne dust can be observed at these wavelengths. This made it possible to track dust clouds crossing the south seasonal cap and the evolution of dust loading at high latitudes [9], with clear similarities with time evolution patterns observed at low latitudes by the MER's confirm the global character

Conclusion and perspectives: Nearly 3 Martian years of spectral imaging observations by OMEGA/Mex at Vis-NIR wavelengths have provided major results on the role of CO_2 ice, H_2O ice and dust in the evolution of Martian seasonal and perennial caps. The focus of on-going and scheduled OMEGA observations of polar regions is on inter-annual variability and on multi-instrument investigations of regions of interest. Higher resolution IR observations are now provided by CRISM/MRO, which can be set within the wider context provided by OMEGA tracks. The results of a coordinated observation campaign of the cryptic region with OMEGA, CRISM, HIRISE and THEMIS are presented in a companion abstract.

References:

[1] J-P. Bibring et al., *Nature*, **428** p. 627 (2004);
[2] S. Douté et al., *Planet. Space Sci.* **55**, p. 113 (2007)
[3] Y. Langevin et al.., *Science* **307**, 1581 (2005);
[4] M. Vincendon et al., *J. G.. Res.* **112**, E08S13 (2007)
[5] Y. Langevin et al., *J. G. Res.* **112** E08S12 (2007)
[6] H. Kieffer et al., *J. G. Res.* **105**, 9653 (2000)
[7] Y. Langevin et al.., *Nature* **442**, 790 (2006)
[8] F. Schmidt et al., *Icarus* **200**, 374 (2008)
[9] M. Vincendon et al., *Icarus* **196**, 488 (2008)

INVESTIGATIONS OF THE CRYPTIC REGION OF THE SOUTH SEASONAL CAP OF MARS IN 2009.

Y. Langevin[1], C. Hansen[2], N. Thomas[3], M. Vincendon[4], T. Titus[5], S. Piqueux[6], J-P. Bibring[1], B. Gondet[1], K. Seelos[7]. [1]IAS CNRS / Univ. Paris Sud 11, Bat. 121, 91405 Orsay Campus, Orsay, France, yves.langevin@ias.u-psud.fr, [2]Jet Propulsion Laboratory, Pasadena USA, [3]University of Bern, [4]Brown University, [5]USGS Flagstaff, [6]Arizona State University, [7]APL, John Hopkins University

Introduction: Our understanding of the origin and evolution of the "cryptic" region [1], a dark and cold area observed over a large fraction of the South seasonal cap of Mars in mid spring, has made major progresses with observations in the near-IR (OMEGA/Mex since early 2004, CRISM/MRO since late 2006). It is now clear that low albedo areas correspond to contamination of CO_2 ice by dust at or near the surface [2,3] instead of a dark surface observed through CO_2 ice, as initially proposed. The contrast of the cryptic region with respect to brighter surrounding areas decreases after mid spring, which corresponds to a partial clean-up of the surface dust contamination [2]. A study of spectral characteristics of south seasonal deposits during retreat [4] demonstrates a complex interplay between the three main factors controlling surface albedo (CO_2 frost, H_2O frost and dust).

The dark areas show a wide range of spectral signatures, with stronger CO_2 ice bands at latitudes ~ 85° S ("A" type) than at latitudes of ~80°S or less ("B" type). Region A also exhibits much stronger signatures of the venting process which results from sub-ice surface heating, leading to the formation of fans, spots and spiders [5, 6]. A series of coordinated observations of the south seasonal has been set up combining OMEGA/Mex, CRISM/MRO, HIRISE/MRO and THEMIS/Odyssey. We report the results of this coordinated campaign for heavily dust contaminated areas ("B" type) which provide new insights on the origin of the highly heterogeneous dust contamination of the surface of the CO_2 ice layer in the cryptic region and its interannual variability. Observations after mid-spring have been focused on the evolution of H_2O ice deposits, which nearly disappear before the summer equinox, according to OMEGA observations during previous martian years.

Combined observations of the cryptic region in mid-spring: areas in cryptic region B exhibiting a rapid decrease of spectral signatures of CO_2 ice in early southern spring have been selected for oibservations by OMEGA, CRISM, HIRISE and THEMIS (Fig. 1). These observations indicate that dust contamination follows a pattern similar to that observed in cryptic region A, but with smaller spot sizes and an onset of spot formation very early after equinox, when the Sun begins to rise over the horizon.

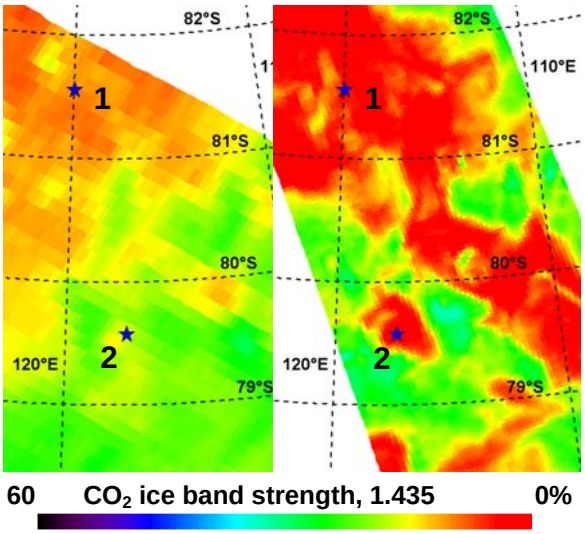

Figure 1: spectral signatures of CO2 ice at Ls 190° (left) and Ls 225° (right) observed by OMEGA in 2007. Two regions of interest showing a strong increase in surface dust contamination ("1": 120°E, 81.55°S and "2": 117°E, 79.55°S) have been selected for combined observations.

In cryptic region "B", the pattern of spots is defined very soon after the sun rises. Once established, it appears very stable with time. The dust contamination, initially mainly confined to the vicinity of spots, spreads over the whole area in mid spring, when the contrast in albedo is strongest (Fig. 2)

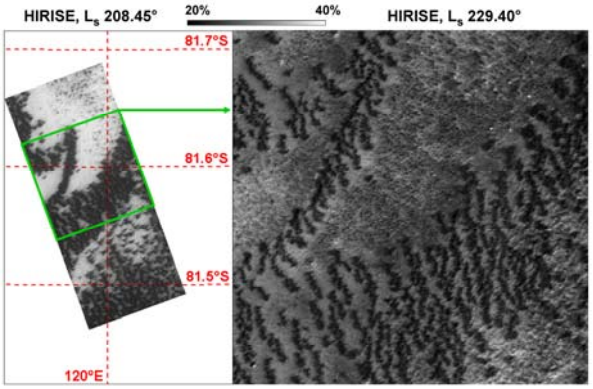

Figure 2: evolution of ROI A from early spring (left) to mid-spring (right) as observed by HIRISE. The spot pattern persists with smaller spots and a weak contrast

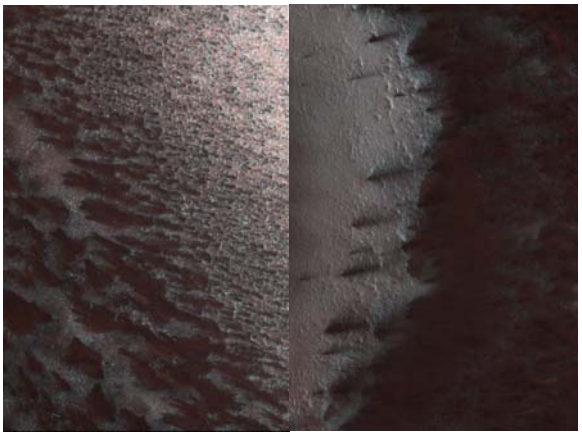

Figure 3: image of ROI 2 by HIRISE at Ls 222°; left: southmost areas; right: northmost areas.

HIRISE observations in mid-spring of ROI 2, which is at a lower latitude than ROI 1 (79,55°S instead of 81.55°S), reveal a significantly different pattern (Fig. 3), with spots of all sizes (to the South) and widespread dust contamination even in spot free regions (to the North). This dust contamination can be attributed to redistribution of dust from the spot covered areas and to a scavenging process of aerosols by precipitation of water ice at latitudes lower than 80° [7].

The post cryptic phase: After mid-spring, the albedo contrast between the cryptic region and the bright areas of the seasonal cap decreases.

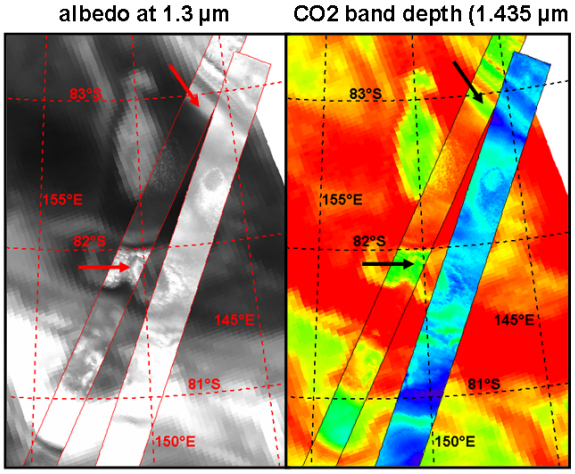

Fig. 4: OMEGA observations of cryptic region B after mid-spring; two higher resolution tracks obtained in 2009 at Ls 208.3° (left of center) and Ls 239.3° (right of center) are superimposed over a lower resolution spectral image obtained at Ls 215.4° in 2007

Observations by OMEGA (Fig. 4) and CRISM (Fig. 5) demonstrate that this is linked to a decrease in surface dust contamination. At Ls ~ 240°, ROI 1 has recovered spectral and albedo characteristics similar to that shortly after equinox. OMEGA observations reveal overall similarities and some discrepancies in the pattern of light and dark areas in 2007 and 2009.

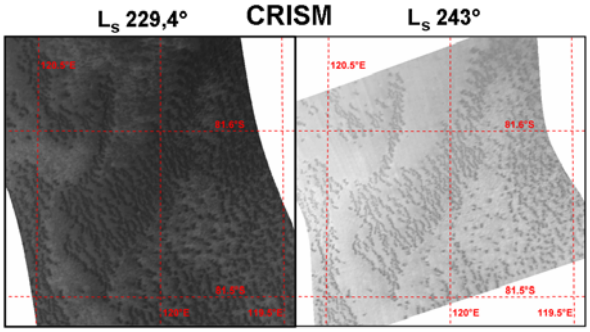

Fig. 5: CRISM, ROI 1 after mid-spring.

Conclusion: Observations of the cryptic region of the south seasonal cap during spring reveal a very complex and dynamic environment. The sublimation of CO_2 ice and the sedimentation of H_2O frost then its sublimation are strongly linked to the evolution of surface dust contamination. As soon as the sun rises over polar regions, a venting process deposits dust on the surface, initially confined close to vents (fans and spots). Until mid-spring, dust is redistributed by CO2 ice sublimation in the cryptic region, which leads to an overall decrease of the albedo. Additional widespread dust contamination can be attributed to a scavenging process by H2O ice aerosols. After mid-spring, the increasing solar flux triggers a clean-up of surface layers, small particles being carried away from the cap while larger particles sink progressively towards the underlying surface [1, 5].

The remaining major puzzle is the origin of the strong surface variegation between brighter and darker areas, with a pattern which exhibits overall consistency over several martian years. Early sedimentation of H_2O or CO_2 frost in the fall, before the onset of direct CO_2 condensation, would effectively protect the surface from the first rays of the Sun in spring. The larger thermal inertia of near surface water ice could play a role in preventing the formation of frost in the fall in specific areas.

References:

[1] H.H. Kieffer et al., *JGR* 105, 9653 (2000);
[2] Langevin et al., *Science* 307, 1581-1583 (2005);
[3] H.H. Kieffer et al., *Nature* 442, 793 (2006) ;
[4] Langevin et al., *J. Geophys Res.* 112 E08S12 (2007) , [5] H.H. Kieffer, *JGR* 112 E08005 (2007),
[6] S. Piqueux et al., *JGR* 108, E8 3-1 (2003), [7] M. Vincendon et al., *Icarus* 196, 488 (2008)

Seven years of observations of Martian Seasonal Caps onboard Mars Odyssey by HEND instrument.

M.L. Litvak[1], W.V. Boynton[2], A.S. Kozyrev[1], I.G. Mitrofanov[1], A.B. Sanin[1],V. I. Tretyakov[1], A. Varenikov[1], D. Golovin[1] [1]Space Research Institute, RAS, Moscow, 117997, Russia, litvak@mx.iki.rssi.ru, [2]University of Arizona, Tucson, AZ 85721, USA.

Introduction: Analysis presented in this study is based on neutron spectroscopy data gathered with HEND/GRS instrument onboard Mars Odyssey. Starting from 2002 this mission passed through primary and several extended phases getting more and more science data including results of global mapping of Martian neutron albedo. It is very efficient technique for exploration of water ice distribution [1-6] as well as for observation of martian seasonal caps [7-9]. Hydrogen in the upper (1-2 m) layer of subsurface in polar areas is very efficient moderator of fast and epithermal neutrons which are produced by Galactic Cosmic Rays. It leads that neutron albedo (above thermal neutron energy range) is very low in high latitude areas of Mars [1-6]. But it is true only for summer period of time when CO_2 is not condensed on the ground from atmosphere. Presence of seasonal dry CO_2 frost with thickness more than several centimeters up to 1 m changes the structure of subsurface and distribution of water ice in upper layers of regolith causing significant variations of neutron flux. These variations may be used for observations of growing and sublimation of Martian snow caps.

Data Analysis: At near polar latitudes difference in neutron flux value between summer and winter seasons may achieve as high as 3-5 times and ~20% at the border of snow cap. It means that counting statistic in neutron detectors may be used to map contours of snow caps at different seasons to be valid to discover areas with presence of > 5 g/cm^2 of CO_2 frost.

But to convert counts in neutron detectors to real physical values such as column depth (g/cm^2), mass, density it is necessary to use more complicated approach based on numerical modeling of nuclear processes happened when neutrons are produced, scattered and captured in martian regolith, atmosphere and spacecraft body. Comparison between modeled counting rate (numerically simulated for the given model of regolith + CO_2 frost) and observed counting rate (in HEND detectors) is the main factor to extract best fit parameters of model: water ice distribution and column density of CO_2 frost (see example on figure 1-2).

Now Mars Odyssey operates at Martian orbit more than 7 years which corresponds to 4 Martian years. It has been used to search for inter annual variations of seasonal cycles trying to compare dimensions and thickness of snow caps for different Martian years.

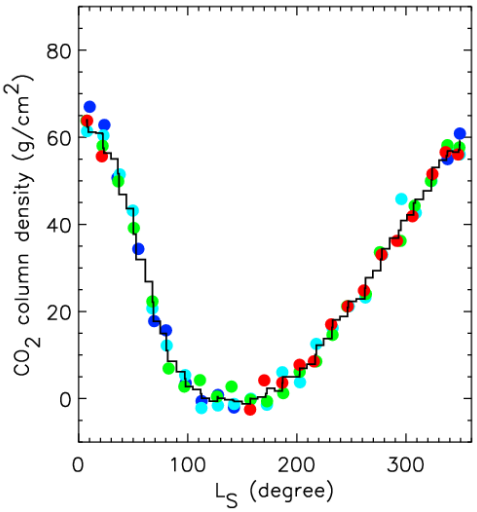

Fig. 1. The seasonal profile (deconvolved from HEND data) of snow depth at north polar latitudes. Color circles correspond to different Martian years; black curve is average seasonal profile for fourth Martian years.

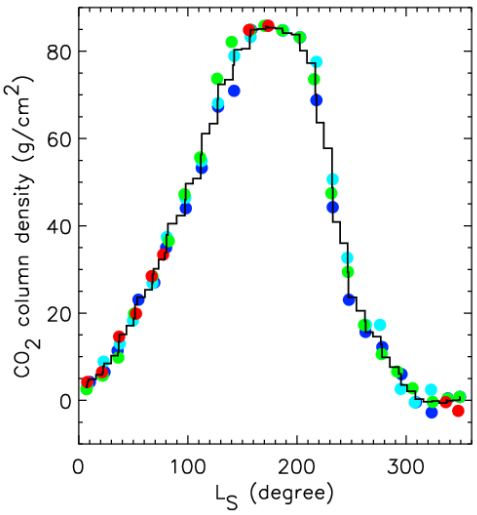

Fig. 2. The seasonal profile (deconvolved from HEND data) of snow depth at south polar latitudes. Color circles correspond to different Martian years; black curve is average seasonal profile for fourth Martian years.

Results: Concluding results of our investigations we may list them in the following order:

1) Using of neutron counting statistic to follow up contours of Martian snow caps for different seasons.

2) Comparison with the visual and infrared observations.

3) Modeling of snow caps with estimations of column density and mass of snow deposit.

4) Comparison with other nuclear instruments such as NS, GRS and climate models.

5) Calculation of volume density through comparison with MOLA.

6) Search of inter annual variations in growing/sublimation of snow caps and thickness of snow deposit.

References: [1] Feldman W.C. (2002), *Science*, 297, 5578, 75-78. [2] Mitrofanov I.G et al. (2002), 297, 5578, 78-81. [3] Boynton W.V. et al. (2002) *Science*, 297, 5578, 81-85. [4] Mitrofanov I.G. et al. (2003) *Science*, 300, 2081-2084. [5] Litvak M.L. et al. (2006) *ICARUS*, 180, 1, 23-37. [6] Feldman W.C. et al., (2004), 109, *J. Geophys. Res*., E09006. [7] Feldman, W. C., et al. (2003) *J. Geophys. Res*., 108. [8] Kelly N. J. et al (2006) *J. Geophys. Res*., E03S07. [9] Litvak M.L. et al (2007) *J. Geophys. Res*., E03S13.

PUSHING FROST UPHILL : THE MARTIAN POLAR CO_2 CYCLE AS A HEAT ENGINE.

R. D. Lorenz[1], [1]JHU Applied Physics Laboratory, 11100 Johns Hopkins Road, Laurel, MD 20723, USA. (Ralph.lorenz@jhuapl.edu).

Introduction: The first steam engines were built to raise water against gravity. The Martian seasonal frost cycle entails the evaporative removal of some $3x10^{15}$kg of material from the northern lowlands, its transport as gas through the atmosphere, and its deposition as snow or frost some 5km higher up in the south, and vice-versa : a cycle entailing considerable mechanical potential energy. While thermodynamic models have been applied to Martian dust devils, the concept of a heat engine has not been quantitatively applied to the Martian seasonal cycle. I discuss the energetics and entropy budget of this process.

Frost Cycle: The frost cycle on Mars has been observed from Earth for centuries. Orbital measurements (e.g. MGS laser altimeter data [1]) show that about 1m of material is deposited polewards of about 60^o, corresponding to ~$3x10^{15}$kg of snow. The cycle is not quite symmetric, for two reasons. First the orbital eccentricity makes southern summer hotter but shorter in duration. Second, the northern summer entails deposition of heat at a lower altitude (and thus a higher pressure). The thermodynamic implications of this have not received much attention in the literature.

Energetics: Whatever the climatic details of albedo effects, partitioning into sensible heat, radiation to space etc., the net effect of the seasonal cycle is to evaporate the material. With a latent heat of ~575 kJ/kg, this amounts to $1.7x10^{21}$ J, or about 10 MJ/m^2 of heat (per cap sublimation) averaged over the area of the planet. For the northern summer, the uphill transport of CO_2 yields 400 kJ/m^2, or a thermodynamic efficiency of 4% (this assumes the material is deposted on the surface as frost – if the material condenses at higher altitudes, more potential energy is generated, but is lost as frictional dissipation as the snowflakes descend.) Averaged over the surface of Mars, the mechanical work generated (and dissipated) by this transport is ~6mW/m^2.

Engine Efficiency: The 5km difference in elevation between northern lowlands and the south (ignoring the very localized topography of the permanent caps) leads to a pressure difference of about 50%, or in engine terms, a compression ratio (CR) of 2. The ideal thermodynamic efficiency of an engine is $1-(1/CR)^{\gamma-1}$, with γ the ratio of specific heats (1.28 for CO_2). Thus the ideal efficiency is ~18%.

Comparison with Earth's Hydrological Cycle: Water substance is evaporated at the surface and forms clouds and precipitation. To a first order 1000kg (1m) of water is evaporated per m^2 per yr and is raised a few km before condensing : if 3km is adopted the dissipation corresponds to $3x10^7$ J/m^2 or ~1W/m^2 (though [2] gives ~2) This may be compared with the latent heat involved ~$2x10^9$ J/m^2/yr to give a thermodynamic efficiency of only ~1.5%. Why so low? A factor may be the fact that the condensable is a minor constituent, so that its dilution after evaporation generates entropy by mixing [3] – this process may be factor on Mars as well, since Argon and Nitrogen can build up locally as the frost caps form (e.g. [4]).

Comparison with Frictional Dissipation: The mechanical work dissipated by surface friction is ~$1/2\rho C_d V^3$, where for Mars ρ~0.02 kg/m^3, and we assume a typical drag coefficient C_d~0.003. Note that a mean windspeed should not be used uncritically as the result depends on the cube of windspeed (i.e. the dissipation may be dominated by the high speed tail of the wind probability distribution [5]) – the Viking windspeed statistics [6], we suggest $<V^3>^{1/3}$~10m/s. As a result the frictional dissipation is ~0.03 Wm^{-2}. On Earth, the corresponding quantity is of order ~$2Wm^{-2}$ [7,8,9] Thus on Earth, the vertical transport of condensable material causes mechanical dissipation comparable with friction at the surface, but on Mars the condensable cycle is only about 2% as important.

Conclusions: The thermodynamic efficiency of the polar cycle is comparable with, and perhaps larger than, that of precipitation on Earth. Perhaps because the condensable does not intercept the abundant sublight at low latitudes, however, the Mars frost cycle generates with a smaller proportion of the total dissipation in the climate system than water does on Earth.

References: [1] Smith, D. E., M. T. Zuber and G. E. Neumann, Science, 294, 2141-2146, 2001 [2] Pauluis, O., V. Balaji, and I. Held, J. Atmos. Sci., 57, 989–994, 2000. [3] Pauluis, O. and I. M. Held, J. Atmos. Sci., 59, 140-150, 2002 [4] Sprague, A. L. et al., J. Geophys. Res., 112, E03S02, 2007 [5] Lorenz, R. D., J. Non-Equilibrium Thermodynamics, 27, 229-238, 2002 [6] Lorenz, R. D., J. Spacecraft and Rockets, 33, 754-756, 1996. [7] Lorenz, E. N., pp. 86–92 in Dynamics of Climate, R. L. Pfeffer (ed), Pergamon Press, 1960. [8] Wulf, O. R., and L. Davis, Jr., J. Meteorology, 9, 79–82, 1952. [9] Peixoto, J. P., and A. H. Oort, Physics of Climate, AIP, 1992

Additional Information: I acknowledge the NASA AISR Program.

HIGH-ALTITUDE CO_2 CLOUDS ON MARS: OMEGA AND HRSC OBSERVATIONS. A. Määttänen[1], F. Montmessin[1], B. Gondet[2], H. Hoffmann[3], F. Scholten[3], E. Hauber[3], F. Gonzalez-Galindo[4], F. Forget[4], J.-P. Bibring[2], J.-L. Bertaux[1], and G. Neukum[5].
[1]LATMOS, Verrieres-le-buisson, France (anni.maattanen@latmos.ipsl.fr), [2]Institut d'astrophysique spatiale, Orsay, France, [3]German Aerospace Center (DLR), Berlin, Germany, [4]Laboratoire de meteorologie dynamique, Paris, France, [5] Freie Universitaet, Berlin, Germany

Introduction: The Martian climate hosts a rare phenomenon of condensation of the bulk atmosphere. CO_2 condenses on the polar ice caps, but also forms clouds in the atmosphere. The existence of low-level, convective CO_2 clouds in the polar night was indirectly discovered by MOLA [1,2] and modeled in some studies [3-5]**.** Recently several satellite instruments [6-9] have observed CO_2 clouds also near the equator, but at high altitudes where the temperatures are low enough for CO_2 condensation. Montmessin et al. [7] identified spectroscopically from MEx/OMEGA observations these high-altitude clouds to be composed of CO_2 ice crystals by modeling the CO_2 ice spectral signature that was observed in a deep CO_2 gas absorption band at around 4.3 μm. In this work we have used the OMEGA [10] and HRSC [11] observations to map the occurrences of the high-altitude CO_2 clouds and their properties. We have also compared the observations to the predictions of the LMD Mars Global Climate Model (LMD-MGCM) [12] and in particular its improved version that extends to the upper atmosphere [13].

Instruments: OMEGA is an imaging spectrometer working in the wavelength range 0.4-5.1 μm. It can operate in nadir, limb and EPF modes: in this study only nadir observations have been used. The clouds can be seen in several wavelengths in the OMEGA data: visible (0.5 μm), slightly farther in the infrared (1.3 μm) and in the near-IR CO_2 absorption bands at 2.7 and 4.3 μm. The spectroscopic identification of the clouds was done using OMEGA data [7]. The HRSC is a camera imaging the Martian surface in stereo and color. It images the surface through several channels that are looking slightly off-nadir. When atmospheric features, like clouds, are imaged through two (or more) filters, the apparent parallax of the features enables very accurate determination of the cloud altitude. The possible across-track movement of the cloud in different images, taken at slightly different times, gives an estimate of the local winds.

Results: Mars Express has acquired already more than 2.5 years of data with varying spatial and temporal resolution. The OMEGA dataset has revealed about 60 occurrences of these high-altitude CO_2 clouds. These observations show that the clouds are mainly confined to the equatorial region (20°S – 20°N) and to a quite specific longitudinal band (-120°E – 30°E, between Tharsis Montes and Terra Meridiani). Only a handful of observations lie outside these limits, most notably two clouds at midlatitudes (one at 50°S, other at 45°N). The seasonal variations are notable, since the clouds appear mainly right after the spring equinox, disappear between Ls=60°-90°, and reappear after the summer solstice. The activity seizes rapidly after Ls=150°, but one cloud has been observed at Ls=250°. When observed from high altitudes (2500 to 4000 km), the clouds show convective morphologies (roundish shapes) in about 10 cases (15%). From lower altitudes (< 500 km), the width of the OMEGA image limits the interpretation: the narrow image reveals only a part of the cloud and any extrapolation would be very difficult. However, simultaneous HRSC observations may shed light on the morphologies.

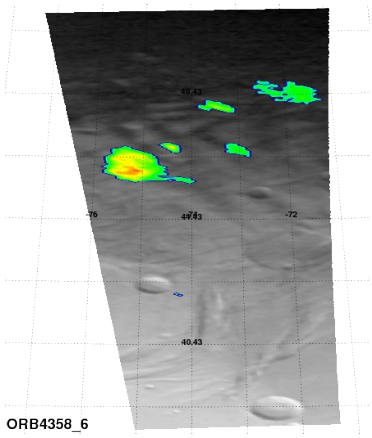

Figure 1: OMEGA observation of a convective-type cloud: the surface of Mars in grayscale and the analyzed cloud signal intensity in color.

Two shadow observations have been used to analyze the cloud optical thickness and particle size, as already mentioned by Montmessin et al. [7]. These authors also calculated the cloud altitude to be around 80 km. In our study we have also mapped the variations of these parameters inside the cloud by analyzing them pixel-by-pixel. These observations have confirmed the previous results of Montmessin et al. [7] as well as produced size distributions of the

cloud particle effective radii and optical thickness. The effective radii vary mainly in the range 1-2 μm and the optical thickness between 0.2-0.7.

The HRSC has imaged clouds in several occasions and clearly two kinds of clouds can be separated from the HRSC dataset: the low- (< 40 km) and high-altitude clouds. The low altitude clouds are thoughts to be primarily H_2O rich, while the high altitudes ones are made of CO_2, as confirmed by a simultaneous observation by OMEGA. These clouds are observed close to the equator, show similar seasonal behavior, and the hygropause level should be at significantly lower altitudes thus limiting the amount of water vapor in the upper atmosphere.

The HRSC cloud altitudes vary from 53 km to 84 km (±2 km) and they exhibit mainly cirrus-like, filamented shapes instead of convective, round shapes (see Fig. 2). The East-West cloud speed (related to the local wind speeds) range is 15-105 m/s but mainly in the range 60-90 m/s (±13 m/s). One cloud, observed in southern midlatitudes, is actually moving from West to East with varying wind speeds of 5-40 m/s.

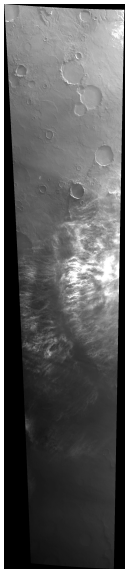

Figure 2: An example of a high-altitude cloud observed by HRSC (orbit 0567).

The cloud observations have been compared with the LMD-MGCM climatology. The MGCM shows strong diurnal temperature variations caused by the strong thermal tides in the mesosphere of Mars at the cloud altitudes. At the altitudes of our interest (60-80 km), the coldest temperatures are attained in the afternoon (16 local time) and the warmest temperatures in the morning hours (04 LT). Most of the clouds are observed in the afternoon, but in a few cases they have been observed before noon. The model reproduces the shutdown of cloud formation at Ls=60°-90°, but the reason for that is out of the scope of this study. The HRSC cloud altitude and wind observations show good general agreement with the MGCM results.

Implications: Formation of CO_2 ice clouds is known to affect the CO_2 cycle as a whole [3,4]. Although the cloud species reported here does not belong to the class of low-altitude clouds encountered in the polar night, it shares similar formation processes with the latter, and thus offers a unique opportunity to decipher the microphysical and dynamical processes at work. This in turn may help us derive a unified and robust theory for the formation of CO_2 clouds in the Martian atmosphere.

References:

[1] Pettengill, G. H. and Ford, P. G. (2000) *GRL, 27*, 609–612. [2] Ivanov, A. B. and Muhleman, D. O. (2001) *Icarus, 154*, 190-206. [3] Colaprete, A. and Toon O. B. (2002) *JGR, 107*,. [4] Colaprete, A. et al. (2003) *JGR, 108*,. [5] Tobie, G. et al. (2003), *Icarus, 164*, 33-49. [6] Montmessin F. et al. (2006) *Icarus 183*, 403-410. [7] Montmessin F. et al. (2007) *J. Geophys. Res. 112*, E11S90. [8] Clancy, T. R. et al. (2007) *J. Geophys. Res. 112*, E04004. [9] Inada, A. et al. (2007) *Icarus 192*, 378-395. [10] Bibring, J.-P. et al. (2004) *ESA SP-1240*, 37-49. [11] Jaumann, R. et al. (2007) *Planet. Space Sci., 55*, 928-952. [12] Forget, F. et al. (1999) *JGR, 104*, 24155-24176. [13] González-Galindo, F. et al. (2009) *JGR, 114*, E04001.

Additional Information: AM wishes to thank the financial support from Centre National d'Etudes Spatiales.

MODELING MICROSCALE MARS POLAR PHENOMENA RELATED TO CO_2 ICE. Tim I. Michaels[1], [1]Southwest Research Institute (Department of Space Studies, Boulder, Colorado, USA, tmichael@boulder.swri.edu).

Introduction: It is now generally understood (from decades of global-scale computer modeling work) that the details of the net energy balance of Mars' near-polar regions (particularly near/during winter) significantly modulate the planet's contemporary climate. Four broad categories of processes and phenomena comprise this regional energy balance near/during winter: Dynamics (atmospheric), radiative transfer, thermal conduction, and phase changes of volatile substances (carbon dioxide and water). All of these do not truly occur independently of one another, at times resulting in substantial feedback. Furthermore, these processes and phenomena occur at widely varying spatial and temporal scales, often with two-way feedbacks between the different scales.

Global and regional climate models must parameterize the effects of processes and phenomena they cannot resolve. Such models for Mars are increasingly requiring more realistic parameterizations to further validate/refine their solutions in the presence of substantial quantities of relevant spacecraft observations. Perhaps the most practical method of obtaining the copious information necessary to construct a more realistic Mars parameterization is to conduct microscale simulations. Such microscale model runs are performed with quite small grid-spacings (10s to 100s of meters) and are often three-dimensional, since many phenomena that occur at such small spatial scales are significantly 3-D in nature.

Targeted Phenomena: The work discussed here involves the microscale modeling of two Mars polar phenomena that are currently unable to be tackled with a global or regional climate model: (1) carbon dioxide ice clouds (and precipitation) in the polar nights and (2) the genesis of the south polar early springtime transient small-scale albedo features (e.g., dark fans, bright streaks) present in spacecraft imagery.

Observations supporting the suspected presence of clouds composed of carbon dioxide ice crystals in the lower atmosphere of Mars date to at least the early part of the Mars Global Surveyor (MGS) mission. Intriguing MOLA laser ranging results in the polar night indicate the nearly undeniable presence of populations of unidentified aerosol particles capable of reflecting or absorbing/scattering a significant portion of the near-infrared laser pulse. Furthermore, MGS radio science temperature retrievals in the polar night often exhibit regions aloft where the air temperature is significantly less than the carbon dioxide ice saturation temperature.

In the south polar region of Mars in early spring, numerous small-scale albedo features (e.g., dark fans, spots, and bright streaks) are present in spacecraft imagery. These features can change relatively rapidly (e.g., [2]), an observation that constrains potential genesis processes. The formation hypothesis proposed by [2], which entails a pressurized venting (or "jet") of carbon dioxide gas and entrained dust through weaknesses in the overlying CO_2 ice sheet, is explored here via microscale modeling. In such a scenario, much of the dust should preferentially deposit onto the ice surface downwind of the vent site, and a bright streak originating at the vent may be due to CO_2 snowfall resulting from a jet event.

Methodology: The quasi-idealized microscale mode of the Mars Regional Atmospheric Modeling System (MRAMS; [1]) is used here. Capabilities relevant to this work include non-hydrostatic dynamics, a size-resolved aerosol microphysics submodel (CO_2 ice and dust species; also subject to turbulent diffusion, advection, and gravitational sedimentation processes), and a detailed surface/subsurface model.

The quasi-idealized carbon dioxide cloud simulations were initialized with a plausible thermodynamic sounding and surface/subsurface characteristics from a relevant mesoscale model (MRAMS) run. Cyclic lateral boundary conditions were employed, the vertical and horizontal grid spacings were 50 meters, and no topography was imposed. Random potential temperature perturbations of 0.1 K were imposed on the initial state at the vertical level nearest the surface. A initial mean wind (isotropic with height) of 5 m/s was also specified.

The carbon dioxide jet simulations were also quasi-idealized, with cyclic lateral boundaries, and no topography. A grid spacing of 0.5 meters was employed, and the jet was initialized in varying ways as a warm, dusty mass of gas with a specified vertical velocity at the model level nearest the surface.

Preliminary Results: Carbon dioxide clouds of a convective nature are evident (dominant) in the cloud simulations, and often exhibit precipitation streamers. The carbon dioxide jet simulations exhibit many characteristics similar to the observed surface albedo features.

References: [1] Rafkin, S. C. R. et al. (2001) *Icarus, 151,* 228–256. [2] Kieffer, H. et al. (2006) *Nature, 442,* 793–796 .

SIMULATING THE MARTIAN CO2 CYCLE WITH THE LMD GLOBAL CLIMATE MODEL. E. Millour[1], F. Forget[1], B. Diez[2] and L. Montabone[3], [1]Laboratoire de Météorologie Dynamique, UMR 8539, IPSL, Université P.&M. Curie, BP99, 4 place Jussieu, 75252, Paris Cedex 05, France, ehouarn.millour@lmd.jussieu.fr, [2]Centre d'Etude Spatiale des Rayonnements, 9 avenue Colonel Roche, BP 44346, 31028 Toulouse Cedex 4, France, [3]Department of Physics and Astronomy, The Open University, Milton Keynes, UK

Introduction: The carbon dioxide (CO_2) Martian atmosphere undergoes large-amplitude seasonal variations due to CO_2 condensation and sublimation in the polar regions. This atmospheric mass cycle, present in surface pressure measurements (such as those obtained by the Viking landers), is clearly a first order effect which must be well represented by Global Climate Models (GCMs) which aim to realistically represent the Martian climate and meteorology.

The Martian GCM developed at LMD [1] is constantly evolving (thanks to numerous and ongoing collaborations) and improved [2]. We present here some of these developments such as the inclusion of realistic subsurface water ice tables in the polar regions, taking into account the impact of CO_2 condensation in the atmosphere (clouds) and including the effect of non-condensable gases. We moreover show and discuss how comparisons between the simulated CO_2 cycle and Viking Lander surface pressure measurements can be used to constrain some of these parameterizations.

CO_2 condensation and subsurface thermal processes in the LMD GCM: The LMD GCM [1,2] includes condensation of CO_2 on the surface (condensation and sublimation of polar caps) as well as a scheme [3] for CO_2 condensation (clouds) , the effect of the presence of non-condensable gases [4,5] and the inclusion of realistic subsurface water-ice tables in the polar regions.

Non condensable gas enrichment and depletion: The model includes a parameterization of non condensable gas enrichment suitable for GCMs which is combined with a modified convection scheme able to simulate the convection forced by the enrichment of lighter gas near the surface. This scheme, combined with recent improvements of the GCM's dynamical core, yields non condensable gas enrichments which compare well with available data [4,5].

Condensation of atmospheric CO_2 into CO_2 clouds: The GCM includes a parameterization [3] for CO_2 condensation of the atmosphere on the ground, but also in the atmosphere, allowing for sedimentation (and possible sublimation) of CO_2 particles. This parameterization which is based on physical considerations (radiative transfer through the CO_2 ice particles and snow metamorphism on the ground) reproduces accurately the general behavior of measurements obtained by Mariner 9 and Viking during the polar nights of both hemispheres.

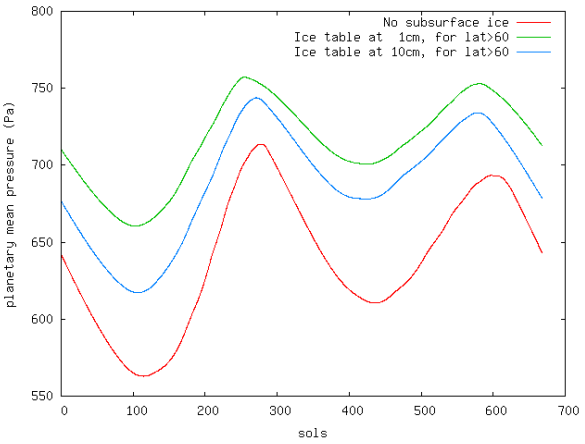

Figure 1: Annual planetary mean surface pressure obtained by the model without subsurface ice tables (red) and when high thermal inertia water ice tables are added 1cm (green) or 10cm (blue) below the surface in the polar (latitudes above 60°) regions.

Thermal conduction in heterogeneous soil: The model has always included thermal conduction in the Martian soil (which acts as a thermal reservoir which stores and restores heat to the surface) but until now the subsurface was considered to be homogeneous (and of properties set to the known surface values).We have recently improved the representation of thermal conduction in the subsurface of the model by switching to a scheme which includes the possibility of varying the thermal properties (volumetric specific heat C and conductivity λ, or equivalently thermal inertia $I=(C.\lambda)^{1/2}$) of the soil. With this implementation, we can now directly include some (high thermal inertia) water-ice tables in the GCM.

The importance of the presence of subsurface polar ice tables which act as thermal reservoirs, storing and restoring large amounts of heat, and thus significantly affect the Martian CO_2 cycle has been demonstrated in [6]. An illustration of this effect is shown in Figure 1 which displays the annual CO_2 cycle obtained with a homogeneous soil (no subsurface ice table) and tuned (emissivities and albedos of polar caps are constrained so that the resulting cycle matches Viking Lander surface pressure measurements, see next section), and the

CO_2 cycles obtained if ice tables (high thermal inertia: I=2000 $J.s^{-1}.m^{-1}.K^{-1}$) are added 1cm or 10cm below the surface of polar regions. In the latter cases the model has not been retuned and less CO_2 is trapped in the polar caps since the subsurface ice layers act as thermal reservoirs which provide heat to the surface during fall and winter.

The next step is obviously to include realistic maps of the ice tables in the model. Such maps have been derived using measurements by the Mars Odyssey Neutron Spectrometer (MONS): of the abundance of hydrogen near the surface [7,8] and an inversion model [9]. Unfortunately these maps describe the shape of the ice tables but not the exact geometrical depth at which they lay (to derive this depth accurately would require precise knowledge of the macroscopic absorption cross section of the ice-poor upper layer of soil). It is however possible to constrain the latter, as discussed in the next paragraphs.

Using the Viking Lander surface pressure measurements to constrain parameterizations and parameters: The Viking Landers have almost continuously monitored the Martian surface pressure over almost two Martian years for Viking Lander 2 and more than three Martian years for Viking Lander 1. This dataset is extremely useful to help constrain and validate GCM parameterizations.

In [10] is described an automatic procedure which minimizes differences between model output (a few control simulations) and Viking Lander 1 surface pressure and yields optimal values of "free" parameters such as polar cap albedos and emissivities. Since (as mentioned above) the exact depth at which the polar H_2O ice tables lay is not known, we have extended the best-fit procedure to include theses depths as parameters for the fit (the shapes of the ice tables remain those derived by [9]). An illustration of the results of the minimization process is given in Figure 2: although the process is 4 dimensional (minimization is with respect to Northern cap albedo AN, Southern Cap albedo AS and coefficients DN and DS which represent proportionality constants to apply to the Mars Odyssey maps to determine the true depth at which the ice table of each hemisphere lays), only the effect of parameters DN and DS are displayed. We find that a best fit is obtained when DS is large (i.e. the ice table in the southern hemisphere is buried deep) and DN minimum (i.e. the ice table in the northern hemisphere is barely buried).

Failing to obtain any clear minimum for coefficients DS and DN (unlike cap albedos values which minimize the fit when AN=0.52 and AS=0.42) hints to the fact that further improvements are required before our procedure can be applied to obtain trustworthy ice table depths. This is currently subject to ongoing work; we are, among other things, considering the possibility of switching to more realistic albedo maps (instead of the cruder approximation of fixing a globally constant value for each cap).

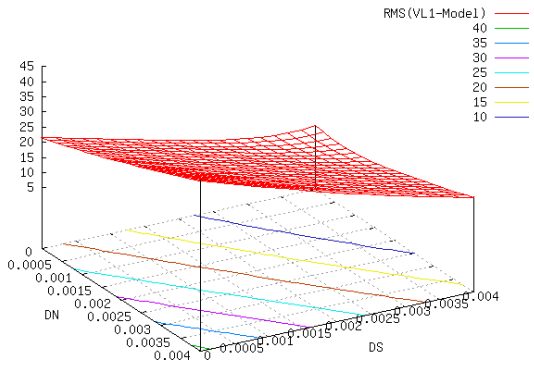

Figure 2: Illustration of the minimization process: Control simulations (with fixed, extreme cases, of parameters AS and AN, respectively southern and northern cap albedoes –not shown here- and DS and DN, proportionality coefficients of the depth at which southern and northern polar ice tables are buried) are used to establish synthetic outputs of what the surface pressure at Viking Lander 1 site would be in intermediate cases. Minimizing the RMS between the modeled output and measured surface pressure by Viking Lander 1 then provides optimal values of the coefficients.

References: [1] Forget F. et al. (1999) *JGR, 90, 104, E10* [2] Forget F. et al. (2008) *Third International Workshop on the Mars Atmosphere, Abstract N°1447, p9029.* [3] Forget F. et al. (1998) *Icarus, 131, 302-316* [4] Forget F. et al. (2008) *Third International Workshop on the Mars Atmosphere, Abstract N°1447, p9106* [5] Forget F. et al. (2009) *This Workshop* [6] Haberle R. M. et al. (2008) *Planetary and Space Science, 56, 251-255* [7] Feldman W. C. et al. (2002) *Science, 297, 75-78* [8] Feldman W. C. et al. (2004) *JGR, 109, E09006* [9] Diez B. et al. (2008) *Icarus, 196, 409-421* [10] Hourdin F. et al. (1995) *JGR, 100, 5501-5523*

A PHYSICAL MODEL OF SURFACE CO_2 ICE: NEW CLUES TO DARK SPOTS FORMATION.

C. Pilorget[1], F. Forget[1], E. Millour[1] and J-B. Madeleine[1]
[1]Laboratoire de Météorologie Dynamique, Université Paris 6, BP 99, 75005 Paris, France
(cedric.pilorget@lmd.jussieu.fr)

Introduction: Observations of the southern and northern seasonal caps have revealed the presence of dark spots and fans. These exotic features with no equivalent on Earth could result from the characteristics and behavior of solid CO_2 on Mars. A proposed explanation is that solar flux penetrates into the CO_2 ice and heats the regolith. Once the sublimation temperature is reached at the bottom of the slab, gas forms and tries to escape. When a path to the surface is created, CO_2 gas and dust are ejected, forming these dark spots [1].

The full model that we developed solves conduction, radiation and mass evolution equations in the CO_2 slab as well as in the underlying regolith.

In this paper, we present some simulations results aiming at better understanding these exotic features. We first investigate on the validity of the scenario previously described on the "Manhattan Island" region example and then try to understand why dark spots appear at some places and not another on Mars.

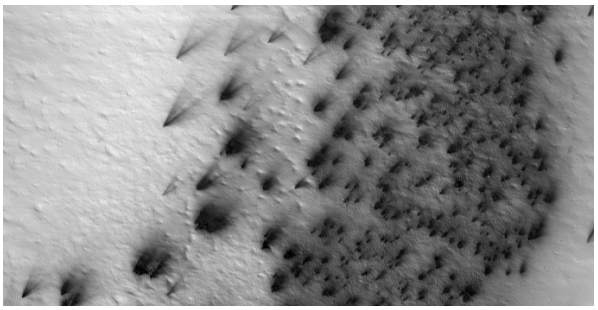

Figure 1: *HiRISE picture of the South part of the Manhattan Island region (99.0°E, -87.0°S) at Ls=188.2° (NASA/JPL/University of Arizona)*

Modeling CO_2 polar caps evolution: Our model is a 1D, time-marching model aiming at simulating the details of the physical processes controlling the thermodynamics of surface CO_2 ice on Mars.

Its vertical computational grid is a dynamic layer grid where layers have their own thermal and optical properties. The vertical resolution is 1cm. Two models have been used to simulate the solar flux penetration into the CO_2 ice: a radiative transfer code, which allows us to simulate different scenarios, with different CO_2 ice properties (CO_2 grain radius, amount of dust, dust grain radius), and a translucent slab model derived from [1] model.

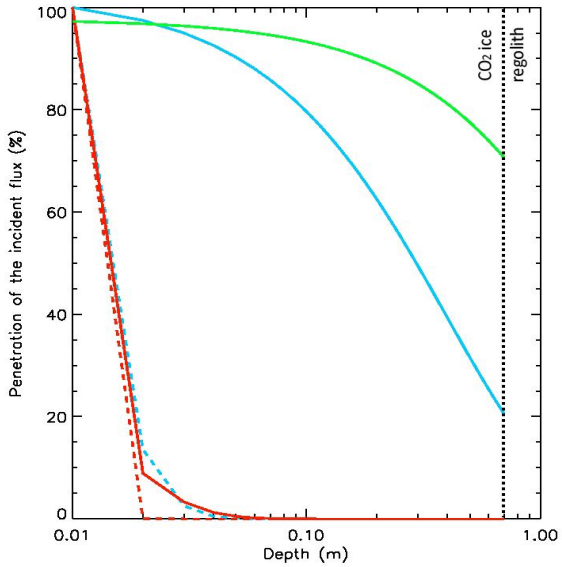

Figure 2: *Penetration of the solar flux in a 70cm CO_2 ice layer for different ice properties. Incident solar angle was set to 60°. In blue: effective grain radius: 20cm; in red: effective grain radius: 100µm; in green: "translucent slab model"; solid line: no dust; dashed line: 500ppmw of dust.*

Our model takes into account the solar flux (0.1−5µm), the thermal flux, the thermal emission, the sensible heat flux, the geothermal heat flux, and the latent heat flux when there is a phase transition. In a case of running simulations on a slope, another term related to the thermal emission and reflexion from surrounding terrains is added [3].

The radiative model is coupled to a complete parametrization of heat conduction and storage by CO_2 and regolith. We also took into account the modification of the thermal et optical behavior of the layers in case there were gas between the CO_2 ice and the regolith.

Different scenarios can be therefore very easily simulated.

Simulating the "Manhattan Island" region conditions: "Manhattan Island" region is centered at 99°E, -86.25°S and follows the classic TES "cryptic" behavior of low albedo while remaining near the CO_2 ice temperature [4]. Based on OMEGA observations

[5], we simulated the behavior of the seasonal cap in this region. Our model confirms that in the case of large CO_2 ice grains and low dust content (which corresponds to OMEGA results in the cryptic region at the end of the polar night), photons penetrate into the CO_2 ice slab and reach the regolith. Model also confirms the fact that the temperature of the slab and the regolith progressively increases after the end of the polar night (which occurs at about Ls=171°), until reaching the sublimation temperature at the bottom of the slab and gas forms. Sublimation also occurs at the same time at the surface but about 5 times slower.

Dark spots can be seen on THEMIS images at Ls=176° [4] and might even appear sooner. Our results show that CO_2 ice properties play an important role on the time of the first gas ejection. The cleaner the CO_2 ice is and the larger the CO_2 ice grains are and the sooner the first gas ejection occurs. Furthermore, the incidence of the terrain as well as its orientation have important effects too, since the incidence angle of the photons, but also the CO_2 ice accumulation during winter depend on these parameters. However, soil thermal inertia seems to have a small impact on the time of the first gas ejection. Indeed, a regolith with a low thermal inertia is much easier to heat, but the amount of CO_2 that condensates during winter is also greater. Photons thus reach the regolith in a smaller proportion. Ground albedo, as well as the optical depth of the atmosphere also play a role but simulations show that their influence is limited.

Investigating dark spots formation requirements on Mars: For different places at the same latitude, simulations results tend to prove that only CO_2 ice properties have a major impact on the sublimation process. Other parameters mostly have an impact of the time of the first gas ejection but do not determine if sublimation at the bottom of the slab occurs or not. This would suggest that dark spots formation highly depends on the condensation process during winter (atmospheric CO_2 condensation, dust and water ice deposition, etc.) [6][7].

As for the impact of latitude, many questions were arisen. Dark spots can be observed on the polar caps at many northern and southern latitudes. [8] mentions the presence of a northern dark region which could have the same nature as the "cryptic" sector in the south polar cap. Still, fewer seasonal and perennial features are observed in the north compared to the south [9]. We tried to better understand this feature by running simulations at different northern and southern latitudes. Simulations results tend to prove that for equivalent CO_2 ice properties, dark spots are as likely to occur in the south as in the north.

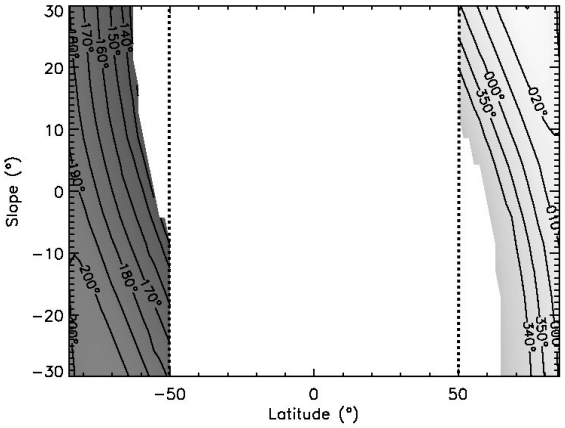

Figure 3: *Time of the first gas ejection for effective CO_2 ice grain radius set to 20cm and no dust, at high latitudes (>50°). Positive slope values are for north oriented slopes and negative values for south oriented slopes. First gas ejection was assumed to occur when the thickness of the CO_2 gas layer reaches 1cm. Surface pressure was respectively set to 400Pa and 1000Pa for the southern and the northern latitudes.*

Conclusion: The model that we developed gives some interesting clues to better understand the dark spots formation process.

First of all, simulations results show that [1] model is plausible and that for certain CO_2 ice properties (like the one that are observed by OMEGA for instance) sublimation of the CO_2 ice slab from the bottom occurs.

In a general way, simulations results tend to show that dark spot formation is highly linked with the CO_2 ice properties. Other parameters mostly have an impact of the time of the first gas ejection but do not determine if sublimation at the bottom of the slab occurs or not.

References: [1] Kieffer (2007) *JGR*, *112*, E08005. [2] Forget et al. (1999) *JGR*, *104*, 155-176. [3] Spiga and Forget (2008) *GRL*, *35*, 15. [4] Kieffer et al. (2006) *Nature*, *442*, 793-796. [5] Langevin et al. (2007) *JGR*, *112*, E08S12. [6] The OMEGA team et al. (2009), *Icarus*, *200*, 374-394. [7] Colaprete et al. (2005), *Nature*, *435*, 184-188. [8] Kieffer and Titus (2001), *Icarus*, *154*, 162-180. [9] Piqueux and Christensen (2008), *JGR*, *113*, E06005.

BASAL SUBLIMATION AND VENTING OF THE NORTH TRANSLUCENT ("CRYPTIC") SEASONAL CAP. S. Piqueux[1] and P.R. Christensen[1], [1]Arizona State University, School of Earth and Space Exploration, Mars Space Flight Facility, 201 E Orange Mall, Tempe AZ, 85287, USA, sylvain.piqueux@asu.edu.

Introduction: The gas venting model of the south seasonal cap developed by [1,2,3] predicts the erosion of the surface of the polar layered deposits, leading to the formation of spiders, and the redeposition through atmospheric settling of dust and/or sand in the vicinity of the spiders (fans and spots), where the seasonal cap is translucent. So far, little work has focused on northern seasonal processes despite numerous similarities with the South [4].

North translucent ice: [5] mention the presence of a northern dark region on the seasonal cap between Ls = 357° and Ls = 60° characterized by an albedo as low as of 0.21 and a CO_2 ice temperature of 152 K. [6] attribute spectra of the north cap acquired by TES to the presence of a transparent slab of CO_2 ice. This dark and cold region (NTSC) is an equivalent of the southern cryptic region. This northern cryptic region is visible between 135°E and 225°E and latitudes 80°N to 85°N, mostly on the polar erg. The TES albedo of the seasonal cap between Ls = 0° and Ls = 10° is shown on Figure 1. Before Ls = 350°, the seasonal cap's albedo is fairly uniform with a typical albedo of 0.40. This darkening has been observed during the 3 consecutive years of TES observations. After Ls = 45°, most of the translucent cap has brightened and displays an albedo of 0.35. After Ls = 60°, the NTSC is not visible anymore and most of the seasonal cap has sublimed away.

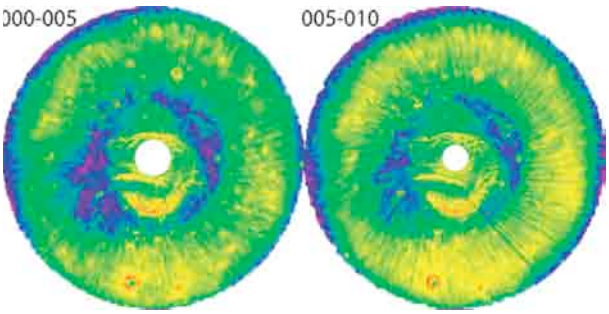

Figure 1: albedo of the north seasonal cap from 90N to 60N by TES from Ls 0 (left) to 10 (right). Albedo values range from 0.65 (red) to 0.15 (purple).

Seasonal features on the cap: The basal sublimation and venting of the south seasonal cap where the cap is translucent lead to the formation of spots, fans, and dark polygons. Temperature data by THEMIS shows that the darker regions of the seasonal cap display a temperature that is consistent with a thin layer

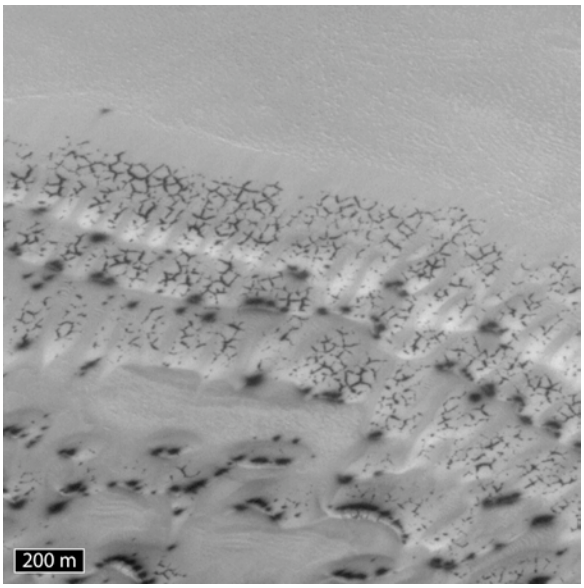

Figure 2: Example of polygons and spots on the North seasonal cap. E2000185, 85.0N, 194.4E, Ls = 64.

(e.g. a few 100s of microns thick) of particulate material in thermal contact with the underlying cap [3]. Similar observations are made during the spring on the North seasonal cap: spots, fans and polygons form where the cap is translucent (Figures 2 and 3). Temperature data by THEMIS shows a clear temperature difference between the bright and dark CO_2, also suggesting that a thin layer of dust coats the cap where it is translucent (Figure 5).

North/South differences: Despite these many similarities, suggesting that the venting model of the cap originally developed for the South also applies to the North, some striking differences must be noticed. First, no spider has positively been identified on the northern polar layered deposits or surrounding terrains. Then, less fans and spots are observed in the North, and no bright fans are visible. Kilometer size dust streaks are commonly associated with defrosting patterns on dunes, suggesting that these aeolian features are a major source of dust (Figure 4). Finally, TES data suggests a large temporal variability of the albedo of the cap shortly after the sun rises.

These differences may partially be explained by the reduced amount of solar energy available near the pole during the northern summer when compared to the southern summer (~20%), the reduced time when the cap is translucent in the North when compared the South [4], a possible difference in the thickness (and

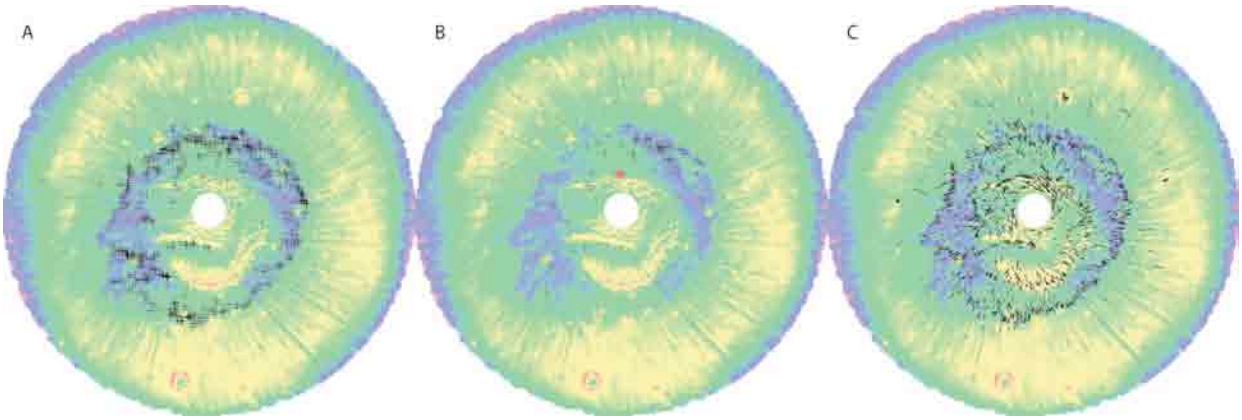

Figure 3: Distribution of (a) fans and spots, (b) dark polygons and possible spiders (red dot) and (c) data used for the mapping of (a) and (b). Background is a contrast reduced TES Lambert albedo Ls = 5° and Ls = 10°, 87°N to 60°N.

therefore mechanical properties) of the South and North seasonal caps [4], which is supported by GCM models [7] and GRS data [8] (but not by MOLA data [9]), a difference of mechanical properties of the substrate, and other unidentified reasons.

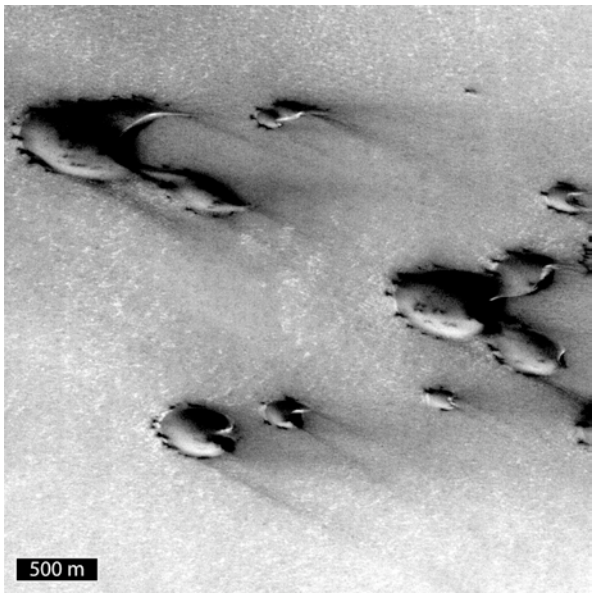

Figure 4. Dust streaks downwind from defrosting dunes. S1501866, 76.8N, 241.5E, Ls = 14.

Conclusions: The south translucent (cryptic) cap has focused most of the attention of the recent polar campaigns [3,9] and studies. The 2008-2009 coordinated polar campaign using OMEGA, CRISM, HiRISE, CTX and THEMIS promises to provide an unprecedented level of constraints on active polar processes. Here, we argue for a similar campaign targeting the North translucent ice, which is shown to present many similarities with the southern "cryptic" region. Future observations should monitor the distribution, magnitude and evolution of 1) the cap's surface dust and 2) water ice contaminations, of 3) the physical properties of the CO_2 ice, of 4) the small scale characteristics of the dark seasonal features forming on the cap (spots, fans, polygons), 5) of the small scale perennial features carved on the frozen polar terrains (etched polygons, [4]), and 6) of the aerosol concentration in the lower atmosphere above the seasonal ice. Whether or not the North seasonal cap physical characteristics are as diverse as the southern cap is not clear. A proper model of seasonal cap evolution will have to satisfy the constraints provided by both North and South observations.

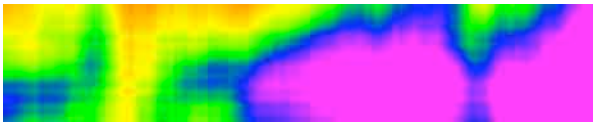

Figure 5: Apparent temperature variations of the North seasonal cap; image I02487005 (purple is at ~148K and red is at ~ 151K), near 76N, 290E, Ls = 38. Warmer surfaces correlate with regions of lower albedo, corresponding to a thin layer of dust in thermal contact with the underlying CO_2.

References: [1] Kieffer et al., 2000, *JGR* 105(E4) [2] Kieffer et al., 2006, *Nature*, 442 [3] Kieffer, 2007, *JGR,* 112(E08005) [4] Piqueux and Christensen, 2008, *JGR,* 113(E2) [5] Kieffer and Titus, 2000, *Icarus*, 154(1) [6] Titus et al., 2001, *JGR*, 106(E10) [7] Smith et al., 1999, *JGR,* 104(E1) [8] Kelly et al., 2006, *JGR*, 111(E03S07) [9] Smith et al., 2001, *Science*, 294 [9] Langevin et al., 2009, *40th LPSC*, #2017.

CONSTRAINTS ON MARS' POLAR ENERGY BALANCE FROM NUCLEAR SPECTROSCOPY.

T. H. Prettyman[1], T. N. Titus[2], and A. Colaprete,[3] [1]Planetary Science Institute (1700 E. Ft. Lowell, Suite 106, Tucson, AZ 85719, prettyman@psi.edu), [2]U.S. Geological Survey (2255 N. Gemini Dr., Flagstaff, AZ, 86001, ttitus@usgs.gov), [3]NASA Ames Research Center (MS 245-3, Moffett Field, Mountain View, CA, Anthony.Colaprete-1@nasa.gov).

Introduction: Since the first Mars Polar Energy Balance and CO_2 Cycle Workshop in 2004 [1], significant progress has been made towards understanding the details of the seasonal cycle of CO_2 and water on Mars from new analyses of orbital remote sensing data and improved modeling of atmospheric and surface processes. Work is now underway to synthesize measurements and models to fully determine unknown terms of the polar energy balance, including regolith energy storage and advection by the atmosphere, on relatively fine spatial scales, limited by the resolution of the remote sensing instruments. Here, we describe measurements of surface and atmospheric properties by the Gamma Ray Spectrometer (GRS) suite of instruments on 2001 Mars Odyssey, with emphasis on results from the Neutron Spectrometer (NS) subsystem. In particular, we report asymmetries in the seasonal CO_2 ice caps, which are caused by spatially and temporally varying thermal surface properties and atmospheric processes.

Nuclear Spectroscopy: Nuclear spectroscopy refers to the detection of gamma rays and neutrons produced by the interaction of cosmic rays with the surface and atmosphere of Mars. Nuclear spectroscopy is sensitive to the elemental composition and layering of the CO_2 frost-free surface, including layering of water ice (depth and water abundance of the ice table at high latitudes) (e.g., [2], [3]). In addition, nuclear spectroscopy is sensitive to the presence of seasonal CO_2 surface ice and noncondensable gas in the atmosphere (e.g., [4], [5], [6]). Depths and thicknesses of layers determined by nuclear spectroscopy are reported as column abundances or areal densities (g/cm^2). Consequently, if the geometric thickness of a layer can be estimated from geophysical constraints or measured (via laser altimetry or photoclinometry), then the bulk density of the layer can be determined. For example, the density of the seasonal CO_2 caps was determined by combining column abundances measured by the GRS instruments and geometric thicknesses determined by the Mars Orbital Laser Altimeter (e.g., [7]). Results indicate that the seasonal ice density is much lower than the theoretical density of CO_2 ice and that the density changes with time, which may point to variations in the emplacement mechanisms (snow vs. direct condensation) and alteration of the surface over time [8].

Nuclear spectroscopy data can be combined with thermal observations, to further constrain surface thermal properties. Since water has relatively high heat capacity, the depth and water abundance of the ice table is an important parameter controlling the deposition and removal of seasonal CO_2 ice. Ice table depths derived from surface thermal properties determined from Thermal Emission Spectrometer (TES) measurements are generally consistent with depths determined by neutron spectroscopy [9,10]. Differences are likely due to assumptions in the analysis, which is dependent of surface physical models, for both TES and NS. For example, the layering is likely more complicated than water-ice covered by a dry lag deposit, which is commonly assumed for both techniques.

We are developing techniques to combine TES and NS measurements to more accurately determine the physical parameters of the layers, which will in turn provide a more accurate model of regolith thermal properties. For example, thermal and epithermal neutrons strongly constrain depth and ice-table content if the "dry" soil composition is known. The addition of thermal inertia to the analysis of thermal and epithermal neutrons will enable neutron absorption by the soil to be determined simultaneously with ice table depth and water-equivalent hydrogen abundance.

Characterizing the seasonal caps: Data acquired by the GRS instrument suite was used to determine the column abundance of CO_2 ice in the northern and southern hemispheres for successive Mars years, independently, by three groups of researchers. Recent results are mentioned here.

Kelly et al. [5] reported zonally-averaged CO_2 ice column abundances on 15° L_S intervals based on measurements of the attenuation of the 2.223 MeV gamma ray (produced by neutron capture with H in the regolith) by the intervening CO_2 ice. Neutron spectroscopy takes advantage of the fact that surfaces with CO_2 ice have higher neutron output than the underlying water-rich regolith, mainly because water-ice more effectively moderates and absorbs neutrons than CO_2-ice. Litvak et al. [6] reported zonally-averaged CO_2 ice column abundances in the southern hemisphere on 12.5° L_S intervals from an analysis of High Energy Neutron Detector data. Finally, Prettyman et al. [Characterization of Mars' Seasonal Caps using Neutron Spectroscopy, *J. Geophys. Res.*, in press] reported maps of CO_2 ice column abundance (2° equal area pixels) of the

northern and southern hemisphere on 10° L_S intervals based on an analysis of NS epithermal counting data.

The intrinsic spatial resolution of all three instruments was about 15° full-width-at-half-maximum (FWHM) of arc length, which is sufficient to resolve local variations in the seasonal caps. All three groups reported relatively small interannual variations in the seasonal ice and similar values for the peak column abundance, peaking time, and seasonal cap mass in comparison to the General Circulation Model calculations "calibrated" to match pressure variations measured by Viking Lander 2.

Seasonal Cap Asymmetry: Maps reported by Prettyman et al. reveal asymmetries in the northern and southern seasonal caps, which have implications for local energy transport and storage. During the advance in the northern hemisphere, the column abundance of CO_2 ice is larger in Acidalia Planitia than in other regions at similar latitude. Enhanced deposition of frost in Acidalia may result from cooling by katabatic winds that flow into Acidalia from Chasma Boreale. The northern seasonal cap is relatively symmetrical in comparison to the southern cap, for which the deposition of CO_2 ice is strongly enhanced in the vicinity of the South Polar Residual Cap (SPRC).

The asymmetry in the southern residual cap is evident in **Figure 1**, which shows the column abundance of CO_2 ice for selected times along an arc of constant longitude, which crosses through the SPRC (see map). During the advance (e.g., L_S = 95°), the cap is asymmetrical, with greater accumulation of CO_2 ice in the vicinity of the SPRC than in adjacent regions. The difference grows with time, resulting in a highly-asymmetrical seasonal cap that recedes to the SPRC.

Increased deposition of CO_2 in the vicinity of the SPRC relative to the surrounding terrain is expected since large portions of the SPRC are covered by CO_2 ice throughout the year. In the regions surrounding the SPRC, energy stored in the water-rich subsurface is conducted to the surface throughout winter, limiting the accumulation of ice relative to the SPRC. Since energy is released in the formation of CO_2 ice, could the asymmetry in CO_2 ice deposition influence atmospheric circulation near the pole? If so, then the asymmetry may influence regional circulation.

Conclusions: Nuclear spectroscopy provides useful information to supplement thermal emission measurements and other remote sensing techniques to determine regolith thermal properties, CO_2 ice column abundance, and the density of CO_2 ice, from which the fine details of the polar energy balance can be determined. Initial results from neutron spectroscopy indicate asymmetrical CO_2 ice deposition resulting from variations in regolith and seasonal cap properties and advection of energy by the atmosphere.

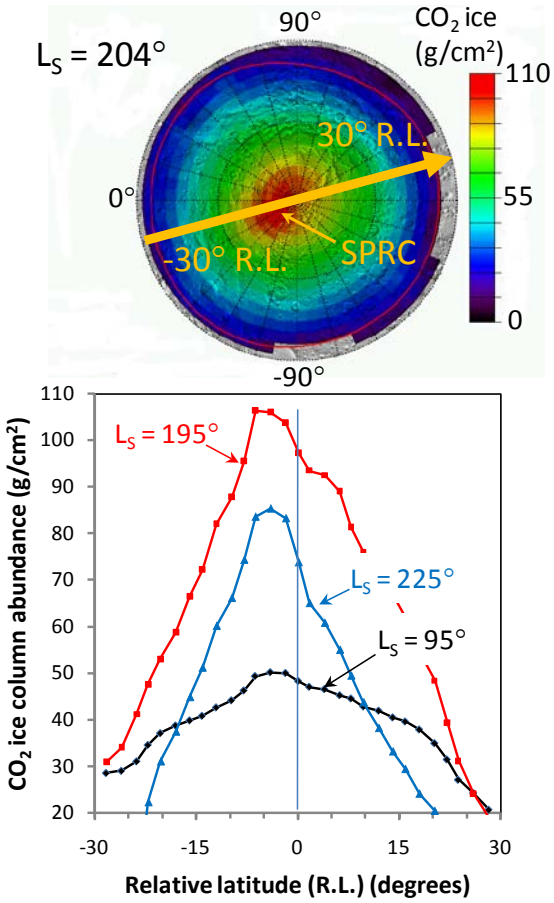

Figure 1. The column abundance of CO_2 ice is shown along an arc of constant longitude (see the arrow on the accompanying map) for selected times. The L_S values are indicated. Spatial deconvolution was used to reduce spatial blurring (resolution < 10° FWHM arc length). The cap edge from TES is shown on the map as a red line (see Titus, T.N., this workshop and [11]).

References: [1] Prettyman, T.H. and T.N. Titus (2004) *EOS Trans.*, *85*(41), 403-403. [2] Boynton, W.V., et al. (2002), *Science*, *297*(5578), 81–85. [3] Mellon, M.T., et al. (2004), *Icarus*, *169*(2), 324-340. [4] Sprague, A.L., et al. (2004), *Science*, *306*(5700), 1364 – 1367. [5] Kelly, N.J., et al. (2006), *J. Geophys. Res.*, *111*, E03S07. [6] Litvak, M.L. (2007), *J. Geophys. Res.*, 112, E03S13. [7] Aharonson, O., et al. (2004), *J. Geophys. Res.*, *109*, E05004. [8] Hecht, M.H. (2008), *Planet. Space Sci.*, *56*, 246–250. [9] Titus, T.N. and T.H. Prettyman (2007) *LPS XXXVIII*, Abstract #2088. [10] Bandfield, J.L. and W.C. Feldman (2008), *J. Geophys. Res.*, *113*, E08001. [11] Titus, T. N. (2005), *LPS XXXVI*, Abstract #1993.

MICROPHYSICAL CYCLE OF EVOLUTION OF THE NORTHERN MARTIAN SEASONAL CONDENSATES

B. Schmitt, T. Appéré, S. Douté, P. Beck *Laboratoire de Planétologie de Grenoble, CNRS/UJF, France (Bernard.Schmitt@obs.ujf-grenoble.fr),* **F. Forget,** *[3]Laboratoire de Modélisation Dynamique, Université Paris 6, Paris, France,* **Y. Langevin, J.-P. Bibring** *Institut d'Astrophysique Spatiale, CNRS - Université Paris-Sud, Orsay,France.*

Introduction: The detailed CO_2 and water cycles on Mars are strongly determined by both the local thermal balance of the surface and the availability of the volatiles in the atmosphere and at the surface. The composition and physical state (mixing modes, temperature, …) of the ices at the surface and in the top layers of soil can determine the exchange fluxes with the atmosphere. It is thus necessary to understand the spatial and temporal evolution of these parameters in the condensate deposits to constrain the sources and sink of volatiles during a seasonal cycle. This may lead to improve the Martian climatic models by taking into account new volatile sources/sinks or processes influencing the thermal and volatile balances.

Overview of the northern condensates cycle: The northern Martian condensate cycle has been only poorly monitored from ground based observations due to unfavorable observation geometry during northern spring. The orbital observations of the past decade have accumulated a large amount of data pertaining to different aspects of the condensation/sublimation cycles both in the southern and northern hemispheres [1,2]. The OMEGA/Mars Express spectroscopic observations are especially well adapted to directly monitor the temporal evolution of the abundance, physical state and distribution of the CO_2, water and dust components of the condensates through their visible and near-infrared spectral signatures [3].

Condensation observations: Water frost condensation and sublimation cycle has been observed around 45° latitude by Viking 2 lander [4] but it has been only poorly monitored at the global scale. Condensation of CO_2 is even less documented because it occurs mostly during the polar night, precluding solar reflectance measurements, down to only a few degrees below the terminator, thus under difficult illumination conditions (low flux, large atmospheric absorption and aerosol scattering).

Sublimation observations: The observation conditions of the spring sublimation of the condensates are much more favorable and a large set of data have now been accumulated over several Martian seasons [1, 2, 5]. A detailed study of the spring evolution of the northern seasonal condensates has been performed over one full Martian year using OMEGA/Mars Express data and is presented in a companion paper [6].

Possible scenarios of microphysical evolution: To understand the possible sublimation scenario, both microphysical and at the hemispheric scale, it is first necessary to infer the structure of the condensates, and thus a condensation scenario, just before the start of the sublimation stage. Then the spatio-temporal evolution of this initial layer subjected to spring sublimation can be followed using the observations.

Condensation scenario: There are typically two stages during the condensation of the frosts occurring during late autumn and winter. First a condensation of a thin layer of pure water frost and then, when the surface temperature decrease, the condensation of the meter thick CO_2-rich ice layer, including small amounts of water ice and dust. The condensation of water frost first starts during the daily night and completely sublimate during the day. The latitude-time dependence of the first frosts will depend on the partial water vapor pressure in the atmosphere. In a second step, when the sun is low enough, the frost persists all day long [4]. At this stage the accumulation rate should increase due to the positive feedback of the surface albedo on the thermal balance. This frost may also partly diffuse inside the upper layer of soil and adsorb on mineral grains or possibly form some ice-cemented crust. Vapor diffusion and condensation at some depth will occurs if a negative thermal gradient occurs at some time of the daily cycle. In a second stage, when the thermal balance allow the surface temperature to drop below the CO_2 freezing point, CO_2 frost can start condense including tiny amounts of water ice grains (< 1 %) and dust particles (< 0.1 %). This condensation should be first a daily condensation/sublimation cycle but at high latitudes, typically northern a latitude 5-10° below the mid-day terminator, condensation will occurs continuously at a rate mostly by determined by the surface CO_2 thermal emission. At lower latitudes, although the daily average balance is negative and net accumulation occurs, the daily condensation/sublimation cycle should still be effective. The thin water frost underneath should then be "frozen" at the CO_2 ice tempera-

ture and water vapor diffusion inside the regolith no more efficient. The initial H_2O frost condensation and its associated surface albedo decrease should help in lowering the surface temperature and thus may initiate CO_2 condensation earlier (or at lower latitude) than without this precursor frost. During the water frost stage and roughly the first half of the CO_2 frost condensation stage the thermal inertia of the first decimeters of the surface should play a major role on the surface temperature and thus in determining whether H_2O ice and then CO_2 ice can condense at the surface. It should also affect the condensation rate [7]. Local and general slope orientations and surface albedos may also play a role on determining the sign of the thermal balance but only up to shortly after the first CO_2 condensations. After this point CO_2 condensation mostly occurs in the polar night at high latitudes where slopes and albedo will have no more effect on the thermal balance. The result should be a layer of CO_2-rich ice, with thickness globally increasing from about 50° latitude to the pole, on top of a millimeter-thick layer of H_2O frost, and possibly a few millimeters or centimeters of icy soil. To which extent microphysical evolutions of these frosted soil, H_2O frost and CO_2 ice layers occurred during these condensation stages is still an open question. The occurrence of condensation/sublimation cycles at the beginning of each of these stages should have at least modified the bottom part of these layers, especially at low latitudes.

Sublimation scenario: Our microphysical scenario of sublimation is mostly based on the results obtained from the spatio-temporal mapping of the CO_2 and H_2O ices during northern spring [6] completed with global statistical analysis [8] and local radiative transfer modelling of the layered condensates [9] using optical constants of CO_2 and H_2O [10, 11]. The major results are:
- A CO_2-free water ice annulus is present around the CO_2 ice rich deposits. Before the beginning of the recession it likely corresponds to the daily water frost cycle stage and is extended (8°). During the CO_2 ice sublimation stage the narrower dusty water ice annulus (2°-3° wide) correspond to the ice released by the CO_2 ice layer (bottom icy soil and water frost layers + ice and dust grains trapped inside the CO_2 layer). Diffusion of water vapour from this ice layer through the underlying soil may be boosted due to strong negative ice-soil thermal gradient probably present at that stage.
- Water ice detected southern of the albedo limit. It probably corresponds to dusty water ice or icy soil segregated with defrosted soil. Progressive de-icing and water desorption of the soil occurs at this stage.
- CO_2 ice is systematically detected southern its thermal stability limit as determined by TES [12]. A spatial segregation occurs between the dusty water ice lag and the CO_2-rich ice layer.
- CO_2 ice reappear at the surface in late spring (Ls=50-70°) at several locations where it had disappeared. This peculiar behavior may be explained by recondensation at higher latitudes of water vapor sublimated from the ice annulus and cold trapped at the surface of the CO_2 ice rich deposits [6, 8]. A millimetres thick layer of H_2O ice may form, hiding the CO_2 ice, until strong sublimation of CO_2 ice occurs in late spring disrupting the H_2O ice layer.

Difference with the southern volatile cycle: The main differences of the southern condensates are the much lower water vapor amount in the atmosphere. Thus the initial frost condensation should be very limited before CO_2 condensation occurs and the amount accumulated within the CO_2 frost is about an order of magnitude lower [3]. Water ice segregated at the edge of the CO_2 condensates during recession is almost non-existent or should be probably limited to less than a few tenth of a degree. Thus water recondensation on top of the CO_2 condensate should be far less efficient than in the north and certainly not enough to create an optically thick water ice layer that can hidden the infrared CO_2 signatures.

Conclusion: The knowledge of the structure and composition of the condensates and their spatial and temporal evolutions should help to understand the various microphysical processes occurring during their deposition and condensation stages. These processes should strongly constrain the fluxes of volatiles between the atmosphere and the surface. The future climatic Martian models should include the effective locations of the different sources and sinks of water vapour evidenced by these studies.

References: [1] Kieffer H.H. and Titus T.N. (2001) *Icarus* 154, 131-144; [2] James P.B. and Cantor B.A (2001) *Icarus* 154, 162-180 ; [3] Langevin Y. et al. (2007) *JGR E,* 112, E08S12; [4] Jones K.L. et al. (1979) *Science* 204, 799-806; [5] Giuranna, M. et al. (2007) *Planet. Space Sci.,* 55, 1328 ; Wagstaff K. et al. (2008) *Planet. Space Sci.,* 56, 256 ; [6] Appéré T., Schmitt B. et al. (2009) *Mars Polar Energy Balance & CO_2 Cycle Workshop*, this issue; [7] Aharonson, O., et al. (2004) *J. Geophys. Res.* (E) 109, 5004 ; [8] Appéré et al. (2008) *LPI Contribution* 1443, 9008 ; [9] Douté S. and Schmitt B. (1998) *JGR E,* 103, 31367-31390; [10] Quirico E. and Schmitt B. (1997) *Icarus,* 127, 354-378. [11] Grundy W. and Schmitt B. (1998) *JGR E,* 103, 25809-25822; [12] Titus T. N. (2005) *36th LPSC*, 36, 1993+.

ON THE MYSTERY OF THE PERENNIAL CARBON DIOXIDE CAP AT THE SOUTH POLE OF MARS. Alejandro Soto[1], Xin Guo[1], and Mark I. Richardson[1], [1]Caltech, M/C 150-21, Pasadena, CA 91125. asoto@caltech.edu, xinguo@caltech.edu, mir@gps.caltech.edu

Introduction: A perennial CO_2 ice cap has long been observed near the south pole of Mars. The retention of a CO_2 ice cap results from the surface energy balance of the latent heat, solar radiation, surface emission, and subsurface conduction. While models conventionally treat surface CO_2 ice using constant ice albedos and emissivities, such an approach fails to predict the existence of a perennial cap. We explore the role of insolation-dependent ice albedo, which agrees well with Viking, Mars Global Surveyor and Mars Express albedo observations. Using a simple parameterization within a General Circulation Model, in which the albedo of CO_2 ice responds linearly to the solar insolation, we are able to predict the existence of a perennial CO_2 cap at the observed latitude and only in the southern hemisphere [1]. While the single insolation dependent function likely does not capture the full spatial and temporal variations of ice albedo, it provides a demonstration that insolation-dependence of albedo is probably the key factor in the existence of a residual cap. Future work on the microphysical and macrophysical mechanisms of CO_2 ice albedo and emissivity is required, one application of which would be a physically-based parameterization of surface radiative effects of CO_2 ice for climate models.

Insolation-dependent albedo: We use the MarsWRF model, the Martian implementation of the planetWRF model [2]. We calibrate the GCM by tuning the albedos and the emissivities of the seasonal dry ice caps and the total CO_2 inventory in the system to reproduce the VL1 surface pressure cycles. Water cycle and CO_2 cloud microphysics, which are likely aliased to the model parameterization of frost albedo and emissivity, are not explicitly included. At the steady state, the model predicts a pressure cycle that matches the Viking Lander records very closely [3]. The predicted mass of the seasonal caps is consistent with other GCMs and observations[4]. However, like all the other models trying to fit the VL pressure records, a residual CO_2 cap in the south pole is not predicted by MarsWRF with this setup.

The Viking observations suggests that the albedo of the southern residual CO_2 cap changes with time [5] [6]. More usefully, the relationship between the residual CO_2 caps albedo and the incident solar flux is very linear (Figure 1). When we use a least square linear regression method, we obtain an empirical equation that predicts the surface CO_2 frost albedo based on the insolation:

$$A = 0.532 + 8.72 \times 10^{-4} \times F_s \qquad (1)$$

where A is the albedo of the CO_2 ice cap and F_s is the incident solar flux in W/m^2. This linear model fits the Viking albedo observations for the southern residual cap very well, with only several percent of fitting error. In the absence of a proven physical model for the dependence of albedo on insolation or other environmental factors, this empirical relationship is potentially very important for reproducing a perennial cap in a GCM. Larger albedo creates a larger energy deficit that has to be compensated by more surface CO_2 ice condensation or less sublimation. From Equation 1, the albedo is the largest in the summer when the incident solar flux is the most intense, which is ideal for the CO_2 ice to endure the summer.

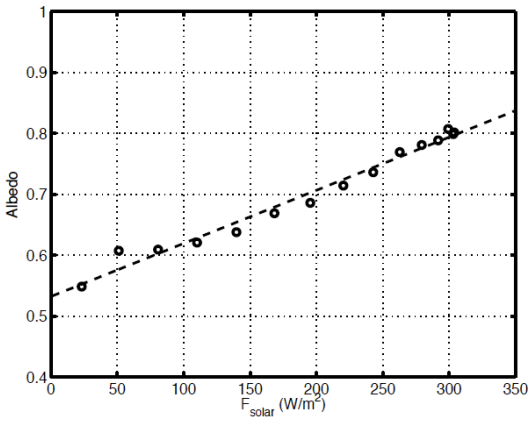

Figure 1: Southern residual cap albedo as a function of incident solar insolation. Open circles: observations from the Viking spacecraft. Dashed line: the line from the linear fitting of the Viking data. Data fit from Guo et al. [1] and data from Paige and Ingersoll [6].

We incorporated this relationship into MarsWRF. For each time step, if the surface is covered by enough CO_2 ice, we calculated the instantaneous incident solar flux and then use Equation 1 to determine the surface albedo for the subsequent radiative calculations (of course the albedo value can not be larger than unity). Results of model runs are shown in the next session. Output from the second year of model simulations is shown.

Results: We first present the control or baseline scenario with time constant albedo. Time constant albedos and emissivities are assigned to the northern and southern CO_2 ice caps. The total CO_2 mass in the system was set to 2.83×10^{16} kg [3]. This setup generates a pressure cycle at the VL1 location agreeing with the VL1 records very well, but without a residual cap at either pole. The annual variation of the zonally averaged surface CO_2 frost is shown in the panel (a) of Figure 2.

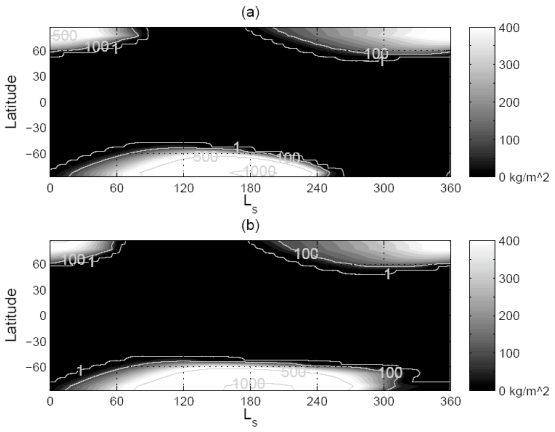

Figure 2: Annual variation of zonally averaged surface CO_2 ice deposition. The grey scale indicates the density of the deposition in kg/m^2. From the lower latitudes to the polar region, the grey contour lines indicate the deposition levels of 1 kg/m^2, 100 kg/m^2, 500 kg/m^2 and 1000 kg/m^2 respectively. Panel (a): This is the case with time-constant CO_2 frost albedos. Panel (b): The setting of this experiment is identical to that of panel (a), except the frost albedo is calculated using Equation 1 in each time step. From Guo et al. [1].

Next the surface CO_2 ice albedo is determined from the local incident solar flux according to Equation 1, while keeping the rest of the model unchanged (note that albedo of CO_2 ice present at any location on the surface is locally determined by this formula). We show the corresponding CO_2 ice surface deposition annual cycle in the panel (b) of Figure 2.

Following the seasonal cap evolution, starting with the onset of polar night in each hemisphere, CO_2 begins to deposit at the winter poles. At this time of the year, the season cap areal coverage in both hemispheres does not differ greatly in the time-varying albedo experiment compared to the control case, because during the polar nights the surface albedo is not relevant to the surface energy balance. When the surface frost is exposed to the sun, the abundance and the longevity of the surface CO_2 ice starts to differ from the control case. As the southern seasonal ice cap is exposed to sunlight as the spring wears on, the albedo is driven to higher values than in the north, and to higher values than those used in the south in the control simulation. This brightening of the southern cap leads to less solar energy absorption and thus reduces the cap sublimation rate. Indeed, thanks to the high albedos generated by Equation 1, the CO_2 ice at the southern pole is able to endure the summer and forms a perennial reservoir.

The reason for the existence of perennial CO_2 ice in the GCM is consistent with the Paige and Ingersoll [6] study of the heat balance of the residual cap. The perennial ice reservoir produced by the GCM is slightly displaced from the geographical south pole, and is longitudinally asymmetric, agreeing with observations [7] [8].

Conclusions: Viking data suggests an empirical linear relationship between the CO_2 ice cap albedo and the incident solar flux. When we include this relationship in the MarsWRF GCM we are able to reproduce a CO_2 cap that persists throughout the full year near the south pole. This perennial cap is not located exactly at the geographical south pole, nor is it zonally symmetric, which agrees with the observations. The predicted perennial cap is not at the same longitude as seen in the observations. The spatially invariant linear fit of albedo and insolation is a major oversimplification, albeit significantly better than time and space invariant treatment in models to date. The improvement in the simulation suggests insolation-dependence should be included in models, but misfits in cap location prediction and errors generated in the simulated pressure cycles also suggest that a more detailed, physically-based model of CO_2 surface ice radiative properties is needed to adequately prognose the Martian CO_2 cycle.

References

[1] X. Guo, M. I. Richardson, A. Soto, and A. Toigo. On the mystery of the perennial carbon dioxide cap at the south pole of mars. *Submitted to JGR*, 2009.

[2] M. I. Richardson, A. D. Toigo, and C. E. Newman. Planetwrf: A general purpose, local to global numerical model for planetary atmospheric and climate dynamics. *JGR*, 112, E09001, 2007.

[3] X. Guo and M. I. Richardson. Fitting the viking lander surface pressure cycle with a mars general circulation model. *Submitted to JGR*, 2009. doi: Guo,X.,etal.(submitted),.

[4] N. J. Kelly, W. V. Boynton, K. Kerry, D. Hamara, D. Janes, R. C. Reedy, K. J. Kim, and R. M. Haberle. Seasonal polar carbon dioxide frost on mars: Co2 mass and columnar thickness distribution. *JGR*, 111(E3):12, 2006.

[5] P. B. James, H.H. Kieffer, and D. A. Paige. *Mars*, chapter 27. The seasonal cycle of carbon dioxide on Mars, page 934. University of Arizona Press, 1992.

[6] D. A. Paige and A. P. Ingersoll. Annual heat balance of Martian polar caps - Viking observations. *Science*, 228: 1160–1168, June 1985.

[7] A. Colaprete, J. R. Barnes, R. M. Haberle, J. L. Hollingsworth, H. H. Kieffer, and T. N. Titus. Albedo of the south pole on mars determined by topographic forcing of atmosphere dynamics. *Nature*, 435(7039):184–188, 05 2005.

[8] H. H. Kieffer, T. Z. Martin, A. R. Peterfreund, B. M. Jakosky, E. D. Miner, and F. D. Palluconi. Thermal and albedo mapping of mars during the viking primary mission. *JGR*, 82(28):4249–4291, 1977.

THE POLAR ATMOSPHERE AS SEEN BY THE RADIO SCIENCE EXPERIMENT MARS ON MARS EXPRESS. S. Tellmann[1], P. Withers[2], M. Pätzold[1], B. Häusler[3], G.L. Tyler[4] and D.P. Hinson[4], [1] Rheinisches Institut für Umweltforschung, Abteilung Planetenforschung, Universität zu Köln, Aachener Str. 209, 50931 Cologne, Germany (silvia.tellmann@uni-koeln.de), [2]Center for Space Physics, Boston University, 725 Commonwealth Avenue, Boston MA 02215, [3]Institut für Raumfahrttechnik, Universität der Bundeswehr München, Werner-Heisenberg-Weg 39, 85577 Neubiberg, Germany, [4]Department of Electrical Engineering, Stanford University, 350 Serra Mall, Stanford, California, USA

Introduction:

The Radio Science Experiment MaRS on Mars Express is sounding the Martian atmosphere and ionosphere using the spacecraft radio signals at X-band and S-band in Earth occultation geometry. Vertical profiles of pressure, temperature and density of the neutral atmosphere can be derived with an altitude resolution of only a few hundred metres [1].

The elliptical orbit of Mars Express allows to examine a large range of local times and locations and can therefore be used to investigate latitudinal, diurnal and seasonal variations.

Observation Method: Within the atmosphere and ionosphere the gradient of refractive index of the gas deflects the direction of propagation, resulting in a curved propagation path. In this way atmospheric refraction alters the path geometry by an amount that is controlled by the radial variation of refractivity. The resulting frequency shift of the signal can be used to calculate the degree of bending, the ray periapsis, and the projection of the ray path onto the planetary surface. The refractivity of the atmosphere at the ray periapsis is obtained from the bending angle via an Abel transform [2]. The neutral number density is directly related to the refractivity profile through a constant factor C_1 which depends on the atmospheric composition of the atmosphere. Temperature and pressure profiles follow by use of the ideal gas law and assuming hydrostatic equilibrium.

The Data Set: MaRS could observe the southern winter hemisphere during the second occultation season (OCC 2) at the end of 2004 (Ls ≈ 130°) and in 2008 (OCC 8, Ls ≈ 94°) (Figure 1).

The northern high latitudes were investigated during the third occultation season in 2005. More than 70 profiles covering all latitudes between 50° N and 76° N at solar longitudes between 259.6° and 289.5° were retrieved (Figure 2).

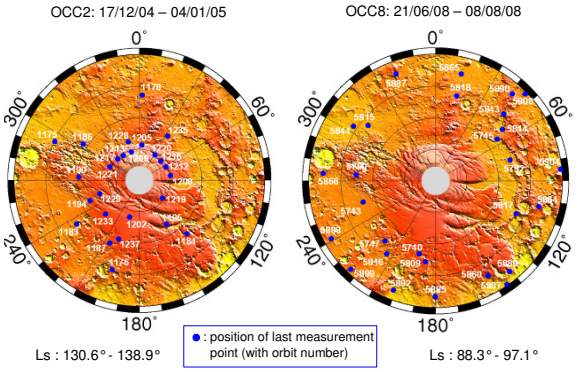

Figure 1: Geographical position of the MaRS measurements from occultation season number 2 (left) and 8 (right) in 2004/2005 and 2008, respectively, in the southern hemisphere. The blue dots indicate the position of the lowest measurement sample above the surface. Each measurement is identified by its orbit number.

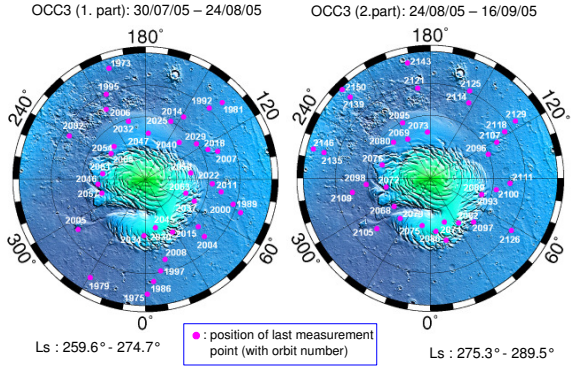

Figure 2: MaRS measurements in the northern middle and high latitudes (OCC season 3, 2005). The first (second) part of the occultation season is shown on the left (right). The pink dots indicate the position of the lowest measurement sample above the surface. Each measurement is identified by its orbit number.

Temperatures: Figure 3 shows a typical temperature profile in the northern winter hemisphere (lat: 75.8° N). The temperature stays close to the CO_2 condensation temperature which indicates CO_2 precipitation up to a pressure level of 70 Pa (≈ 20 km). The data set allows comparisons between both hemispheres for the different seasons, latitudes, and Mars years. Small scale fluctuations indicating atmospheric waves can be found in several temperature profiles.

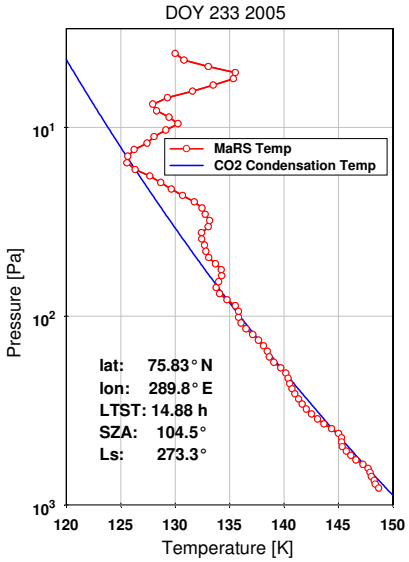

Figure 3: Typical temperature profile from the northern high latitude region (DOY 233 2005) at northern winter solstice. The red curve shows the MaRS profile, the blue line indicates the CO_2 condensation curve. An upper boundary condition of 130 K is used.

Neutral Number Density: The neutral number density profiles can be used to examine the effect of CO_2 condensation in the winter hemisphere at different locations, seasons and altitude levels. Figure 4 shows the neutral number densities at a geopotential altitude of 20 km for parts of the third OCC season. The measurements started at mid latitudes, moved close to the northern polar region and returned to the mid latitudes after winter solstice. Two effects are clearly visible: the density decreases with increasing latitudes and the ongoing CO_2 condensation leads to decreasing densities over the course of the winter season. These effects can be studied for both hemispheres in different Mars years to investigate the interannual variability.

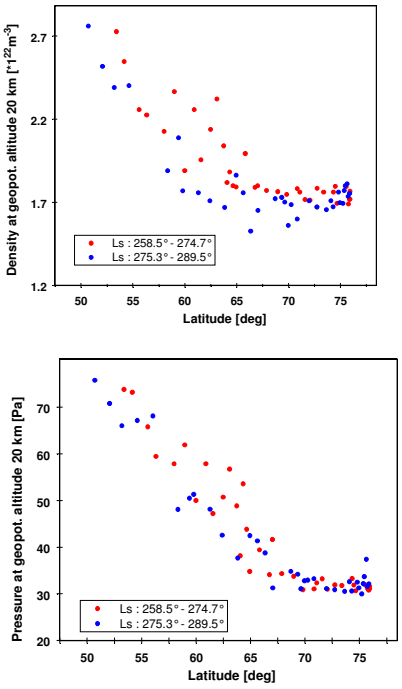

Figure 4: Neutral number densities (upper panel) and pressure (lower panel) at a geopotential altitude of 20 km for the third OCC season in 2005. Each dot indicates one measurement. The red dots show the first part of the OCC season, starting at mid latitudes and moving closer to the pole, the blue dots show the second part of the OCC season starting the high latitudes and coming closer to lower latitudes.

Pressure: The effect of CO_2 condensation leads to a strong pressure gradient in the highly dynamical winter atmosphere (Figure 4). Latitudinal pressure gradients indicate distinctive zonal winds on the winter hemisphere.

Conclusions: The MaRS data set allows to study the effect of CO_2 condensation on the atmospheric pressure, temperature and number density for different Mars Years, seasons, and geolocations. The high vertical resolution can be used to examine the CO_2 condensation and resulting dynamical effects at different altitude levels.

Acknowledgements: The MaRS experiment is funded by DLR under grant 50QP9909.

References:

[1] Pätzold, M. et al. (1994), *ESA Special Publication*, SP-1240.

[2] Fjeldbo, G. et al. (1971), *Astron. J., 76*, 123-140.

RESIDUAL SOUTH POLAR CAP: HOW OLD, HOW IS IT CHANGING? P. C. Thomas[1], P. B. James[2], W. M. Calvin[3], R. M. Haberle[4] [1]Center for Radiophysics and Space Research, Cornell University, Ithaca NY 14853, USA [2]Space Science Institute Boulder CO [3] Department of Geological Sciences, University of Nevada, Reno NV [4]Space Science Division, NASA Ames Research Center, Moffet Field CA.

Introduction: We examine the occurrence and likely minimum ages of units that make up the residual south polar cap (RSPC) of Mars and examine the current mechanics of erosion. Mars Reconnaissance Orbiter has provided new perspectives on the RSPC with Context Imager (CTX) data over the whole cap at ~5m/pixel, with the 25-50 cm scale pixels of the High Resolution Imaging Science Experiment) HiRISE camera, and with data from the Compact Reconnaissance Imaging Spectrometer (CRISM).

Unit geography, volumes, age: Units can be defined by their thickness, surface character, and types of erosional depressions [1,2] The thickest and oldest units, "A", shown in Fig. 1 as purple (hard to see), orange and cyan cover only a small fraction of the cap. The thinner "B" unit covers most of the RSPC. Beneath and beyond these CO_2 materials is water ice material and the Polar Layered Deposits [3]

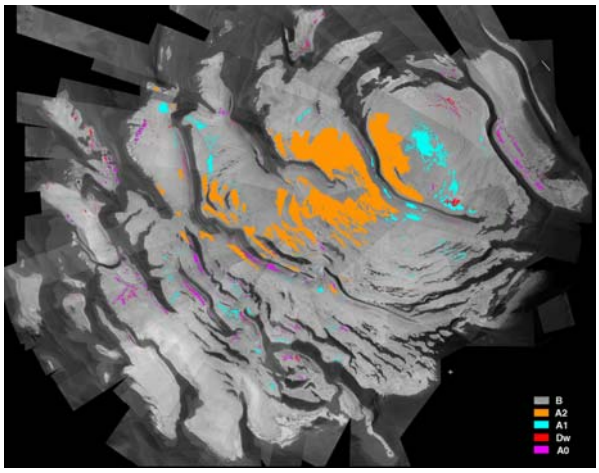

Figure 1. Units in the RSPC. CTX late summer base map, Mars year 28. Bright, uncolored areas are unit B. Purple is A0, thickest, oldest unit. Cyan is A1, characterized by heart-shaped to curled depressions. Yellow is "fingerprint" terrain [1]. Red (almost impossible to see at this scale) is "downwasted" materials.

From measured thicknesses of examples of these units and the exposure areas, we may estimate maximum total volume of the current RSPC, which is <376 km^3. Depending upon the density assumed, the mass therein is ~2-3% of the total atmorpheric mass.

The older, thicker exposures although accounting for very little volume, are widely scattered over the RSPC. They include several elongate exposures near the edges of troughs in the PLD, most often on the lower elevation, lower latitude side of the troughs which are usually asymmetric in cross profiles.

The 500m + depressions in unit A0, currently expanding (single face) at ~3.6 m/Mars year, suggest an age of well over 100 Mars years for the oldest, thickest unit. Depressions in the thinner, younger "B" materials are expanding over a 4-Mars year period at a slightly lower rate, ~2.2 m/MY. Some expanding linear gaps between materials that were apparently deposited after Mariner 9 observations (Mars year 9) are predicted to have started eroding in Mars year 8 or 9 at current rates. This result gives some confidence in reconstrcutions over a few Mars decades, but caution is always warrented in such caculations because of possible variations in erosion rates.

Since Mariner 9 observations the depressions within all units have been eroding, yet some areas have accumulated CO_2 covering, and the late summer extent of the RSPC is slightly larger in many places than in 1972 [4]. There is no general on-off mode for the polar deposition/erosion environment in recent Mars decades.

Erosion: backwasting of scarps Expansion of depressions by scarp retreat is not simple sublimation of an exposed face of ice. Both the thick and thin units retreat leaving behind a series of ridges of progressively lower height that can take many Mars years to completely decay. The scarps in the thicker A units (Fig. 2 top) show separation, slumping, and possible rotation of blocks from the scarp face. These units leave about one block or remnant ridge per Mars year. MOC images revaled the presence of the resulting debris ramps; MRO coverage by HiRISE has shown the details of the detachment of blocks [5] and merging of the debris into the wormy-appearing debris ramps. The thinner B unit also retreats leaving ridges, but their frequency is is closer to once every two Mars years in areas so far examined. There are even precursor markings, up to tens of meters from the scarp that appear years before the scarps pass a point.

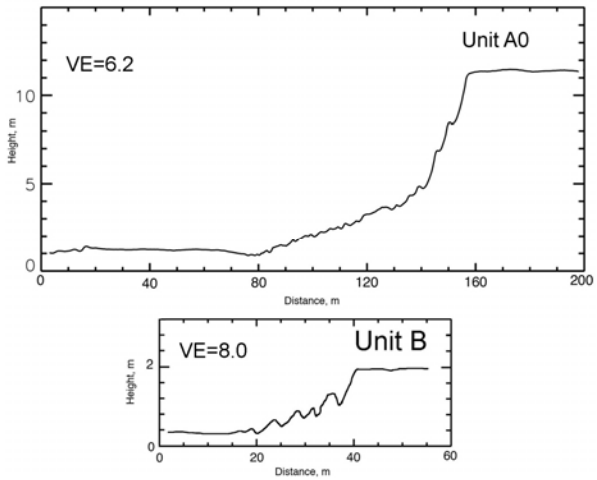

Figure 2. Typical profiles of retreating scarps in the thick A unit and thinner B units of the RSPC, derived from simple photoclinometry of HiRISE images. Note large vertical exaggerations and horizontal extent of the debris from the scarp crest is many times that of annual retreat distance.

Erosion: downwasting: Some areas of the thicker units experience loss of material by downwasting, rather than by backwasting of scarps [1]. The MRO HiRISE data show that the debris left from downwasting has a similar wormy ridge and trough topography as the aforementioned debris ramps, and that it can require more than 18 Mars years to completely disappear. Areas of downwasting are, as is the A unit itself, scattered widely over the cap, and at least two areas of downwasting since Mariner 9 observations have been identified [2].

The downwasting debris provides one of the best windows into the materials making up the thicker parts of the RSPC, and is included in high-priority targets for several MRO instruments in the southern summer of Mars year 29.

Overview: The age, the variety of units, the presence of both erosion and deposition in the last two Mars decades, and the complex, multi-year process of eroding scarps show that the RSPC has no one simple mode of development or loss. The complexities offer opportunities for elucidating the controls on deposition and erosion over lengthy periods well before the arrival of spacecraft at Mars, and thus may help untangle Mars climate variability and climate change.

References:

[1] Thomas, P. C. et al. (2005) Icarus 174,535-559. [2] Thomas, P. C. et al. 2009, Icarus, submitted [3] Piqueux, S. et al. 2008 J. Geophys. Res. 113, E08014. [4] Piqueux, S. and P. Christense 2008 J. Geophys. Res. 113, E02006. [5]Byrne, S. et al., 2008 Lunar. Planet. Sci. 39, abs # 2252.

MARS POLAR CAP EDGES TRACKED OVER 4 FULL MARS YEARS USING MGS TES. T. N. Titus[1], [1]U.S. Geological Survey, Flagstaff, AZ 86001 (ttitus@usgs.gov).

Introduction: The polar caps of Mars have been observed since 1666 [1]. In the late eighteenth century, Herschel [2] observed the advance and retreat of the polar caps, thus being one of the first observers of Mars' seasonal cycles. In more recent history, the polar caps have gained significance in that they are one of the driving forces of Martian climate, with approximately 25% to 30% of the atmosphere being cycled through the polar caps annually [3,4].

Understanding the nature of the seasonal polar caps is imperative if we are to understand the current Martian climate. The retreat of the Martian seasonal caps has been monitored by both satellite and telescopic observations. Most of these studies utilized visible imaging to determine the albedo contrast between the edge of the seasonal cap and the volatile-free soil [5,6]. This use of visible imaging, while widely used, has some limitations. Cap edge detection depends on albedo contrast between the polar cap and the soil. This contrast is below reliable detection methods where the CO_2 cap is dark, as in the south polar cryptic region [7], or during the advance of the seasonal cap [8]. The visible method also fails to distinguish between CO_2 and H_2O ices. Kieffer & Titus [9], using the Mars Global Surveyor (MGS) Thermal Emission Spectrometer (TES), observed a warm and bright annulus around the retreating northern seasonal CO_2 polar cap. They concluded that this annulus was most likely water ice. This was later spectroscopically confirmed with near-infrared spectroscopy [10].

There are currently 3 instruments in Mars orbit that are capable of monitoring the growth and retreat of the seasonal caps: the Mars Odyssey (ODY) Thermal Emission Imaging System (THEMIS), the Mars Express (MEx) Observatoire pour la Mine´ralogie, l'Eau, les Glaces et l'Activite´ (OMEGA), and the Mars Reconnaissance Orbiter (MRO) Compact Reconnaissance Imaging Spectrometer for Mars (CRISM). While these instruments continue to monitor the seasonal cap edge, TES provides the longest continuous record of the seasonal caps in both the visible and the infrared.

Data Processing: The first step in monitoring the seasonal cap edge is the construction of a data hypercube, with 2 spatial dimensions (Polar Stereographic projection at approximately 60 km resolution), 2 temporal dimensions (700 seasons at 2 local times of day), and 1 parameter dimension (albedo and 30 μm brightness temperature). Data extracted from the TES database are averaged and binned into the hypercube per every 12 orbits (approximately 23.55 hours), separated into ascending and descending data, which roughly defines day and nighttime data. This creates a hypercube of dimensions 90 x 90 x 700 x 2 x 2. Five of these hypercubes were constructed: 3 complete mapping years in the north and 2 complete mapping years in the south. The hypercubes were constructed so that the seasons start and end in the summer in order to capture both the advance and the retreat of the seasonal cap.

IR Cap Detection Technique: For this study, we applied the cap edge detection techniques used by Kieffer et al. [7] and Kieffer & Titus [9]. They made use of the rapid rise in surface temperature that occurs when CO_2 ice is removed. For this study, we defined the advancing cap edge, or frost date, to be when the 30 μm brightness temperature drops below 155 K. We defined the retreating cap edge, or crocus date, as the date when the 30 μm brightness temperature rises above 165 K. The springtime threshold temperature is set slightly higher due to effects from atmospheric dust that are common during the cap retreat.

Once the frost and crocus dates have been determined for each 60km x 60km cell, we fit the latitude of the cap edge to a series of sine and cosines which are functions of season and longitude. The sine and cosine fit is effectively a low-pass filter that removes the high frequency artifacts caused by the data being collected at only 12 longitudes per day.

VIS Cap Edge Detection Technique: The MGS TES solar bolometer can also be used to detect the cap edge. We fit an arc tangent curve to the albedo as a function of season, and define the cap edge as the inflection point. Because of a lack of albedo contrast between the soil and CO_2 in the early spring and a lack of contrast between the water ice northern residual cap and the seasonal CO_2 cap, this analysis is restricted to the latitude range of ±60° to ±80°.

Once the VIS cap crocus dates have been determined, we fit the latitudes of retreat to a quadratic (to account for the mean zonal retreat) and to series of sine and cosines (to account for asymmetries in the cap retreat).

Analysis: The results of this study will compare the interannual variation of the polar cap edges for both the spring (cap recession) and autumn (cap advance). The cap edge determined from albedo observations will be compared to the cap edge as determined from the thermal infrared data. Where appropriate, these cap edges will be compared to OMEGA and THEMIS observations. TES thermal observations are also useful in tracking the cap edge during predawn hours. Comparisons of diurnal cap edge variations will also be presented.

References: [1] Kieffer H. H. et al. (1992) in *Mars*, 1-33. [2] Herschel, W. (1784) *Philos. Trans. R. Soc. Lond. 74*, 233–273. [3] Tillman et al. (1993) *JGR*, *98*, 10963-10971. [4] Kelly et al. (2006) *J. Geophys. Res. 111*, E03S07, doi:10.1029/2006JE002678, [5] James P. and Cantor B. (1997) *JGR, 90,* 1151–1154. [6] James, P. B. et al. (1996) *Icarus,* 123, 87. [7] Kieffer H. et al. (2000) *JGR*, 105, 9653–9699. [8] Titus et al. (2001) *JGR*, 106, 23181–23196. [9] Kieffer H. and Titus T. (2001) *Icarus*, 154, 162-180. [10] Bibring J.-P. et al. (2005) *Sci.* 307, 1576–1581.

3 MARS YEARS OF DUST OPTICAL DEPTH MAPPING BY OMEGA ABOVE THE SOUTH POLE. M. Vincendon[1], Y. Langevin[2], S. Douté[3], J.-P. Bibring[2], [1]Department of Geological Sciences, Brown University, Providence, Rhode Island, 02912, U. S. A. (mathieu_vincendon@brown.edu). [2]Institut d'Astrophysique Spatiale, Orsay, France. [3]Laboratoire de Planétologie de Grenoble, Grenoble, France

Introduction: The varying amount of airborne dust particles observed at high latitudes directly affects the polar energy balance of Mars [1]. The behavior of aerosols above the south polar cap differs from that seen in equatorial and mid-latitude regions ([2], [3], [4]). It can however not be determined by classical thermal infrared methods of optical depth retrieval as the thermal contrast between surface ice and atmosphere is too low [5]. The strong near-IR absorptions of CO_2 ice enabled the development of a new method to retrieve optical depths which requires the presence of clean CO_2 ice at the surface [4]. We have extended the application of this method to 2007 and 2009 springs and summers and compared the results to the 2005 retrievals presented in [4]. This new time range includes the planet-encircling dust event of July 2007. Modeling results which aim at determining the amount of deposited dust during this global dust storm will also be presented at the conference.

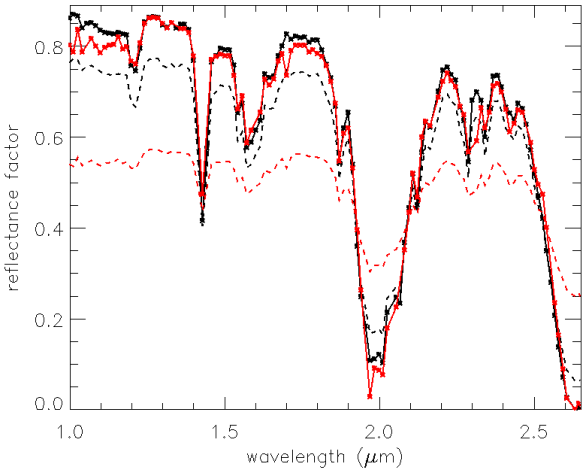

Figure 1: The CO_2 covered surface at 301°E and 84°S is observed by OMEGA in 2005 (black dotted line, moderate opacity period) and 2007 (red dotted line, beginning of the global dust storm) at the same L_S (272°). The observed spectral contrast is significantly reduced during the dust storm. The reflectance at 2.64 µm is used [4] to estimate the optical depth of dust aerosols: 0.4 in 2005 compared to 1.7 in 2007. Using this optical depth to correct observations from aerosols scattering leads to very similar surface spectra (solid lines), which validates the method in case of very high opacities.

Method: The reflectance observed by OMEGA at 2.6 µm has been demonstrated to be uniquely due to the light scattered by the whole layer of aerosols when clean CO_2 ice covers the surface (Figure 1). We can therefore convert this reflectance to an optical depth of dust particles using a RT code [4].

Results: The time variations of the optical depth above the South Pole are presented in Figure 3 for three martian years. They show a high level of consistency in the L_S 180°-250° range. As the summer solstice approaches, optical depths are strongly affected by the dust events occurring at equatorial latitudes: the increase of optical depth seen by Opportunity at L_S 315° in 2005 [6] propagates up to the south pole, as well as the 2007 planet encircling dust event (L_S 265°).

While a significant part of OMEGA low to mid latitude observations show no evidence for persistent surface dust deposits during the months following the decay of the 2007 planet encircling dust event [7], evidence for the deposition of a thin layer of dust above the south cap have been obtained (Figure 2). After L_S 292° a significant decrease (10/15%) of the ice albedo is observed in MY28 compared to MY27. This change can not be attributed to aerosols or photometric conditions which are alike. As the spectral properties of ice are similar in MY27 and MY28 before the storm (Figure 1), we attribute this change to the deposition of a thin layer of dust. The amount of dust deposited at the surface will be estimated using the model of [8].

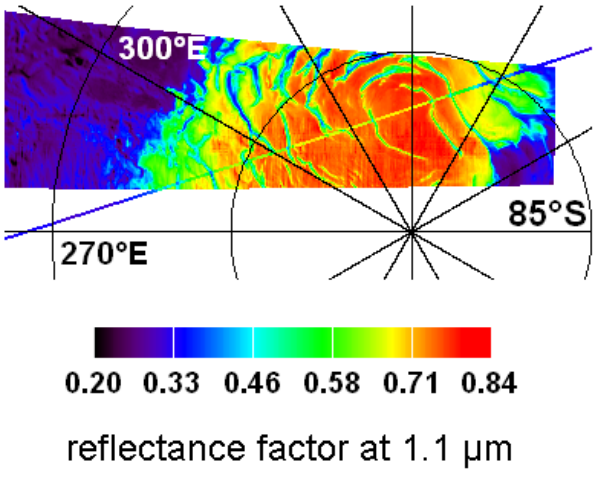

Figure 2: Comparison of OMEGA observations of the south cap at L_S ~ 293° obtained in 2005 and

2007 (observed albedo map: I/F/cos(i) at 1.1 µm). A thin track obtained in 2007 overlaps a large track obtained in 2005. The conditions of observations are similar (photometric angles and aerosols optical depth).

References: [1] Paige et al. (1994), J. Geophys. Res., 99, 25,993-26,013. [2] Neumann et al. (2003), J. Geophys. Res., 108, 5023. [3] Montmessin et al. (2006), J. Geophys. Res., 111, E09S09 [4] Vincendon (2008), Icarus, 196, 488, 505. [5] Smith (2004), Icarus, 167. [6] Lemmon (2006), Lunar Planet. Sci. Conf. 37, #2181. [7] Vincendon et al. (2009), Icarus, 200, 395-405. [8] Douté and Schmitt (1998), J. Geophys. Res., 103(E13), 31,367-31,390

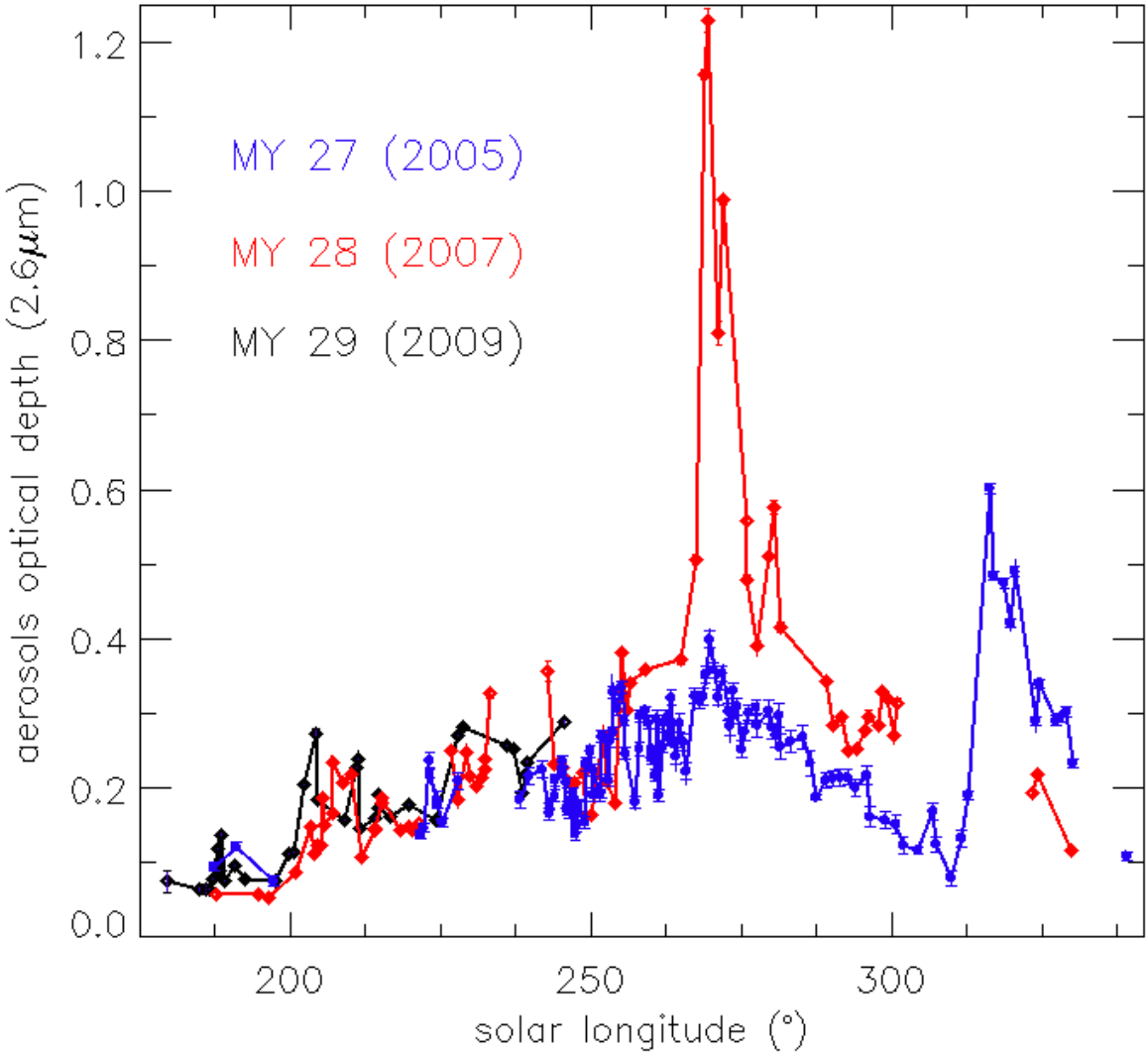

Figure 3: Time variations of the optical depth of dust aerosols during southern spring and summer as seen by OMEGA during 3 Mars Years (MY27 in blue – from [4], MY28 in red and MY29 in black). The 2.6 µm normal optical depth of the whole aerosols layer is derived from OMEGA observations above the south cap summit at 87°S, 355°E. Relative error bars are indicated. See [4] for a discussion of the absolute uncertainties (estimated to be reduced to a multiplicative factor in the [1. – 1.3] range).

MID LATITUDE CO_2 ICE DEPOSITS ANALYZED WITH CRISM AND OMEGA. M. Vincendon[1], J. Mustard[1], F. Forget[2], M. Kreslavsky[3], A. Spiga[4], S. Murchie[5], J.-P. Bibring[6], [1]Department of Geological Sciences, Brown University, Providence, RI, USA. (mathieu_vincendon@brown.edu) [2]Laboratoire de Météorologie Dynamique, Université Paris 6, Paris, France. [3]Earth and Planetary Sciences, University of California - Santa Cruz, CA, USA. [6]Department of Physics & Astronomy, Open University, Milton Keynes, UK [5]Johns Hopkins University/Applied Physics Laboratory, Maryland, U.S.A. [6]Institut d'Astrophysique Spatiale, Université Paris Sud, Orsay, France.

Introduction: The near-IR orbital experiment OMEGA onboard Mars Express has detected seasonal CO_2 ice deposits in the mid-latitudes regions of Mars ([1], [2]). Small patches of seasonal frost with temperature consistent with CO_2 ice have been also observed in high-resolution visible MOC images [3]. Whereas the surface of Mars is totally covered by ice during a part of the year at latitudes higher than 45-50°, only patches of ice frequently linked with pole facing slopes have been found at lower latitudes. We will present a study of the CO_2 ice deposits observed by the CRISM and OMEGA imaging spectrometers. The distribution and properties of these deposit as a function of latitude, season, surface slope, thermal inertia, landform… for both hemisphere will be discussed and compared to the predictions of the LMD GCM [4] adapted to account for surface slopes [5].

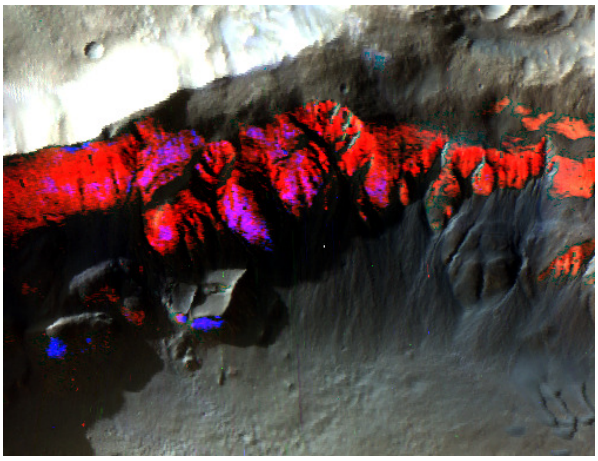

Figure 1: Example of CRISM high resolution observation (# FRT3266) of a pole facing crater rim (located at 38.88°S, 164.07°W) showing CO_2 ice (in blue, detections based on the 1.43 µm band). Water ice (1.5 µm band) is indicated in red. This observation was acquired at L_S 140.6°.

Data processing: More than 8000 spectral cubes have been obtained by OMEGA up to mid March 2009. The spatial resolution of these observations ranges from 0.3 km to 5 km. This dataset is automatically processed to detect points containing a 1.43µm band depth greater than 5%. This 5% limit results from the random noise of the OMEGA instrument and from the uncertainties of the atmospheric CO_2 gas band removal. We consider only observations with solar zenith angles lesser than 70°, as the noise strongly increases after that limit.

The CRISM dataset is composed of multispectral observations with a spatial resolution of 200 m and hyperspectral targeted observations with a spatial resolution ten times better. Due to the more complex structure of the noise of this dataset ([6], [7]), the selection of observations containing CO_2 ice is manually performed with a visual inspection of averaged spectra and spectral ratios. This approach also results in a 5% detection limit (in terms of 1.43 µm band depth) for most deposits considering their limited spatial extent (which limits the possibility of averaging spectra).

The link between the observed band depth and the amount of ice that condense at the surface is not straightforward as it depends on the structure of the ice (grain size…). We estimate that a 5% band depth requires a deposit with a thickness of at least a few tens of µm from laboratory measurements and modeling results [8, 9]. As observations of these CO_2 ice deposits are frequently obtained in shadowed regions with high solar zenith angles, the contribution of aerosols is high, which reduces the apparent band depth of surface components. According to Monte-Carlo modeling of the radiative transfer [10], a 10% band depth at the surface is required to obtain a 5% band depth in the final observation. Our detection limit thus approximately corresponds to a 200 µm thick CO_2 ice deposit at the surface. Thicker deposits can however be undetectable if composed of very small grains size [8], or if their extent is smaller than the pixel size. Latitude and season of deposits identified so far are shown in Figure 2.

Modeling: We use local 1D energy balance code from the LMD Global Climate Model [4] to predict the stability of CO_2 ice on the ground. Surface slopes are accounted for [5]. The ground is composed of two layers for which the thermal inertia and the depth of the interface can be adjusted. The model is run for three years so as to stabilize (the results of the last year are presented). We explore the effect of changing the properties of the ground, the atmospheric dust scenario, the slope angle as well as the slope orientation. An example of simulation is shown in Figure 3.

Results: In the southern hemisphere (Fig. 2), CO_2 ice deposits are observed up to 35°S, and between L_S 80° and L_S 175°. OMEGA and CRISM observations provide complementary L_S coverage. The higher spatial resolution of CRISM gives access to smaller deposits observed higher in latitude or later in the season. Modeling results strongly depend on the thermal inertia of the ground, as observed by [13] for flat surfaces. Grounds with higher thermal inertia store more heat during summer and do not reach temperatures cold enough for CO_2 ice to condense during winter. First modeling results indicate that the ice is expected to be easily stable in the southern hemisphere, i.e. no extreme conditions in terms of thermal inertia or slope angles are required to explain the stability range derived from the observations (Figure 3). Actual slopes on which CO_2 ice is observed (estimated using MOLA measurements) are in good agreement with modeling results: 28 of the 30 craters for which it has been possible to use MOLA profiles show slopes greater than 18°.

In the northern hemisphere, no CO_2 ice deposits have been detected so far for latitude lesser than 45°. Only a minor part of CRISM observations have however been processed for the moment in that region. First modeling results seem also to indicate that CO_2 ice is significantly less stable in the northern hemisphere. The differences between the northern and the southern hemisphere that are accounted for in the model are differences linked with the orbit of Mars (southern summers are warmer but shorter) and differences linked with the L_S dependent atmospheric dust amount. The smaller area of surfaces with high angle slopes in the northern hemisphere could also contribute to the absence of detections (available observations do not cover all these regions around the winter solstice).

Further work is now being carried out to refine the calculation of incoming radiation on slopes, notably by looking in more detail at the impact of atmospheric dust. Spatial variations of the ground inertia, as well as variations with latitude of the density and distribution of slopes, are also being explored.

References: [1] Langevin et al. (2007), *J. Geophys. Res.,* 112, E08S12 [2] Gondet et al. (2008), *Mars Water Cycle Workshop*. [3] Schorghofer and Edgett (2006), *Icarus*, 180, 321-334. [4] Forget et al. (1999). , *J. Geophys. Res.*, 104, 24155-24176. [5] Spiga and Forget (2008), GRL, 35, L15201 [6] Murchie et al. (2007), *J. Geophys. Res.*, 2007, 112, E05S03. [7] Parente (2008), LPSC 39, #2528 [8] Schmitt et al. (2005), LPSC 36, #2326 [9] Dupire et al. (2009), LPSC 40, # 1242 [10] Vincendon et al. (2007), *J. Geophys. Res.,* 112, E08S13. [11] Putzig et al. (2005), *Icarus*, 175, 325-341. [12] Ahronson and Schorghofer (2006), *J. Geophys. Res.,* 111, E11007 [13] Haberle et al. (2008), *Planet. Space Sci.*, 56, 251-255.

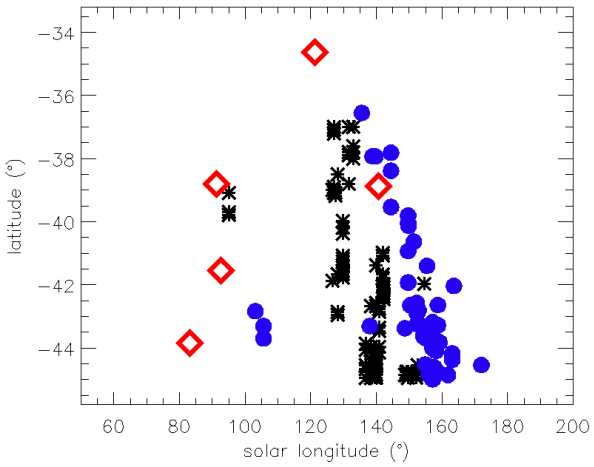

Figure 2: Latitude and season of observed CO_2 deposits (southern hemisphere). OMEGA detections are shown with black stars. Blue dots correspond to CRISM multispectral observations, and red diamonds correspond to CRISM high resolution observations similar to the example of Figure 1.

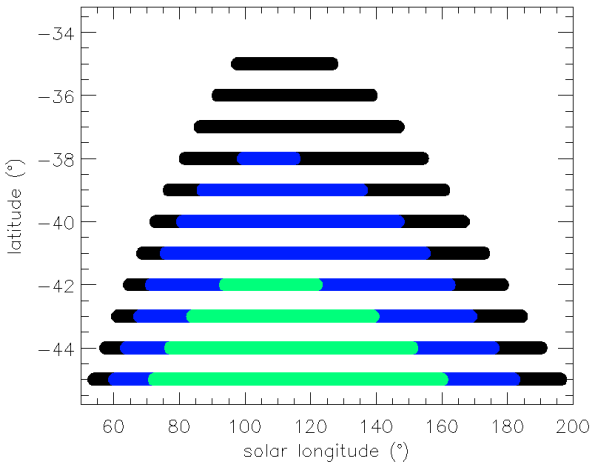

Figure 3: Modeled stability of CO_2 ice on pole facing slopes (black: 30° slopes; blue: 25° slopes; green: 20° slopes) in a latitude / solar longitude diagram (southern hemisphere). The ground is composed of a 10 cm thick soil of thermal inertia 260 SI that cover a layer with a higher inertia (2200 SI) according to ([11], [12]). The MGS atmospheric dust scenario is used.

SIMPLIFYING THE MARTIAN CARBON DIOXIDE CYCLE: AN EMPIRICAL METHOD FOR PREDICTING SURFACE PRESSURE. Paul Withers[1] and Silvia Tellmann[2], [1]Center for Space Physics, Boston University, 725 Commonwealth Avenue, Boston MA 02215 (withers@bu.edu), [2]Rheinisches Institut fur Umweltforschung, Abteilung Planetenforschung, Universitat zu Koln, D-50931, Cologne, Germany (stellman@uni-koeln.de).

Introduction: Temporal and spatial variations in martian surface pressure are strongly influenced by the exchange of carbon dioxide between solid and gaseous phases at the polar caps. Martian surface pressure is thus a sensitive indicator of polar cap processes. Many studies of martian polar energy balance and the carbon dioxide cycle use a model for surface pressure as a constraint or input. Typically, each of these studies uses a different model for surface pressure, often the output from a general circulation model, and it can be difficult for other scientists to replicate the assumed surface pressures in their studies. Here we report a simple empirical model for martian surface pressure and total atmospheric mass. This can provide a common reference surface pressure, thereby eliminating one possible cause of differences between models. It is also useful for a range of other applications.

Available Data: Surface pressure on Mars has been measured by landers and orbiters. Landed measurements of surface pressure come from Viking Lander 1, Viking Lander 2, Mars Pathfinder and Phoenix. Orbital measurements of surface pressure by radio occultation experiments come from Mariner 9, Viking Orbiter 1, Viking Orbiter 2, Mars Global Surveyor and Mars Express. These datasets are consistent, with the exception that Pathfinder's surface pressures seem 0.1 mbar too small. This is probably due to poor knowledge of the gain of the Pathfinder pressure sensor [1].

We tested different empirical expressions for surface pressure against these datasets to identify the best empirical expression. The most useful datasets are Viking Lander 1 and Viking Lander 2, because of their long durations, and Mars Global Surveyor, because of its extensive spatial coverage, long duration and tens of thousands of measurements.

Empirical Expression: We found that the following empirical expression gave reasonable predictions of diurnal mean surface pressure, p_s:

$$p_s(z,Ls) = p_{0,VL1}(Ls) \exp(-(z-z_{VL1})/H) \times (1 + s1 \sin(Ls) + c1 \cos(Ls) + s2 \sin(2Ls) + c2 \cos(2Ls)) \quad \text{[Eqn 1]}$$

where z is altitude and Ls is season, $p_{0,VL1}$ = 7.9723740 mbar, z_{VL1} = -3.63 km, H = 11 km, s1 = -0.068622849, c1 = 0.060390972, s2 = 0.044663631, c2 = -0.050183946. All parameters except z_{VL1} and H were found by a fit to Viking Lander 1 surface pressure data. The value of H was found by trial and error using 21243 MGS measurements of surface pressure. The functional form of this expression was selected because variations in surface pressure due to variations in season and altitude are much greater, and much simpler to model, than those due to variations in latitude, longitude, local time, interannual variability and day-to-day variability. The dependence of surface pressure on altitude is represented by a constant and uniform scale height (11 km, equivalent to a reasonable 215 K). The dependence of surface pressure on season is represented by a truncated harmonic series. Additional terms did not significantly improve the accuracy of predictions.

This expression was tested on Viking Lander 2, Pathfinder, Phoenix and Mars Express data with satisfactory results. Figures 1-3 demonstrate the accuracy of this expression. This work has been performed to support the safe landing of Mars Science Laboratory, so validation has focused on latitudes within 45^o of the equator and altitudes below +1 km. These contraints, and many others, must be satisfied by candidate landing sites. Analyses to date suggest that, at a 1-σ confidence level, the diurnal mean surface pressure predicted for the MSL landing by Equation 1 will be within 3% of the actual value.

Other Applications: According to this expression, the total atmospheric mass is proportional to p_0R^2/g, where R is the planetary radius and g is the gravitational acceleration, and has the same seasonal dependence as surface pressure. Integration of Equation 1 across the surface of Mars gives a mean total atmospheric mass of approximately 2.4E16 kg, consistent with previous results [2]. Predicted atmospheric masses can be used by geodetic studies of topics such as the martian rotational state and gravitational field.

This expression can be used to support landing site selections, the determination of absolute altitude scales for atmospheric T(p) profiles, and theoretical simulations of topics as diverse as dust lifting and aeolian modification of surface features, the thermodynamic stability of near-surface liquids, and the radiation environment at the surface.

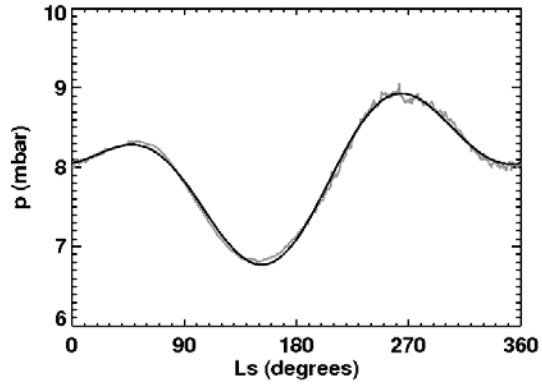

Figure 1: The grey line shows diurnal mean surface pressures observed by Viking Lander 1. The black line shows the corresponding predictions.

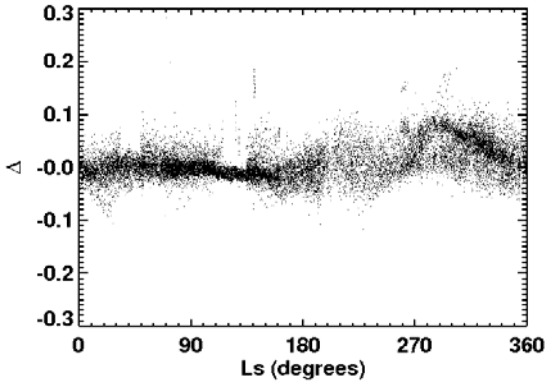

Figure 2: Δ for 21243 MGS surface pressure measurements as a function of season. Δ is defined as $(p_{pred}-p_{meas})/p_{meas}$, where p_{meas} is a measured pressure and p_{pred} is the corresponding prediction.

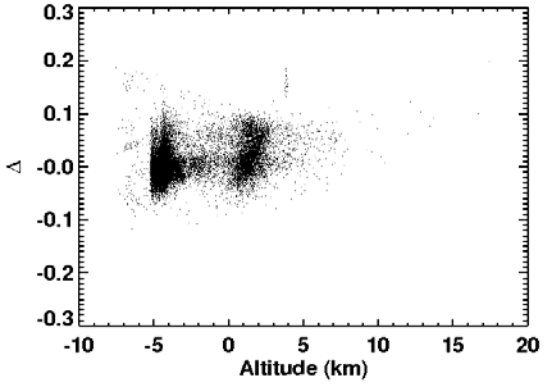

Figure 3: Δ for 21243 MGS surface pressure measurements as a function of altitude. Δ is defined as $(p_{pred}-p_{meas})/p_{meas}$, where p_{meas} is a measured pressure and p_{pred} is the corresponding prediction.

Conclusions: The simple expression reported here can be used to predict martian diurnal mean surface pressures to approximately 3% accuracy (1-σ). Predictions of surface pressure are important for a range of applications.

Acknowledgements: Support from the JPL Mars Critical Data Products program to Boston University.

References: [1] Haberle et al. (1999) JGR, 104, 8957-8974. [2] James et al. (1992) Mars, University of Arizona Press, 934-968.

Epochal Seasonal Thermal Modeling of Mars' Polar Surface Energy Balance: Perennial CO_2 Ice and Atmospheric Collapse. S. E. Wood[1] and S. D. Griffiths[2], [1]Dept. of Earth and Space Sciences, University of Washington, Box 351310, Seattle, WA, 98195-1310, sewood@ess.washington.edu, [2]Dept. of Applied Mathematics, University of Leeds, Leeds, LS2 9JT, UK.

Background: The obliquity of Mars – that is, the angle between its spin axis and orbit normal – undergoes large variations due to a coupling between the motion of its orbit plane and the precession of its spin axis [*1*]. Currently 25.19°, orbital dynamics calculations show that for the past 3 Myr the obliquity has oscillated between 15° and 35° with a dominant periodicity of ~120,000 years and a modulation period of ~1.3 Myr [*2*]. At low obliquity the polar regions receive less annual insolation and can reach a point where the total CO_2 sublimation at the pole becomes less than the total condensation – forming a perennial CO_2 ice polar cap. Below this critical obliquity the mass of the CO_2 polar cap(s) increases at the expense of the atmosphere, potentially leading to atmospheric "collapse". As the atmospheric pressure decreases (more precisely, the partial pressure of CO_2, p_v), so does the CO_2 frost-point temperature (T_f); but any decrease in the temperature of CO_2 ice on the surface decreases the condensation rate because the dominant sink for latent heat is thermal radiation to space. This negative feedback acts to keep the annual average temperature of the perennial CO_2 ice cap and annual average atmospheric pressure in solid-vapor equilibrium, while the obliquity determines which pair of equilibrium values (T_f; p_v) are selected through its control of the polar heat balance [*3,4*].

While the precise magnitude of atmospheric collapse at low obliquity is uncertain, the fact that a significant decrease in atmospheric pressure can occur is a robust conclusion for a wide range of realistic values of CO_2 frost albedo and emissivity. An important consequence of this pressure drop is that it causes a decrease in the thermal conductivity of porous regolith materials. This effect, which has not been considered previously in studies of Mars' climate, can lead to increased subsurface temperatures as the planetary heat flow becomes trapped below a more insulating upper layer [5]. The degree of subsurface warming depends strongly on the minimum atmospheric pressure reached (p_{min}). The value of p_{min} is also important for controlling the flux of micrometeors that reach the surface – evidence for which could provide constraints on atmospheric collapse and/or surface erosion rates [6,7].

Modeling of this process is sensitive to the assumed solar albedo A_f and thermal emissivity ε_f of CO_2 ice at the poles. Values obtained from best-fit modeling of the seasonal pressure cycle may not be representative of the entire seasonal CO_2 polar cap because the atmospheric mass is most strongly affected by the lower latitude portions (50°–70°) where they have the greatest surface area [8], and where they are more likely to be affected by dust storms. Observational studies have shown that the central portions of the seasonal polar caps can be much brighter than the outlying portions, with springtime A_f values as high as 0.83 and ε_f close to unity [9].

The first long-term climate model that included a seasonally-resolved model of polar energy balance [10] used values of $A_f = 0.67$ and $\varepsilon_f = 0.55$ that precluded the formation of perennial CO_2 ice caps unless the obliquity was less than 13°, and therefore predicted no atmospheric collapse during the past 10 Myr. The first long-term climate model to include the latest calculations of Mars' orbital and axial variations [1] predicted a minimum pressure of 30 Pa in the past 1 Myr [*11*], using A_f=0.70 and ε_f =1.0, but did not include the effects of subsurface heat conduction.

Current Work: We have performed seasonally-resolved calculations of the evolution of Mars' atmospheric 4 pressure over the past 1 Myr using a model that includes subsurface heat conduction and the latest calculations of Mars' orbital and axial variations (*1*). The zonally-symmetric model calculates the amount of surface CO_2 condensation or sublimation 12 times per year at 23 latitudes (clustered near the poles) based on a surface energy balance using daily average insolation rates. We found that for values of $A_f = 0.60$, 0.65, and 0.70 (with $\varepsilon_f = 1.0$ in all cases), the minimum pressures reached were 113 Pa, 69 Pa, and 45 Pa, respectively (Fig. 1). Higher A_f values would give lower minimum pressures but would also produce stable perennial CO_2 ice caps at both poles at the present obliquity, which is not observed. In our model, the lowest possible pressure is 29 Pa, due to the presence of 7.9 kg/m^2 of non-condensible gases.

We will present more recent calculations using insolation-dependent albedo as suggested by Viking IRTM observations [9].

References: [1] Laskar, J. *et al.* (2004) *Icarus, 170*, 343-364. [2] Manning, C. V. *et al.* (2006) *Icarus, 180*, 38-59. [3] Toon, O. B. et al. (1980) *Icarus, 44,* 552-607. [4] Ward, W. R. et al (1974) JGR 79, 3387-3395.

[5] Wood, S. E. and S. D. Griffiths (2009) 40th LPSC, Abstract #2490. [6] Vasavada, A. R. et al. (1993) JGR 98, 3469-3476. [7] Paige, D. A. et al. (2007) 7th Int. Conf. Mars, Abstract #3392. [8] Wood, S. E. and D. A. Paige (1992) Icarus 99, 1-14. [9] Paige, D. A. and A. P. Ingersoll (1985) Science 228, 1160-1168. [10] Armstrong, J. C. et al (2004) Icarus 171, 255-271. [11] Manning, C. V. et al. (2006) Icarus 180, 38-59.

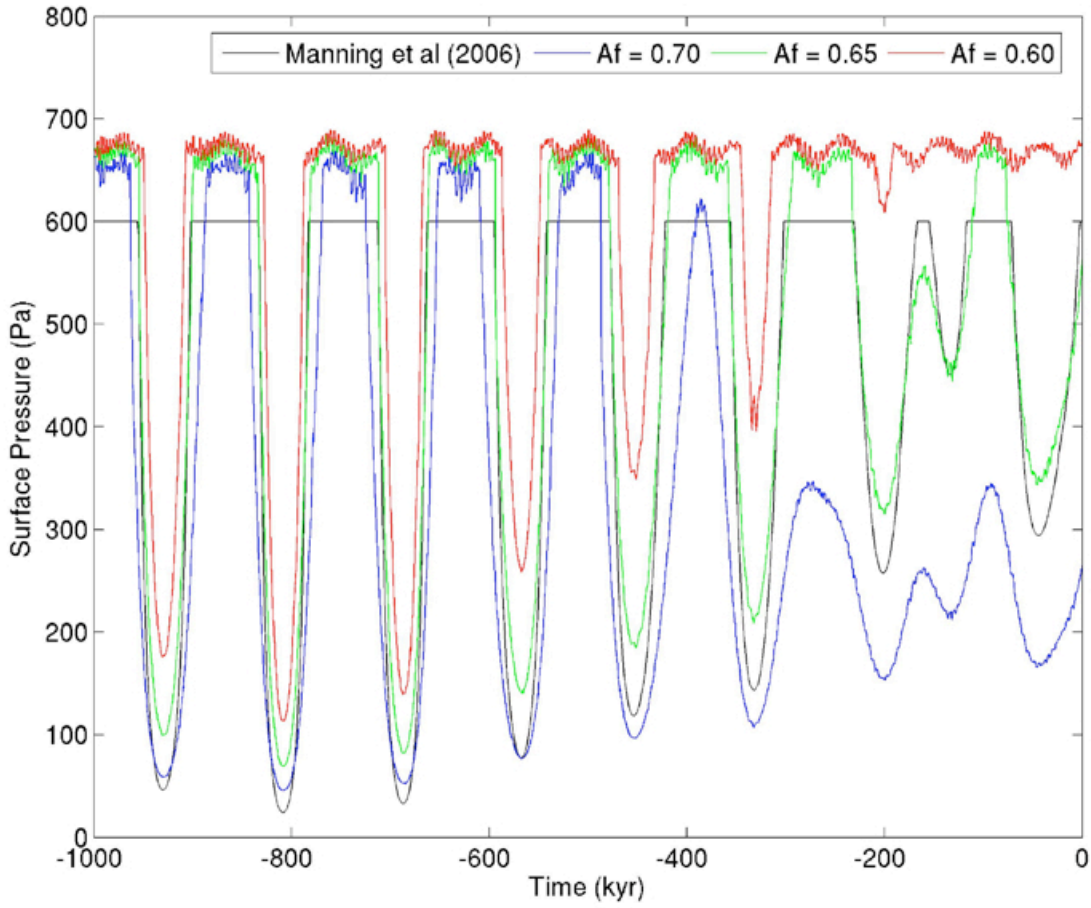

Figure 1

Notes

Notes